

WITH NO GLY-LOOP FAMILY OF KINASES

APPROVED BY SUPERVISORY COMMITTEE

Michael Reese, Ph.D.

Margaret Phillips, Ph.D.

Melanie Cobb, Ph.D.

Vincent Tagliabracci, Ph.D.

Angelique Whitehurst

DEDICATION

To my family, friends, and mentors for all their love and support through the years.

WITH NO GLY-LOOP FAMILY OF KINASES

By

TSEBAOT GHEBRETINSAE BERAKI

DISSERTATION

Presented to the Faculty of the Graduate School of Biomedical Sciences

The University of Texas Southwestern Medical Center at Dallas

In Partial Fulfillment of the Requirements

For the Degree of

DOCTOR OF PHILOSOPHY

The University of Texas Southwestern Medical Center at Dallas

Dallas, Texas

May, 2019

Copyright

by

TSEBAOT GHEBRETINSAE BERAKI, 2019

All Rights Reserved

IDENTIFICATION AND CHARACTERIZATION OF WITH NO GLY-LOOP (WNG)
FAMILY OF KINASES IN *TOXOPLASMA GONDII*

TSEBAOT GHEBRETINSAE BERAKI, Ph.D.

The University of Texas Southwestern Medical Center at Dallas, 2019

Supervising Professor: MICHAEL REESE, Ph.D.

Toxoplasma gondii replicates within a protective organelle called the parasitophorous vacuole (PV). The PV is filled with a network of tubulated membranes, which are thought to facilitate trafficking of effectors and nutrients. Despite being critical to parasite virulence, there is scant mechanistic understanding of the network's functions. Phosphoproteomics data indicated that many PV resident proteins are phosphorylated, including ones that have roles in the biogenesis and maintenance of these tubular networks. Since phosphorylation is a common method to regulate protein functions we hypothesized that PV resident kinases must regulate PV/IVN functions. Protein kinases are enzymes that modify proteins with phosphate molecules.

Using bioinformatics, we identified an unusual family of kinases (WNG kinases) that lack a structural motif, called the Gly-loop, that is absolutely required for the activity of all previously described kinases. In this work, I show that the most conserved WNG kinase, WNG1 as well as WNG2 are catalytically active. The WNG kinases are only found in certain intracellular parasites, such as the human pathogen *Toxoplasma gondii*. I identify the parasite secreted kinase WNG1 as a critical regulator of tubular membrane biogenesis. By solving the crystal structure of a pseudokinase in the WNG1 family, I show members adopt an atypical protein kinase fold lacking the glycine rich ATP-binding loop that is required for catalysis in canonical kinases. Unexpectedly, I find that WNG1 is an active protein kinase that localizes to the PV lumen and phosphorylates PV-resident proteins, several of which are essential for the formation of a functional intravacuolar network. Moreover, I show that WNG1-dependent phosphorylation of these proteins is required for their membrane association, and thus their ability to tubulate membranes. Consequently, WNG1 knockout parasites have an aberrant PV membrane ultrastructure. Collectively, my results describe a unique family of *Toxoplasma* kinases and implicate phosphorylation of secreted proteins as a mechanism of regulating PV development during parasite infection.

TABLE OF CONTENTS

ABSTRACT.....v

TABLE OF CONTENTS VII

LIST OF FIGURES VIII

LIST OF TABLES..... X

LIST OF DEFINITIONS..... XI

LIST OF APPENDIXES..... XIII

CHAPTER ONE: INTRODUCTION 1

 Toxoplasma Parasitophorous vacuole 2

 Introduction to protein kinases 10

 Conserved kinase motifs 11

 Mechanisms of protein kinase activation 12

 Atypical kinases..... 14

 Secreted kinases..... 15

 Proteins and domains that bind phosphoserines and threonines 15

 Kinase substrate specificity 16

CHAPTER TWO: WNG1 regulation of membrane ultrastructure of the *Toxoplasma*
parasitophorous vacuole21

 Introduction 22

 Materials and Methods 23

 Results 30

 Discussion 40

 Future directions..... 43

Chapter 3: WNG2 and WNG3 75

 Materials and Methods 76

 Work on WNG2 and WNG3..... 77

APPENDICES 88

BIBLIOGRAPHY 91

LIST OF FIGURES

Figure 1.1. Cartoon illustration of PV and IVN functions.....	18
Figure 1.2. Toxoplasma PV and IVN ultrastructure	19
Figure 1.3. PKA structure showing conserved active site residues.....	20
Figure 1 : The WNG kinases comprise a phylogenetic clade that is distinct from canonical protein kinases.....	45
Figure S1A: Alignment of Toxoplasma gondii WNG kinase domains.....	46
Figure S1B: Alignment of the N-lobes of human PKA and Toxoplasma gondii WNG kinase domains.	47
Figure 2 : WNG kinases are secreted into the PV lumen from the dense granules.....	50
Figure S2: WNG kinases localize to the dense granules	51
Figure 3: The structure of TgBPK1 reveals an atypical kinase fold lacking the Gly-loop.....	52
Supplemental Figure S3.....	53
Figure S3: BPK1 has a divergent, open active site.....	53
Figure 4: WNG1 has adapted its active site to catalyze phosphoryl transfer without a Gly-loop.	55
Figure S4: Multiple sequence alignment of WNG1 kinase domains with TgBPK1.	56
Figure 5: Vacuoles lacking active WNG1 kinase show disrupted IVN membranes.	57
Figure S5a: Generation of WNG1 knockout parasites	58
Figure S5b: WNG1 complements faithfully localize to dense granules and PV.....	59
Figure S5c : Unusual membrane structures in vacuoles lacking active WNG1 kinase.....	60
Figure 6: Overview of quantitative phosphoproteomics data	61
Figure 7: WNG1 and its substrates are membrane associated.....	64
Figure S6: WNG1 substrates are dense granular proteins.	65
Figure 8: Membrane association of GRA proteins correlates with WNG1 kinase activity.....	66
Figure S7: WNG1 activity does not affect TX-114 partitioning of IVN GRA proteins.	67
Figure 9: Model for WNG1 regulation of IVN GRA protein membrane association.	69
Figure 10: The HRD R is required for WNG1 substrate phosphorylation.	70
Figure 11: WNG1 forms a multimer.....	71
Figure 12: WNG1 autophosphorylation is required for activity.	73

Figure 13: WNG1 autophosphorylation is required for activity.	74
Figure 3.1: Generation of WNG2 knockout parasites	80
Figure 3.2: Generation of WNG3 knockout parasites	81
Figure 3.3: WNG2 is an active kinase	82
Figure 3.4. WNG3 localizes within the parasite	83
Figure 3.5. Vacuole of WNG3 KO parasites showing aberrant cytokinesis.....	84
Figure 3.6. Vacuoles of WNG3 KO parasites show mislocalized organelles (mitochondria)	85

LIST OF TABLES

Table S1C: Gene models (for sequences in ToxoDB) or NCBI accession numbers of sequences used in this study	49
Supplemental Table S2: Crystallographic Data and Refinement	54
Table 1: Phosphosites downregulated in RH Δ wng1 vacuoles	63
Table 2: Phosphosites upregulated in WNG1-deficient vacuoles	63
Table 3.1: Phosphosites downregulated in RH Δ wng2 vacuoles	86
Table 3.2: Phosphosites downregulated in RH Δ wng3 vacuoles	87

LIST OF DEFINITIONS

AMPK-AMP-activated kinase

Aq-aqueous

BPK1-Bradyzoite Pseudokinase 1

CHO-Chinese hamster ovary

C-lobe-C-terminal lobe

CoA-acetyl-coenzyme A

CPC-Carbamyl phosphate synthase

CPL-cathepsin protease L

Det-detergent

DTT-dithiothreitol

GRA-Dense granule

GxGxxG-Gly loop

HFF-Human foreskin fibroblasts

HM-hydrophobic motif

IRG-immunity-related GTPases

IRGs-immunity-related GTPases

IVN-intravacuolar network

KD-kinase dead

KSR-kinase suppressor of Ras

LDL-low density lipoprotein particles

MEK-mitogen activated protein kinase

MHC-major histocompatibility complex I

MS-mass spectrometry

MYR1-major histocompatibility complex I (MHC) Myc regulation 1

N-lobe-N-terminal lobe

PBS-phosphate buffered saline

PFA-paraformaldehyde

PKB/Akt-Protein kinase B

PVM-Parasitophorous vacuole membrane

PV-parasitophorous vacuole

RAH-arginine-rich amphipatic helix

ROPK-rhoptry kinase

SILAC-stable isotope labeling with amino acids in cell culture

TEM-transmission electron microscopy

TFA-trifluoroacetic acid

TM-transmembrane helices

VLK-vertebrate lonesome kinase

WNG-With-No-Gly-loop kinases.

WT-wild-type

LIST OF APPENDIXES

Table 3.3. Primers used in this study.....87

CHAPTER ONE: INTRODUCTION

Toxoplasma gondii

Toxoplasma gondii is a protozoan parasite that belongs to the phylum Apicomplexa. *Toxoplasma* is capable of infecting almost all nucleated cells in nearly all warm blooded animals. A third of the world population is chronically infected with *Toxoplasma gondii*, a parasite that causes severe encephalitis in immune compromised individuals (1). During infection, tachyzoites, the fast growing form of the parasite cause an acute and systemic infection. Then, in response to stress conditions such as host immune response, tachyzoites differentiate into the slow growing bradyzoites. Bradyzoites form tissue cysts in the brain, muscles and visceral organs. This chronic infection is lifelong with no treatments available. While chronic toxoplasmosis is typically asymptomatic, in immunocompromised individuals, parasites within tissue cysts can reemerge and cause severe disease affecting the heart, lungs and eyes. These, tissue cysts are a reservoir for the reactivation of toxoplasmosis in immune compromised hosts such as AIDS and organ transplant patients (2).

Toxoplasma Parasitophorous vacuole

During invasion, *Toxoplasma* invaginates the host plasma membrane, encloses itself within a host cell derived membrane and forms the parasitophorous vacuole (PV). The PV fails to fuse with endocytic compartments of nonphagocytic cells, suggesting this vacuole is maintained as distinct from host endosomal trafficking and is protected from fusion with host lysosomes. This in turn raises the question, *Toxoplasma* grows and replicates inside this non-fusogenic vacuole and is protected from immune detection by the PV membrane (PVM). One of the most striking features of the PV is the intravacuolar network (IVN) of membranous tubules of 20-50nm diameter that appear to bud from the PV membrane into the vacuolar lumen (15) (Figure 1.2). Notably, the inside of the tubules is topologically contiguous with the host cytosol (15, 16). In vacuoles that have 16 parasites or more not all the parasites within are in direct contact with the PVM. This would limit their ability to access nutrients. The IVN tubules increase

the surface area of the PVM and may facilitate access to nutrients, by acting as a network that allows distribution of materials acquired from the host (3). The IVN has been associated with diverse phenomena (Figure 1.1), including:

Nutrient uptake: Although the PVM protects the parasite from fusion with and degradation by host endolysosomes, it also acts as a barrier between host parasite interactions. *Toxoplasma* is auxotrophic for many nutrients including but not limited to cholesterol, purines, arginine and tryptophan. Recently, two dense granule proteins, GRA17 and GRA23 have been shown to be essential for trafficking of small molecules across the PVM. To assess the role of GRA17 and GRA23 in the uptake of small molecules the fluorescent dye 5-(and-6)-carboxy-20,70-dichlorofluorescein diacetate (CDCFDA) was used. This dye has a molecular weight of 445 Da, is PV-permeable and has the ability to fluoresce after entering live cells and getting converted to a membrane impermeable fluorescent form by esterases. Invaded GRA17 and GRA23 KO parasites showed reduced permeability to the dye. GRA17 is a homolog of *Plasmodium* translocon protein EXP2 and GRA17 knockout phenotypes are rescued by complementation with EXP2. Unlike EXP2 which transports both small molecules as well as proteins, the pore created by GRA17 and GRA23 has only been shown to be involved in transporting small molecules.

Mammalian cells obtain cholesterol by uptake of plasma low density lipoprotein particles (LDL) and by de novo synthesis via the mevalonate pathway in the ER (4). LDL binds LDL receptors and is endocytosed through clathrin mediated endocytosis. *Toxoplasma* diverts LDL-derived cholesterol from host lysosomes as demonstrated after incubation of infected cells with labelled cholesterol incorporated into LDL (5). *Toxoplasma* also sequesters cholesterol-filled host lysosomes within the IVN (17). These data suggested that the IVN mediates the transport of host endocytic vesicles from the cytoplasm to the PV.

A membrane-bound host cell P-glycoprotein transporter is required for cholesterol transport to the PV (6). Cholesterol delivery into the PV is then facilitated by host Niemann-Pick type C proteins (7). Once at the PV, a lipid translocating importer of the ATP-binding cassette transporter G subfamily located at the parasite plasma membrane delivers cholesterol to the parasite interior (8). Inside the parasite, a D-bifunctional protein promotes the circulation of cholesterol, phospholipids and fatty acids between parasite organelles and the plasma membrane.

Toxoplasma lacks the ability to *de novo* synthesize purines. *Toxoplasma* salvages purines through adenosine kinase or hypoxanthine-xanthine-guanine phosphoribosyltransferase (HXGPRTase) (9,10). Although the parasite lacks the means for uptake of adenine nucleotides (11), *Toxoplasma* can incorporate adenosine directly into AMP via adenosine kinase. Hence, adenosine has been proposed as the preferred source of purines for the parasite (9). Consistent with this idea, two adenosine transporters (AT1 and AT2), have been identified in the plasma membrane of *Toxoplasma* tachyzoites (12),(13). *Toxoplasma* also expresses a transporter for hypoxanthine, guanine and xanthine (9). Hypoxanthine and guanine are taken up by extracellular parasites (14) and incorporated into nucleotides via a phosphoribosyl-transferase (9,15).

A role for NTPases in purine nucleoside salvage has been proposed. The parasite secretes a family of NTPases into the vacuole from the dense-granule (16). The secreted soluble NTPase then associates with the IVN and becomes a membrane associated insoluble enzyme (17). The NTPase is highly abundant, accounting for about 2-8% of the total tachyzoite proteins (18). The enzyme seems to be a dormant enzyme under ordinary conditions and requires reducing conditions for activation *in vitro*. Two isoforms of NTPase, NTPase-I and NTPase-II, have been characterized (19,20). Although NTPase-I preferentially hydrolyses

triphosphate nucleosides while NTPase-II hydrolyses tri and diphosphate nucleosides, both are capable of hydrolyzing ADP to AMP.

The precursor molecule for both pyrimidines and arginine, carbamoyl phosphate, is produced by Carbamyl phosphate synthase (CPS) activity. Eukaryotes have two CPS genes with distinct activities. The glutamine dependent CPSII is linked with pyrimidine biosynthesis and CPSI is required for arginine biosynthesis (21,22). CPSI produces a carbamoyl phosphate which is converted to citrulline via ornithine carbamoyltransferase. Arginine is then produced from citrulline in two steps by the sequential actions of argininosuccinate synthetase and argininosuccinate lyase (21,22). Through a CPSII knock-out mutant, it was demonstrated that the *Toxoplasma* CPSII is responsible for pyrimidine biosynthesis.

T. gondii is an arginine auxotroph and this auxotrophy can be rescued by supplementing growth media with either arginine or citrulline (20). Arginine is produced from citrulline through the activities of argininosuccinate synthetase (AS) and argininosuccinate lyase (AL) (21). In mutant host cells, rescue with citrulline was dependent on the presence of host cell AS and AL activities. These experiments demonstrated the functional absence of arginine biosynthetic enzyme activity in *Toxoplasma*. The arginine auxotrophy and arginine depletion during *Toxoplasma* infection have been linked with the differentiation of tachyzoites to bradyzoites in vitro. This suggests that local depletion of arginine during the host immune response to parasite infection may play a role in signaling which leads to the formation of slow growing bradyzoites or cyst development and maintenance (2).

Tryptophan auxotrophy of *Toxoplasma* has also been linked to host immune response and control of infection. Tryptophan auxotrophy resulted in reduced growth rate of tachyzoites during tryptophan depletion caused by the host immune response to parasite infection. These data suggest that host immune responses that result in local depletion of amino acids, at sites of

parasite infection, serve as a general mechanism to slow parasite growth or trigger differentiation of rapidly replicating parasites into slow growing encysted bradyzoite forms (2).

Ingestion of host soluble proteins by the parasite: Extracellular parasites are able to internalize fluorescent heparin bound to the parasite surface (23). In addition to the presence of early and late endosome markers, these data suggested that *Toxoplasma* has the ability to endocytose host-derived macromolecules. *Toxoplasma* has also been shown to “ingest” host cytosolic proteins and digest them using proteases within its endolysosomal system (24). *Toxoplasma*’s ability to uptake host-derived proteins was probed by transiently transfecting cytosolic green fluorescent protein (GFP) constructs into Chinese hamster ovary (CHO) cells and fluorescence microscopy. The role of the endopeptidase cathepsin protease L (CPL), in the degradation of host-derived proteins, was also tested by infecting the transfected CHO cells with parasites of the wild type, cpl knockout strain, or ones complemented with catalytically active or inactive CPL. The ingested GFP is exclusively seen in CPL-deficient strains, suggesting that proteolytic activity of CPL is important for digesting incorporated proteins in a lysosomal-like compartment. Reduced ingestion of host-derived GFP in GRA2 KO parasites suggests that an intact IVN facilitates the ingestion of host cytosolic proteins.

Effector translocation across the PVM: The parasite modulates host signaling from within the PV via exported proteins. Several GRA proteins have been identified that are exported outside the PV (). Recently, GRA protein export to the host nucleus was shown to depend on a secreted protein Myc regulation 1 (MYR1). A genetic screen originally set up to identify the effector protein responsible for c-Myc induction by *Toxoplasma* led to the identification of MYR1 and thus why it is called MYR1. Mutant parasites defective in this host c-Myc up-regulation were identified by sorting (using flow cytometry) of infected mouse cells expressing green fluorescent protein fused to c-Myc (c-Myc–GFP). Whole-genome sequencing of three independent mutants

led to the identification of MYR1. MYR1 is a secreted protein that requires the activity of the aspartyl protease TgASP5 to be cleaved into two stable portions, both of which are ultimately found within the parasitophorous vacuole and at the parasitophorous vacuole membrane. Deletion of MYR1 revealed that in addition to its requirement for c-Myc up-regulation, the MYR1 protein is needed for the export of several proteins. The export of GRA16, GRA24, and TgIST was impaired in cells infected with $\Delta myr1$ parasites. The functions of proteins that translocate through the PV to localize to the PVM (with parts exposed to the host cytosol), such as MAF1 and GRA15, were not altered, suggesting that MYR1-dependent export is limited to dense granule proteins that translocate across the PV membrane and accumulate in host cell organelles. Two other proteins, from this myc screen were later identified as being essential for export and named, MYR2 and MYR3 (25). MYR1 is cleaved into N- and C-terminal fragments that run at approximately 80 kDa and 32 kDa, respectively. Immunoprecipitations using anti-HA antibodies on HFFs infected with MYR1-3xHA tachyzoites expressing C-terminally tagged MYR1 and probing with anti-bodies against the C or N terminal protein showed that the N terminal fragment co-precipitated with the C terminus, suggesting that the two proteins are associating. A similar IP and WB experiment showed that MYR3 but not MYR2 associates with MYR1. Together, these data were used to suggest that MYR1, 2 and 3 are critical components of an export complex.

Protection from antigen presentation: CD8 T-cells detect *Toxoplasma* invasion by recognizing short antigenic peptides bound to major histocompatibility complex I (MHC). The IVN protein GRA6 gives rise to a decamer epitope which is presented by MHC (26). In GRA2 knockout parasites, which result in loss of the IVN, there was a substantial increase in the GRA6 antigen presentation. The GRA6 also showed an increased localization at the PVM in the absence of the IVN perhaps due to loss of IVN surface area. This indicates that the IVN decreases

presentation of the membrane-bound GRA6 and thus has an immune modulatory role in which it interferes with MHC processing of membrane-bound vacuolar antigens.

Parasite effector localization to PVM: During invasion, *Toxoplasma* secretes rhoptry effector proteins into the host cytosol. The ROP2 family is one such effector family and it associates with the PVM through an arginine-rich amphipathic helix (RAH) domain (27). While YFP-RAH fusion proteins localized to the PVM in WT parasites, in IVN deficient parasites, they could not localize to the PVM regions between parasites. This demonstrated that the IVN plays a role in the membrane localization of effector proteins.

Protection of PVM from destruction by host immune effectors: ROP18 is a ROP2 family serine/threonine kinase that phosphorylates host targets and modulates acute virulence (28). During infection, host cells translate immunity-related GTPases (IRGs) that localize to and destroy the PVM. ROP18 localizes to the PVM and disrupts this host immune response by phosphorylating IRGs and preventing loading on the PVM. Mutants of ROP18 that couldn't target to the PVM failed to phosphorylate and clear IRGs from the PVM. This resulted in the mutants being avirulent in a mouse model of acute toxoplasmosis. Thus, localization of effector proteins to the PVM is necessary for its protection.

The parasite proteins in the intravacuolar network are phosphorylated, presenting likely points of regulation by kinases. Several Dense granule (GRA) proteins have been shown to be essential for the biogenesis and maintenance of the intravacuolar network.

GRA2: Is a 25 KDa protein that is secreted to the PV. Upon secretion, GRA2 localizes to the IVN as an integral membrane protein. Two amphipathic helices are involved in targeting the protein to the IVN (53). KO of GRA2 results in loss of the tubular structure of the IVN (25). GRA2 forms a complex with GRA4 and GRA6 (29). Recombinant GRA2 tubulates large unilammellar vesicles (LUVs) (20).

GRA3: is a 30 KDa protein that is secreted to the PV and associates with the PVM as an integral membrane protein. It contains a transmembrane domain (30). The N-terminus of the protein faces the PV lumen while the C-terminus is in the host cytosolic side.

GRA4: is a 40 KDa protein that associates with the IVN. The association of GRA4 with the IVN is mediated by protein-protein interactions with GRA6 that has been predominantly influenced by hydrophobic interactions (124). GRA4 forms a complex with GRA2 and GRA6 (29).

GRA5: is a 20 KDa protein that is secreted as a soluble protein into the PV and then associates with the PVM as a transmembrane protein, with its N-terminal domain extending into the cytoplasm and its C-terminus in the vacuole lumen (125). GRA5 contains a transmembrane domain and helices that target it to the PVM.

GRA6: is a 32 KDa protein that is secreted into the PV and associates with the IVN (131). KO of GRA6 results in loss of the tubular structure of the IVN. GRA6 deforms large unilamellar vesicles (LUV) in vitro (29).

GRA7: Triton X-114 partitioning of isolated parasites suggests that GRA7 is an integral membrane protein that localizes to the PVM (31). This is consistent with its having a transmembrane domain. The N terminus of GRA7 faces the PV lumen while the C-terminus is in the host cytosolic side. GRA7 forms a complex with ROP5/ROP18 and ROP17. GRA7 also binds oligomers of Irga6 resulting in disassembly (32). The IRGs are then phosphorylated by ROP18 which prevents their recruitment to the PV.

GRA8: Is a proline rich, 38 KDa protein that associates with the PVM. It contains a TM domain in the C-terminus (33).

Introduction to protein kinases

Protein phosphorylation is the most common type of post-translational modification used in signal transduction. Phosphorylation plays a role in various cellular processes such as growth, division, differentiation, membrane transport, immunity and organelle trafficking (34). Protein kinases catalyze phosphoryl transfer to protein substrates. In eukaryotes, the phosphorylation occurs on serine, threonine and tyrosine residue. Another class of protein kinases, the histidine kinases, are found in prokaryotes. Protein kinases are regulated by gene transcription, translation, protein degradation and cellular localization which in turn limits access to substrates and regulatory binding partners. Phosphorylation of substrates can lead to enzyme activation, enzyme inhibition, and the creation of recognition sites for recruitment of other proteins.

The earliest report of a phosphoprotein was in 1883 by Olof Hammarsten which detected phosphorous in the secreted protein casein (35). Current concepts of protein phosphorylation as a method of regulation grew out of work on glycogen metabolism. In the 1940s researchers showed the enzyme phosphorylase, which catalyzes the first step in glycogen breakdown exists in active and inactive forms (36). In 1954, Burnett and Kennedy were the first to characterize protein kinase enzyme activity using a rat liver mitochondrial fraction as the source of their enzyme (37). They found that casein was readily phosphorylated and were able to isolate and identify [³²P]-phosphoserine following acid hydrolysis of the casein product. They also showed that chemically isolated [γ -³²P]-ATP serves as substrate and that Mg²⁺ is required for protein kinase activity. Soon after, Earl Sutherland *et al*, working with liver phosphorylase, and Fischer and Krebs working with the muscle enzyme, discovered that the active form of phosphorylase is a protein kinase (38,39). They showed that the interconversion of phosphorylase b to phosphorylase a (the enzyme that catalyzes the rate-limiting step of glycogenolysis) involves enzyme catalyzed phosphorylation and dephosphorylation steps. The enzyme catalyzing the

phosphorylation of phosphorylase was named phosphorylase kinase. Researchers soon discovered that phosphorylase kinase also requires phosphorylation in a process that is stimulated by cyclic AMP (40). From these studies, it became clear that phosphorylation increases the activity of phosphorylase and phosphorylase kinase but decreases the activity of the biosynthetic enzyme, glycogen synthase.

In 1958, Sutherland's group described the role of cAMP, a second messenger that leads to the activation of phosphorylase (41). This led to the search and discovery of protein kinases activated by second messengers. Protein kinase A (cyclic AMP-dependent protein kinase), a protein-serine/threonine kinase, protein kinase G (activated by cGMP) and protein kinase C (activated by Ca^{2+}) were thus characterized (42–44). Many more protein kinases were discovered in rapid succession using cDNA cloning methodologies and there are more than 500 human protein kinases (33).

Conserved kinase motifs

The first crystal structure of a kinase showed the protein kinase core consists of two lobes: an N-terminal lobe (N-lobe) and a C-terminal lobe (C-lobe) (45). The two lobes form a cleft that serves as a binding site for ATP. Activation is achieved through changes in the orientation of the C helix in the small lobe and the activation segment in the large lobe. The GxGxxG (Gly-loop) that is present in almost all nucleotide binding proteins, is essential for ATP binding (78). The first Gly interacts with the ribose and the second Gly with the β -phosphate. The VAIK motif where the Val may play a role in positioning the conserved glycines and the Ala faces the adenosine ring. While the Lys interacts with the α and β -phosphate of the ATP. The catalytic core is defined by the HRD and DFG motifs. The Asp is responsible for correct orientation of the P-site hydroxyl acceptor group in the peptide substrate (8). The Arg often coordinates a phosphorylatable residue in the activation loop thus acting as a sensor of phosphorylation. The Asp is the catalytic aspartate. The DFG constitutes the magnesium-

binding loop. The Asp in the DFG forms contacts between the three phosphates of the ATP, either directly or through the coordination of magnesium ions. The Phe in the DFG is involved in the proper positioning of the DFG aspartate and accommodation of the α -C helix. The Asn in the KPEN also binds the second magnesium.

Mechanisms of protein kinase activation

Kinases can be activated by phosphorylation on the activation segment, phosphorylation at other sites, removal of inhibitory sequences or subunits, and/or association of other domains or subunits. Engagement of the C helix hydrophobic patch by internal regions or by external subunits has emerged as a common theme for activation of some kinases. Protection of the activation segment by regulatory domains is another theme.

The cell cycle kinase Cdk2 is dependent on cyclin binding for activity. The cyclin binds in the region of the C helix and leads to a rotation which results in the Cdk C helix hydrophobic residues being shielded by cyclin binding (46). At the same time, the activation segment starting at the DFG motif, moves out of the catalytic site rendering the threonine accessible for phosphorylation. The aspartate of the DFG shifts to an internal site where it chelates the Mg²⁺ ion for ATP binding. In another variation of this activation mechanism, the constitutively active kinase, the PhK catalytic subunit in isolation possesses a canonical amphipathic C helix is fixed in the active conformation without requiring additional interactions (22). In contrast, the kinase domain of Src is held with the C helix in an inactive conformation by interactions with its SH2 and SH3 domains that pack on the opposite side of the kinase and are not in direct contact with the C helix (47). These restraints can be removed, either through the SH2 and SH3 domains docking to recognition proteins or by phosphatase-mediated hydrolysis of the phosphorylated tyrosine that forms the SH2-docking site, allowing the kinase to relax to its active conformation of the C helix (48).

The AGC family of kinases are activated by phosphorylation on both the activation segment and on a hydrophobic motif (HM) located toward the C terminus with consensus sequence FXXF(S/T/D)Y (49). Phosphorylation on the HF motif promotes the intramolecular association of this region with an N-terminal lobe groove, where hydrophobic interactions from the two phenylalanines promote the active conformation of the C helix leading to activation. Protein kinase B (PKB/Akt) is activated by phosphorylation on a serine residue in the hydrophobic motif and by phosphorylation on the activation segment (50). PDK1 is a member of the AGC family that phosphorylates several AGC kinases on their activation segment. PDK1 autophosphorylates on the activation segment and is constitutively active, but activity for substrates is augmented by recognition through the phosphorylated HM motif. PDK1 does not possess an HM in its C-terminal region, but it does have the hydrophobic pocket in the N-terminal lobe (51). Kinases such as S6K, SGK, and RSK are recognized by PDK1 through binding of their phosphorylated HM motifs to the PDK1 hydrophobic pocket.

AMP-activated kinase (AMPK) maintains ATP levels by phosphorylating and inactivating two enzymes in the fatty acid and cholesterol biosynthesis (52). It is a complex of three proteins in which the α -subunit, the catalytic kinase, requires phosphorylation on the activation segment for activity. The β - and γ -subunits play regulatory roles.

Dimerization is another activation mechanism by which many proteins are activated. In such cases, either both partners phosphorylate and activate one another or one partner activates the other through an allosteric mechanism. This activation mechanism was first observed in the receptor tyrosine kinases where binding of a ligand to the extracellular portion of a receptor tyrosine kinase results in activation of the protein kinase domain. An inhibitory sequence is removed from the active site allowing the rearrangement of the activation segment to form the peptide substrate-binding site. The rearranged structure is then secured by phosphorylation on a conserved threonine or tyrosine residue. Dimerization-dependent

phosphorylation of the activation segment in trans to activate a kinase has also been observed in serine/threonine protein kinases (53).

The EGFR kinase is unusual among the family of receptor tyrosine kinases in that it does not require phosphorylation of the activation segment for full activity and its juxtamembrane sequence is required to activate, rather than to inhibit, the kinase domain. Analysis of multiple structures has revealed a conserved mechanism of allosteric activation where one kinase is remodeled and activated following formation of an asymmetric dimer with a second activator kinase (54).

Another example of where kinase dimerization plays a crucial role in kinase activation and in which it now appears one of the monomers plays a scaffolding role and need not have catalytic activity is provided by the cytoplasmic serine/threonine kinase, RAF, and kinase suppressor of Ras (KSR) (55). RAF, together with mitogen activated protein kinase kinase (MEK) and the ERKs, comprises one of the evolutionarily conserved MAPK pathways that collectively signal to regulate cell growth, differentiation, and survival (56).

Atypical kinases

Many proteins have now been shown to be missing some of the canonically conserved motifs and yet are still active. The WNK kinases that are missing the K in the VAIK motif use another K upstream to perform the same role (57). Similar to the WNGs, the kinase VRK3 is also missing a Gly-loop (58,59). On the other hand, the alpha-kinase family consists of atypical protein kinases that have little sequence similarity to canonical protein kinases (60). Kinases in this family have a unique mode of substrate recognition. Unlike canonical kinases that target phosphorylatable residues in non-structured regions, alpha-kinases can phosphorylate residues found in alpha-helical regions.

Secreted kinases

Recently, kinases that phosphorylate secreted proteins in metazoa have been identified (61). These localize within the endoplasmic reticulum, Golgi apparatus and the extracellular space. The identified family includes members of the family with sequence similarity 20 (Fam20) and comprises three members: Fam20A, Fam20B, and Fam20C, all of which have been genetically implicated in mineralized tissue homeostasis. Fam20B is not a protein kinase and instead, it phosphorylates xylose (62). Also in the family of ffx1-related proteins are members of the family with sequence similarity 198 (Fam198), which include Fam198A and Fam198B (found in all vertebrates) and have yet to be functionally characterized. Fam20C phosphorylates secreted proteins with Ser-x-Glu/pSer motifs, including casein (35). Fam20A forms a complex with Fam20C and allosterically activates it leading to efficient phosphorylation of secreted proteins by Fam20C. Although the vast majority of these protein substrates are involved in biomineralization, cytokines, neuropeptide hormones, proteases and extracellular matrix components have also been identified as putative Fam20C substrates (35).

Another group of secreted kinases includes the vertebrate lonesome kinase (VLK) which phosphorylates extracellular proteins on tyrosine residues (63). Proteins related to VLK also localize in the secretory pathway, have a predicted kinase like fold and have been implicated in neurological disorders (64).

Proteins and domains that bind phosphoserines and threonines

Serine/threonine phosphorylation can result in multi-molecular signaling complexes through specific interactions between phosphoserine/threonine binding domains and phosphorylated sequence motifs (65). These domains mediate regulatory protein complexes in signaling networks. However, these domains are absent in the *Toxoplasma* PV, which begs the question: how are phosphoserine/threonines recognized in *Toxoplasma*? Phosphoserine/threonine binding proteins and domains include:

14-3-3 proteins are a family of dimeric α -helical pSer/Thr-binding proteins that are found in eukaryotic cells (65). 14-3-3 proteins recognize the sequences R(S/Ar)XpSXP and RX(Ar/S)XpSXP.

WW domains are signaling elements that bind short proline-rich sequences, mainly containing PPXY, PPLP or PPR motifs (66). These domains are found in proteins that are involved in a variety of cellular processes, including RNA transcription and processing, protein trafficking, receptor signaling, and control of the cytoskeleton.

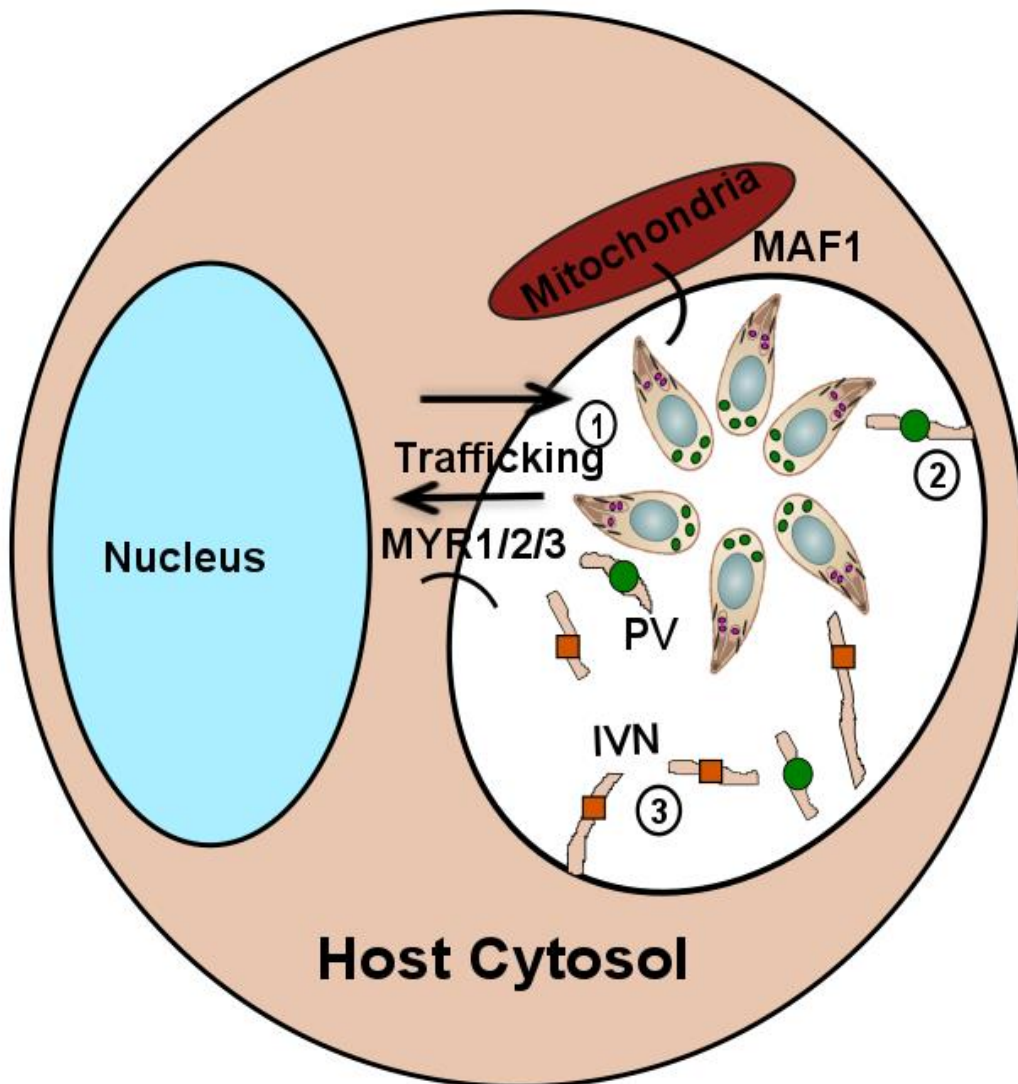
The forkhead-associated (FHA) domain is a signaling element that recognizes phosphothreonines (67). It is found in kinases, phosphatases, kinesins, transcription factors, RNA-binding proteins, and metabolic enzymes.

F-box motif containing proteins recognize substrates of Skp1–Cdc53/Cullin–F-box (SCF) ubiquitin ligases and target them for degradation (68). The F-box motif is commonly found in the amino-terminal half of proteins. Leucine-rich repeats (LRRs) and WD repeats, which are thought to recognize pSer/Thr, are found in the carboxy-terminal part of the protein.

Kinase substrate specificity

Both primary sequence and secondary structural features are important for substrate specificity. The amino acids that are found immediately N-terminal and C-terminal to the phospho-site are involved in substrate recognition (69). Another way kinases achieve substrate specificity is through docking motifs on the substrate or on separate domains or subunits that increase their affinity for that specific substrate. Scaffolding proteins that target the kinase to a specific substrate also allow for substrate specificity. Consensus sequences for phosphorylation can be determined using peptide variants in either a manual screening (70) or a random library (35,71). In a manual screening, phosphorylation sites in substrate proteins are identified and short peptides, based on the local sequence surrounding this site, are synthesized. The

significance of each residue is then tested by making mutations and measuring steady-state kinetic parameters. In the random peptide library approach, all possible amino acids except the P-site are inserted at each position in a short peptide sequence. The best peptide substrates are then selected from the library using peptide sequencing coupled with statistical methods to determine the preference for a certain residue in each position.



- GRA proteins in the IVN
- RAH containing protein

Figure 1.1. Cartoon illustration of PV and IVN functions. The IVN has been associated with diverse phenomena 1) Trafficking of proteins across the PVM and nutrient acquisition 2) Parasite effector localization to the PVM and protection of PVM from by host immune effectors 3) Protection from antigen presentation.

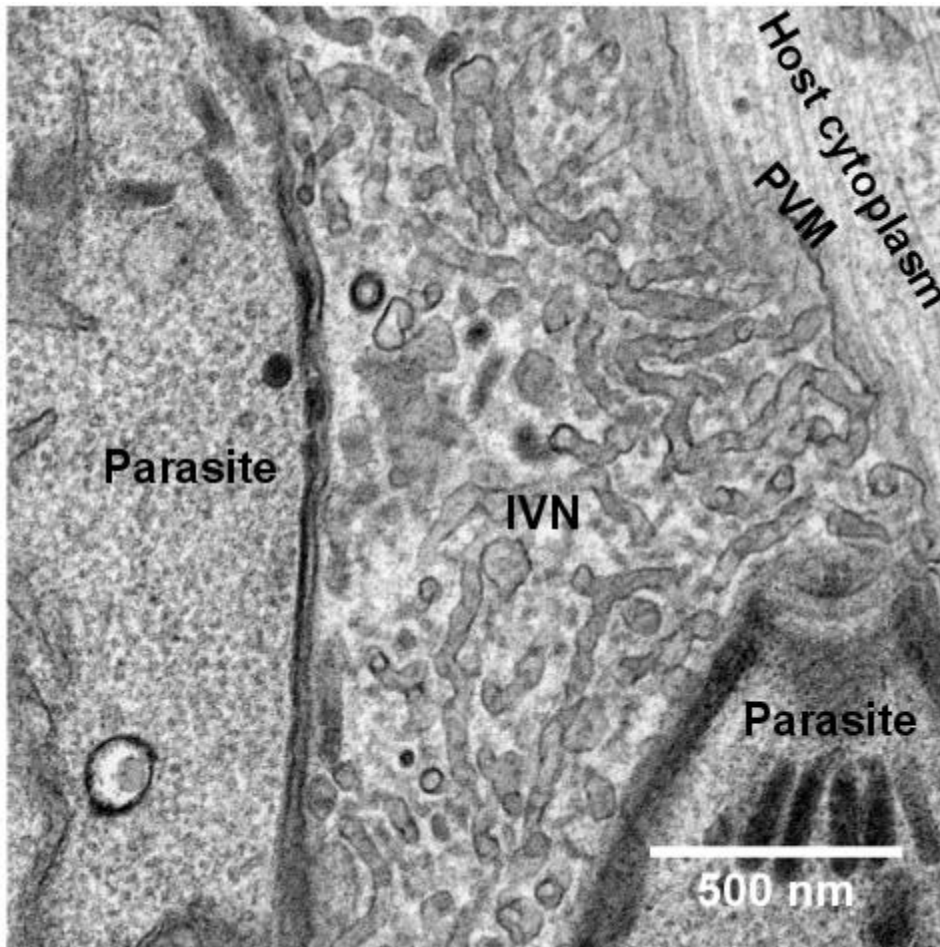


Figure 1.2. Toxoplasma PV and IVN ultrastructure. Transmission electron micrograph of WT parasites showing IVN tubules that have insides that are contiguous with the host cell cytosol.

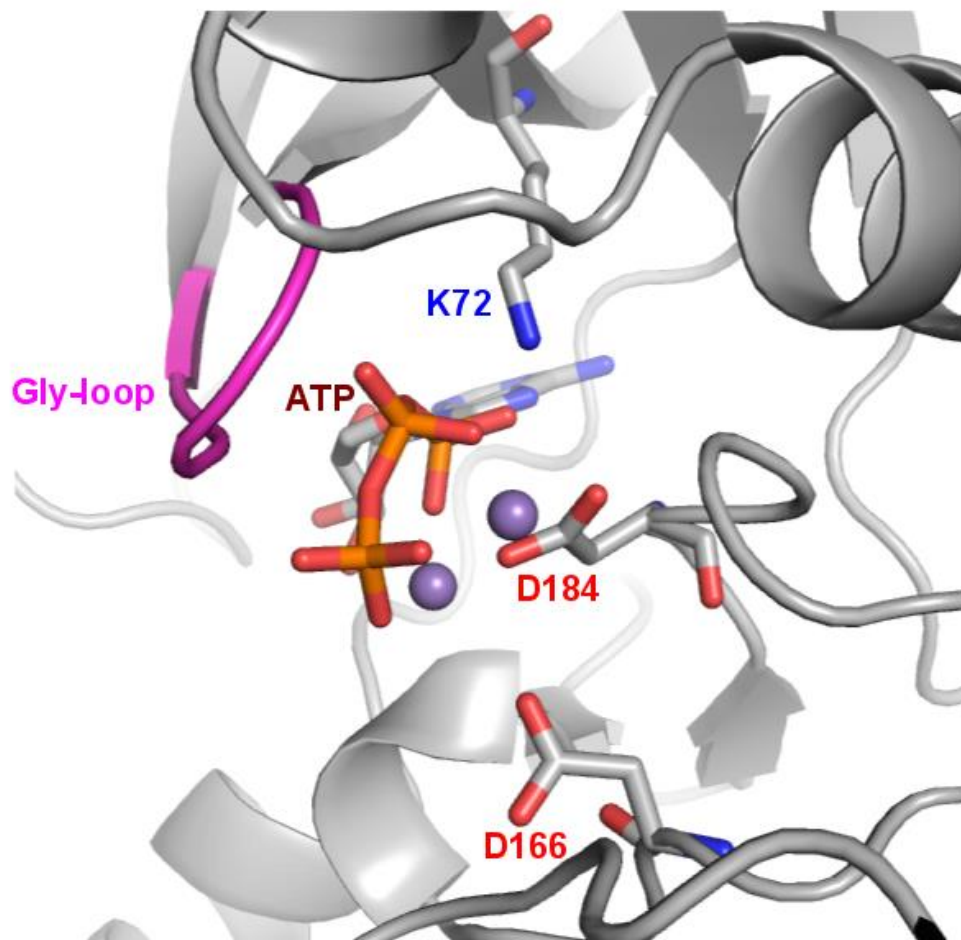


Figure 1.3. PKA structure showing conserved active site residues.

**CHAPTER TWO: WNG1 regulation of membrane ultrastructure of the
Toxoplasma parasitophorous vacuole**

Introduction

Protein phosphorylation is the most common post-translational modification in eukaryotic cells. The addition and removal of specific phosphates is a key mediator of cellular information processing and signal transduction. Phosphorylation is catalyzed by protein kinases, which form one of the largest families of enzymes in mammals (72). The interface between an intracellular pathogen and its host cell is a special case in cellular signaling that defines both a pathogen's ability to manipulate its host and the host's ability to respond to and control the pathogen. The parasite *Toxoplasma gondii* is one of the most successful pathogens in the world, as it can infect virtually any cell type of almost all warm-blooded animals, including approximately one third of humans worldwide (73). *Toxoplasma* directly manipulates signaling at the host-pathogen interface by secreting a variety of effector proteins (74,75), including ~50 protein kinases and pseudokinases (76,77). However, the functions of most of these effectors are unknown.

One vital role for these secreted kinases is to maintain the parasite's replicative niche within its host cell. Like many intracellular pathogens, *Toxoplasma* survives in a specialized membranous organelle called the parasitophorous vacuole (PV). The PV is a complex cellular compartment that mediates sophisticated, multidirectional trafficking, though the molecules that regulate its functions are largely a mystery. Many of the known components of the PV, and of the IVN in particular, are highly phosphorylated after they have been secreted from the parasite (78). About one third of the *Toxoplasma* kinome contains signal peptides but lack transmembrane domains, and are thus predicted to be secreted. Most of these kinases belong to a parasite-specific family that includes a number of virulence effectors (79–81) secreted into the host cytosol from the parasite rhoptries during invasion (82), and have been dubbed the “rhoptry kinase (ROPK)” family. A previous bioinformatic effort annotated the majority of predicted secreted kinases in *Toxoplasma* as ROPKs (76). Notably, vertebrate or ROPK effector kinases localized in the host cytosol cannot access PV-resident proteins on the luminal side of the PV membrane. However, two members of the ROPK family, ROP21/27, were recently found to be secreted into the PV

lumen, rather than localizing to the rhoptries (83). Because ROP21/27 are expressed mainly during the chronic stage of the parasite (83), they are unlikely to function in the regulation of processes during the acute stage, such as the biogenesis of the IVN.

In the present work, we identify a specialized family of kinases that lack the glycine-rich loop that is critical for nucleotide-binding in canonical kinases, leading us to name them the With-No-Gly-loop, or WNG, family. These WNG kinases are conserved throughout the coccidian family of parasites to which *Toxoplasma* belongs and are secreted into the PV. We solved the crystal structure of a family member which demonstrates that the N-lobe of the kinase does indeed lack the structural elements that form the Gly-loop. We found that at least one member of the family, WNG1/ROP35, is catalytically active, and we identified a number of proteins associated with the IVN membrane as phosphorylated in a WNG1-dependent manner. Finally, we demonstrated that loss of these phosphorylation sites correlates with aberrant PV ultrastructure, likely due to the loss of membrane association of proteins that drive the biogenesis of IVN tubules. Taken together, our data show the WNG family of kinases mediates specialized functions in regulating the proteins that create and maintain the intravacuolar network of tubules, which is crucial to the coccidian host-parasite vacuolar interface.

Materials and Methods

PCR and plasmid generation – All PCR was conducted using Phusion polymerase (NEB) using primers listed in Dataset S2. Constructs were assembled using Gibson master mix (NEB). Point mutations were created by the Phusion mutagenesis protocol.

Parasite culture and transfection – Human foreskin fibroblasts (HFF) were grown in Dulbecco's modified Eagle's medium supplemented with 10% fetal bovine serum and 2 mM glutamine. *Toxoplasma* tachyzoites were maintained in confluent monolayers of HFF. Epitope-tagged and knockout parasites were generated by transfecting the RH $\Delta ku80\Delta hxcprt$ strain (84) with 15 μ g of linearized plasmid and selecting for HXGPRT expression, as previously described

(85). The loxP-flanked HXGPRT selection cassette in knockout parasites was removed by transient transfection with a plasmid overexpressing Cre recombinase, and selecting with 6-thioxanthine. WNG1 complement parasites were created by targeting 3xHA-tagged WNG1 (either wild-type or kinase-dead) driven by its native promoter, together with a bleomycin resistance cassette, to the empty Ku80 locus, and selecting with bleomycin, as previously described (86).

Immunofluorescence – HFF cells were grown on coverslips in 24-well plates until confluent and were infected with parasites. The cells were rinsed twice with phosphate buffered saline (PBS), and were fixed with 4% paraformaldehyde (PFA)/4% sucrose in PBS at room temperature for 15 minutes. After two washes with PBS, cells were permeabilized with 0.1% Triton-X-100 for 10 minutes and washed 3x with PBS. After blocking in PBS + 3% BSA for 30 min, cells were incubated in primary antibody in blocking solution overnight at room temperature. Cells were then washed 3x with PBS and incubated with Alexa-fluor conjugated secondary antibodies (Molecular Probes) for 2 h. Cells were then washed 3x with PBS and then mounted with mounting medium containing DAPI (Vector Laboratories). Cells were imaged on a Nikon A1 Laser Scanning Confocal Microscope. Primary antibodies used in this study include rat anti-HA (Sigma; 1:500 dilution), mouse anti-GRA2 (BioVision; 1:1000 dilution), mouse anti-GRA6 (gift of David Sibley; 1:1000 dilution), rabbit anti-ROP2 (1:10,000 dilution).

In vitro kinase assays – The kinase assays comparing WT and mutant activities were run using 2 μ M of His₆sumo-WNG1, 4 mM MgCl₂, 200 μ M cold ATP, 1 mM DTT, 1 mg/mL BSA, 10% glycerol, 300 mM NaCl, 20 mM HEPES pH 7.5. Reactions were started by adding a hot ATP mix, that contained 10 μ Ci γ [³²P] ATP and 5 μ g MBP. The $K_{M,ATP}$ kinase assays were run using the same mix as above except non-radioactive ATP was used in a range of concentrations from 1 mM to 32.5 μ M. The 25 μ L reactions were incubated at a 30°C water bath for 2 h. Reactions were stopped by adding 9 μ L 4x SDS-buffer. 20 μ L samples were then run on an SDS-PAGE

gel. The gels were coomassie stained and the MBP bands were excised and radioactivity quantified using a scintillation counter. All data were analyzed using GraphPad Prism 7.

Western blotting – Proteins were separated by SDS-PAGE and transferred to a PVDF membrane. Membranes were blocked for 1 hour in TBST + 5% milk, followed by overnight incubation at 4°C with primary antibody in blocking solution. The next day, membranes were washed 3x with TBST, followed by incubation at room temperature for 1-2 hours with HRP-conjugated secondary antibody (Sigma) in blocking buffer. After 3x washes with TBST, western blots were imaged using ECL Plus reagent (Pierce) on a GE ImageQuant LAS4000. Antibodies used in this study include: mouse anti-GRA1 (BioVision; 1:1,000 dilution), mouse anti-GRA2 (BioVision; 1:1,000 dilution), mouse anti-GRA3 (gift of J-F Dubremetz; 1:2,000 dilution), mouse anti-GRA4 (gift of LD Sibley; 1:2,000 dilution), mouse anti-GRA5 (BioVision; 1:1,000 dilution), mouse anti-GRA6 (gift of LD Sibley; 1:4,000 dilution), rabbit anti-GRA7 (gift of LD Sibley; 1:5,000 dilution), rabbit anti-ROP2 (1:10,000 dilution), rat anti-HA (Sigma; 1:1,00 dilution). Western blots for quantification were performed independently with each antibody to avoid residual signal due to incomplete stripping.

Figure generation – Structural models were generated using PyMOL v1.7 (87). Secondary structure cartoons were generated using the Pro-origami web server (88). Data plotting and statistical analyses were conducted in Graphpad Prism v7.02. All figures were created in Inkscape v0.91.

Protein purification – BPK1 (residues 61-377 cloned into pGEX4T) was expressed as a GST fusion in *E. coli* Rosetta2(DE3) overnight at 16°C after induction with 300 mM IPTG. Cells were resuspended in 50 mM Tris 8.0, 200 mM NaCl, 1% Triton-X-100 and 0.2% sodium sarkosyl, lysed by sonication, and centrifuged at 27k rcf for 30 min. GST-fusion protein was affinity purified using glutathione sepharose, which was washed first with PBS containing 1% Triton-X-100, and then without detergent. Protein was eluted by overnight on-bead thrombin cleavage at

4°C overnight. BPK1 was further purified by anion exchange and size exclusion chromatography, where it was flash frozen in 10 mM HEPES, pH 7.0, 100 mM NaCl for storage. Recombinant wild-type and mutant WNG1 (residues 265-591; cloned into pET28) proteins were expressed N-terminally fused with His₆-SUMO in *E. coli* Rosetta2(DE3) incubated overnight at 16°C after induction with 300 mM IPTG. Bacteria were lysed in 50 mM HEPES 7.4, 500 mM NaCl, 15 mM Imidazole, lysed by sonication, and centrifuged as above. His₆-fusion proteins were affinity purified using NiNTA resin, and eluted in 50 mM Tris, pH 7.0, 500 mM NaCl, 250 mM imidazole and dialyzed in 20 mM Tris, pH 7.0, 300 mM NaCl before concentration and flash freezing for long-term storage.

Protein crystallization – Small hexagonal plates of BPK1 grew in a wide variety of conditions in initial screens. High quality crystals were seeded from initial hits grown in 0.2M Proline, 0.1M HEPES 7.4, 10% PEG- 3350. To generate a platinum derivative, crystals were soaked with reservoir solution containing 10 mM K₂PtCl₄ for 2 h and washed quickly in reservoir solution. All crystals were flash frozen in a cryoprotectant of reservoir with 25% ethylene glycol.

Data collection, structure determination, and refinement – The diffraction data for the native crystals were collected at beamline 19-ID at the Advanced Photon Source at a wavelength of 1.038 Å and a temperature of 100 K. Native crystals diffracted to 2.5 Å, though diffraction was highly anisotropic, ranging from 2.2 Å in the best dimension to 2.8 Å in the worst. Data for the platinum derivatives were collected in an inverse beam experiment at 1.07195 Å, 1.076276 Å, and 1.07229 Å, corresponding to peak, remote, and inflection wavelengths. Integration, indexing, and scaling of the diffraction data were performed using the HKL2000 suite of programs (89). Initial phases at 3.5 Å were determined by multi-wavelength anomalous diffraction from the Pt datasets using the SHELX suite (90) and used to generate a starting model after density modification with the SOLVE/RESOLVE package (91,92). The high resolution native data were incorporated for extension and map improvement in Phenix (93).

Manual rebuilding in Coot (94) and refinement in Refmac5 (95), led to a final 2.5 Å structure of BPK1 (PDB accession: 6M7Z). The structure was evaluated with Molprobit (96).

Homology modeling – A model of the WNG1/ROP35 structure was created in Modeller v9.14 (97) using the BPK1 structure as a template and an alignment of BPK1 and WNG1 created using Clustal Omega (98).

Transmission electron microscopy – Cells were fixed on MatTek dishes with 2.5% (v/v) glutaraldehyde in 0.1M sodium cacodylate buffer. After three rinses in 0.1 M sodium cacodylate buffer, they were post-fixed with 1% osmium tetroxide and 0.8 % $K_3[Fe(CN_6)]$ in 0.1 M sodium cacodylate buffer for 1 h at room temperature. Cells were rinsed with water and en bloc stained with 2% aqueous uranyl acetate overnight. After three rinses with water, specimens were dehydrated with increasing concentration of ethanol, infiltrated with Embed-812 resin and polymerized in a 70°C oven overnight. Blocks were sectioned with a diamond knife (Diatome) on a Leica Ultracut UC7 ultramicrotome (Leica Microsystems) and collected onto copper grids, post stained with 2% Uranyl acetate in water and lead citrate. Images were acquired on a Tecnai G2 spirit transmission electron microscope (FEI) equipped with a LaB_6 source at 120 kV. Images were analyzed and quantified using the Fiji distribution of ImageJ (99).

Cell culture, lysis and protein digestion for MS proteomics – All reagents were obtained from Sigma-Aldrich unless specified otherwise. Parental (WT) and $RH\Delta wng1$ *Toxoplasma* parasites were cultured in either R0K0 (light) or R10K8 (heavy) SILAC medium (Dundee Cell Products) for 8 generations to ensure efficient heavy label incorporation. 24 h prior cell lysis human foreskin fibroblasts (HFFs) were infected (MOI=5) with WT or $RH\Delta wng1$ parasites. Lysis was then performed in 8 M urea, 75 mM NaCl, 50mM Tris, pH=8.2, supplemented with protease (complete mini tablets, Roche) and phosphatase (Phos Stop tablets, Roche) inhibitors followed by sonication to reduce sample viscosity (30 % duty cycle, 3 × 30 sec bursts, on ice). Protein concentration was measured using BCA protein assay kit (Thermo Fisher Scientific) and equal

amounts of heavy and light lysates mixed in 1:1 ratio. Lysates were subsequently reduced with 5 mM dithiothreitol (DTT) for 30 min at room temperature and alkylated with 14 mM iodoacetamide for 30 min at room temperature in the dark. Following quenching with 5 mM DTT for 15 min in the dark lysates were diluted with 50 mM ammonium bicarbonate to reduce the concentration of urea to < 2M and digested with trypsin (Promega) overnight at 37 °C. After digestion samples were acidified with trifluoroacetic acid (TFA) (Thermo Fisher Scientific) to a final concentration of 1 % (v/v), all insoluble material was removed by centrifugation and the supernatant was desalted with Sep-Pak C18 cartridges (Waters). The samples were further digested with LysC (Promega) for 2-3 h at 37 °C and trypsin overnight at 37 °C followed by desalting with Sep-Pak as above.

Phosphopeptide enrichment – Desalted and vacuum dried samples were solubilized in 1 ml of loading buffer (80 % acetonitrile, 5 % TFA, 1 M glycolic acid) and mixed with 5 mg of TiO₂ beads (Titansphere, 5 µm GL Sciences Japan). Samples were incubated for 10 min with agitation followed by a 1 min 2000 × g spin to pellet the beads. The supernatant containing all non-phosphorylated peptides (total proteome) was removed and stored at -80 °C. The beads were washed with 150 µl of loading buffer followed by two additional wash steps, first with 150 µl 80 % acetonitrile, 1 % TFA and second with identical volume of 10 % acetonitrile, 0.2 % TFA. After each wash beads were pelleted by centrifugation (1 min at 2000 × g) and the supernatant discarded. The beads were dried in a vacuum centrifuge for 30 min followed by two elution steps at high pH. For the first elution step the beads were mixed with 100 µl of 1 % ammonium hydroxide (v/v) and for the second elution step with 100 µl of 5 % ammonium hydroxide (v/v). Each time the beads were incubated for 10 min with agitation and pelleted at 2000 × g for 1 min. The two elutions were combined and vacuum dried.

Mass spectrometry sample fractionation and desalting – Both phospho- and total proteome (40 µg) samples were fractionated in a stage tip using Empore SDB-RPS discs (3M). Briefly,

each stage tip was packed with one high performance extraction disc, samples were loaded in 100 μ L of 1 % TFA, washed with 150 μ L of 0.2 % TFA and eluted into 3 fractions with 100 μ L of the following: 1) 100 mM ammonium formate, 20 % acetonitrile, 0.5 % formic acid; 2) 200 mM ammonium formate, 40 % acetonitrile, 0.5 % formic acid; 3) 5 % ammonium hydroxide, 60 % acetonitrile. The fractions were taken to dryness by vacuum centrifugation and further desalted on a stage tip using Empore C18 discs (3M). Briefly, each stage tip was packed with one C18 disc, conditioned with 100 μ L of 100 % methanol, followed by 200 μ L of 1 % TFA. The sample was loaded in 100 μ L of 1 % TFA, washed 3 times with 200 μ L of 1 % TFA and eluted with 50 μ L of 50 % acetonitrile, 5 % TFA. The desalted peptides were vacuum dried in preparation for LC-MS/MS analysis.

nLC-MS/MS and data processing – Samples were resuspended in 0.1 % TFA and loaded on a 50 cm Easy Spray PepMap column (75 μ m inner diameter, 2 μ m particle size, ThermoFisher Scientific) equipped with an integrated electrospray emitter. Reverse phase chromatography was performed using the RSLC nano U3000 (Thermo Fisher Scientific) with a binary buffer system (solvent A: 0.1% formic acid, 5% DMSO; solvent B: 80% acetonitrile, 0.1% formic acid, 5% DMSO) at a flow rate of 250 nL/min. The samples were run on a linear gradient of 2-35% B in 90 or 155 min with a total run time of 120 or 180 min, respectively, including column conditioning. The nanoLC was coupled to a Q Exactive mass spectrometer using an EasySpray nano source (Thermo Fisher Scientific). The Q Exactive was operated in data-dependent mode acquiring HCD MS/MS scans ($R=17,500$) after an MS1 scan ($R=70,000$) on the 10 most abundant ions using MS1 target of 1×10^6 ions, and MS2 target of 5×10^4 ions. The maximum ion injection time utilized for MS2 scans was 120 ms, the HCD normalized collision energy was set at 28, the dynamic exclusion was set at 20 or 30 s for 120 and 180 min runs, respectively, and the peptide match and isotope exclusion functions were enabled. Raw data files were processed with MaxQuant (100) (version 1.5.0.25) and peptides were identified from the MS/MS

spectra searched against *Toxoplasma gondii* proteome (ToxoDB, 2017) using Andromeda (101) search engine. SILAC based experiments in MaxQuant were performed using the built-in quantification algorithm (100) with minimal ratio count = 1, enabled 'Match between runs' option for fractionated samples (time window 0.7 min) and 'Re-quantify' feature. Cysteine carbamidomethylation was selected as a fixed modification whereas methionine oxidation, acetylation of protein N-terminus and phosphorylation (S, T, Y) as variable modifications. The enzyme specificity was set to trypsin with maximum of 2 missed cleavages. The precursor mass tolerance was set to 20 ppm for the first search (used for mass re-calibration) and to 4.5 ppm for the main search. The datasets were filtered on posterior error probability to achieve 1% false discovery rate on protein, peptide and site level. "Unique and razor peptides" mode was selected to allow identification and quantification of proteins in groups (razor peptides are uniquely assigned to protein groups and not to individual proteins). Data were further analyzed as described in the Results section and in the Supplementary Table S6 using Microsoft Office Excel 2010 and Perseus (102) (version 1.5.0.9).

Results

Identification of a divergent family of coccidian secreted kinases that lack the canonical glycine-rich loop

We reasoned that regulatory phosphorylation of PV-resident proteins would most likely be carried out by a conserved resident protein kinase that is secreted from the parasite's dense granules. To identify potential PV-resident kinases, we compared the sequences of the predicted secreted kinases in *Toxoplasma*. We were surprised to find that a small family of parasite kinases appear to completely lack the glycine-rich, or P-loop, that is found in all canonical kinases and is required for binding the ATP in the active site (103,104) (SI Appendix, Fig. S1A,B). These kinases include three proteins annotated as ROPKs (ROP33, ROP34, and ROP35), and a pseudokinase, BPK1, that has previously been identified as PV resident and a component of the bradyzoite cyst wall (105). Phylogenetic analysis gave clear support for these

proteins forming a clade that is distinct from canonical protein kinases (Figure 1), including the parasite ROPKs. Furthermore, we identified members of this family in every species of coccidian parasite for which genomic sequence is available (Figure 1 and SI Appendix, Table S1C), suggesting that they play an important role in the parasite's pathogenic lifestyle. Notably, with the exception of the PV-resident kinases ROP21/27, the majority of ROPKs are not conserved throughout coccidian parasites (106). Given the lack of the glycine-rich loop and phylogenetic evidence that indicates that these proteins form a distinct clade, we propose that the family be named the WNG (With-No-Gly-loop) kinases.

WNG kinases are secreted into the parasitophorous vacuole

As noted above, BPK1 has previously been identified as a PV-resident pseudokinase (83). We thus sought to assess the localization of other WNG kinases and concentrated on the most divergent members of the family in *Toxoplasma*: ROP34 and ROP35 (Figure 1). We engineered parasite strains in which the endogenous copies of each of ROP34 and ROP35 were expressed in frame with a 3xHA tag. While both proteins appeared to be secreted into the PV, neither ROP35 nor ROP34 co-localized with the rhoptry marker ROP2 (Figure 2A), though ROP35 co-localized well with the dense granule marker GRA2 after secretion into the PV (Figure 2B, SI Appendix, Fig. S2). However, both ROP34 and ROP35 appeared to co-localize with puncta of the dense granule marker GRA5 in extracellular parasites (SI Appendix, Fig. S2), suggesting they are dense granule proteins. While these data appear inconsistent with the reported localization of ROP35 to the parasite PV via rhoptry secretion (104), we note that the previous report did not colocalize ROP35 with a known rhoptry marker, nor did it analyze endogenously tagged protein, both of which could lead to misinterpretation of the protein's endogenous localization. Furthermore, both ROP34 and ROP35 have recently been identified as proteolytically processed by the Golgi-resident ASP5 protease (105), which appears to act exclusively on dense granule proteins. As the "ROP" designation was originally created to

indicate localization rather than function (106), we propose that the WNG kinases be renamed to avoid confusion with the unrelated ROPK family. Given its high conservation (Figure 1 and SI Appendix, Table S1C), we propose ROP35 be renamed WNG1, and other family members annotated as in Figure 1 and SI Appendix, Table S1C.

The crystal structure of TgBPK1 reveals a non-canonical active site that lacks the Gly-loop

While the Gly-loop is thought to be both a critical catalytic and structural element of the protein kinase fold, a number of unusual kinases have been demonstrated to have either adapted a canonical kinase fold to perform a specialized non-catalytic function (107–109), or to use an atypical fold and active site to catalyze phosphoryl transfer (110,111). We therefore sought structural information to better understand the topology of the WNG kinase fold. While we were unable to crystallize an active WNG kinase, we readily obtained crystals of the *Toxoplasma* pseudokinase BPK1 (Bradyzoite Pseudokinase 1). We solved the structure of BPK1 to 2.5 Å resolution (Figure 3A and Table S2). Like WNG1, BPK1 is secreted into the lumen of the PV (83), and is a clear member of the WNG family (Figure 1). As such, BPK1 shares both primary identity and predicted secondary structure with other WNG kinases throughout its sequence (SI Appendix, Fig. S1A), indicating that its structure would provide faithful insight into the WNG kinase fold.

The BPK1 structure revealed a divergent kinase fold in which the Gly-loop and the first β -strand that stabilizes it (β 1 in PKA nomenclature) have been replaced by a helical extension that packs against the top of the N-lobe of the kinase (Figure 3). Remarkably, not only do the WNG kinases lack a Gly-rich primary sequence, the structural elements that compose the motif have been replaced, resulting in a reorganized N-lobe architecture (Figure 3C,D). The core of the kinase fold, however, is remarkably well conserved, supporting our phylogenetic data (Figure 1) that suggest the WNG family diverged from a canonical Ser/Thr kinase fold. Two salt bridges help stabilize the BPK1 N-lobe within the pseudoactive site, including the bridge

between the conserved α C-helix Glu and VAIK-Lys (SI Appendix, Fig. S3A). Notably, the lack of the Gly-loop and β 1-strand creates an active site that is much more open than that of a canonical kinase, such as PKA (SI Appendix, Fig. S3B,C).

While BPK1 is a confirmed pseudokinase that cannot bind nucleotide (112), the other WNG kinase family members have conserved the other canonical motifs essential for catalysis (SI Appendix, Fig. S1A and Figure 4A), suggesting they may be active. To better understand how the WNG kinase active site has adapted to bind nucleotide and catalyze phosphoryl transfer without a Gly-loop, we modeled the WNG1/ROP35 active site using the structure of BPK1 as a template (Figure 4B,C). This model, together with analysis of sequence conservation among WNG1/ROP35 orthologs (SI Appendix, Fig. S4), confirmed that the core of the canonical active site appears largely conserved (Figure 4C).

We expressed and purified the kinase domain of *Toxoplasma* WNG1/ROP35 and found that it robustly phosphorylated the generic substrate MBP in an *in vitro* kinase assay. We verified that mutation of each of the canonical motifs that enable catalysis and Mg^{2+} /ATP-binding (HRD*, VAIK*, D*FG) resulted in loss of kinase activity (Figure 4D). We also identified three notable variations from typical motifs within the active site. First, we noted that while substitution of the Ala in the VAIK motif to a bulkier side chain usually interferes with ATP-binding, a Val appears to be preferred at this position in WNG family members. Mutation of V344A in WNG1/ROP35 reduced the specific activity of the kinase to ~20% of wild-type (Figure 4D), consistent with a requirement for repositioning the ATP within the WNG active site. Second, we noted a conserved stretch of basic residues in WNG1/ROP35 orthologs (R312/313 in *Toxoplasma*) that are placed near where the Gly-loop would lie (Figures 4B,C and SI Appendix, Fig. S4). We therefore reasoned that the side chains of these residues may form a degenerate Walker A motif-like cap (80), and help replace the Gly-loop function. Consistent with such a model, both R312A and R313A mutants exhibited reduced specific activity, though R313A

showed a much less severe effect than R312A (Figure 4D).

Finally, we noted that the WNG kinase Mg^{2+} -coordinating DFG motif had an acidic residue (E457 in WNG1) replacing the Gly. As in our BPK1 structure (SI Appendix, Fig. S3A), the WNG1 E457 appears to form a salt-bridge with a conserved basic residue +2 from the VAIK Lys (Figure 4C; K348 in WNG1). This substitution is unusual for two reasons. (i) the DFG Gly is thought to be important for the regulation of many kinases, as it enables the peptide backbone to “flip” between two states (“DFG-in” and “DFG-out”; (113,114)); (ii) the side chain of the Glu would be predicted to point towards the phosphates of the bound nucleotide (Figure 4C), and would thus electrostatically clash. We reasoned that a clash may be prevented, however, if the residue was participating in Mg^{2+} -coordination, as the Asp in the DFG does. The pseudokinase domain of metazoan RNaseL also has this unusual substitution, in this case, a DFD motif. The crystal structure of RNaseL pseudokinase demonstrated that both acidic residues in the DFD motif participate in Mg^{2+} -coordination (115), helping to explain the protein’s unusually high affinity (1 μ M) for ATP. We therefore tested whether mutation of WNG1/ROP35 E457 to either Gly or Ala would affect its activity, and found that both mutant proteins had severely attenuated activity that was not significantly different from the kinase-dead HRD D437S mutant (Figure 4D). We went on to determine that our recombinantly expressed WNG1 has an *in vitro* $K_{M,ATP}$ of 520 ± 90 μ M (Figure 4E), using MBP as a substrate. Given the lack of the Gly-loop, which is a key ATP-binding element, it is unsurprising that this $K_{M,ATP}$, is higher than the 10-100 μ M reported for many canonical kinases (116). However, the mammalian kinases Src and Akt have reported $K_{M,ATP}$ of approximately 200 μ M and 500 μ M, respectively (116), indicating that our value for WNG1/ROP35 is consistent with an active kinase. Furthermore, the PV membrane is permeable to small molecules such as nucleotides (117,118), and cellular ATP concentrations range between 2-5 mM (119), suggesting that PV nucleotide concentrations are well above that needed for activity with such an affinity for nucleotide.

Taken together, our structural and biochemical data suggest that WNG1/ROP35 and other family members are active protein kinases that have evolved multiple alterations to the active site to compensate for the lack of a Gly-loop. Furthermore, these broad structural changes imply an evolutionary pressure to reshape the protein structure to perform a specialized function.

The intravacuolar network of parasites deficient in WNG1 kinase activity is unstable

We next sought to identify potential functions for the WNG kinases. We chose to concentrate our efforts on WNG1 because it is conserved throughout coccidia (Figure 1), concentrates within the PV lumen (Figure 2), and is important for chronic infection in a mouse model of infection (120). We used double homologous recombination to knock out the WNG1 locus in the *RHΔku80Δhxgprt* background (SI Appendix, Fig. S5a). The resulting *RHΔwng1* parasites showed no obvious growth phenotype in normal culture conditions. We also generated WNG1-complemented strains by knocking a wild-type or kinase-dead (D437S; the HRD motif) copy of WNG1 into the empty Ku80 locus of the *RHΔwng1* strain. The kinase was expressed with its native promoter and in-frame with a C-terminal 3xHA. Both the active and kinase-dead complement strains expressed WNG1 at similar levels to the levels in the endogenously tagged parasite strain, and were appropriately localized to the vacuolar space (SI Appendix, Fig. S5b). To examine the ultrastructure within the vacuoles of parasites with and without active WNG1, we used transmission electron microscopy (TEM). We compared the vacuoles of HFFs that had been infected for 24 hours with either parental, *RHΔwng1*, or the complemented strains (Figure 5, SI Appendix, Fig. S5c). The IVN is a complex structure of branching membranous tubules that fills a large portion of the PV lumen (121). As expected, we observed a dense network of tubules filling the luminal space between the parental parasites (Figure 5A). While we did observe regions with IVN tubules in *RHΔwng1* vacuoles, they have been largely replaced with unusual multilamellar structures containing many 70 – 150 nm diameter vesicles within a larger

0.5 – 2 μm membrane-delineated object (Figure 5B). These multilamellar structures appear much less electron dense than the tubular network, suggesting a lower protein content. Consistent with this observation, the internal vesicles appear to have been lost in some structures (Figure 5B, S5c), potentially due to reduced crosslinking before plastic embedding. Importantly, we prepared samples from mutant parasite strains in parallel with a parental control. We never observed loss of tubular structures in the parental strains, suggesting that this phenotype is not an artifact of our preparation. While vacuoles of wild-type WNG1 complemented parasites were indistinguishable from the parental, those formed by the kinase-dead complemented strain exhibited the same loss of IVN tubules and its apparent replacement with large multilamellar vesicles (Figures 5C-D). These changes were quantified in Figure 5E,F. These data indicate that WNG1 phosphorylates one or more proteins involved in IVN biogenesis and/or stability, and that this phosphorylation is required for normal function.

Quantitative phosphoproteomics reveals GRA proteins as candidate substrates of WNG1

To identify potential substrates of WNG1, we compared phosphoproteomes of the parental (WT) and $\text{RH}\Delta\text{wng1}$ strains using stable isotope labeling with amino acids in cell culture (SILAC) quantitative mass spectrometry (MS) based proteomics as previously described (122). Briefly, we infected human foreskin fibroblasts (HFFs) for 24 h with WT or $\text{RH}\Delta\text{wng1}$ parasites previously grown in either “heavy” (H) or “light” (L) SILAC media. After cell lysis we mixed the samples (H and L) in 1:1 ratio applying forward ($\Delta\text{wng1}/\text{WT}$), reverse ($\text{WT}/\Delta\text{wng1}$) as well as control labeling (WT/WT). This mixing strategy ensures that both systematic and technical errors due to stable isotope labeling can be identified and results in high confidence of MS quantifications. Mixed lysates were then digested with LysC/trypsin and phosphopeptides enriched and fractionated as described in the methods section. We prepared 3 biological replicates for WT vs Δwng1 samples and analyzed quantitative differences in the proteome and phosphoproteome between WT and mutant samples by mass spectrometry. We identified

10,301 phosphosites for both human and *Toxoplasma* and obtained quantification (H/L ratios) for 8,755 of them. *Toxoplasma*-specific sites constituted 2,296 (~30%) of all quantified sites (Dataset S1), which is a similar proportion of sites identified in previous studies using intracellular *Toxoplasma* parasites (123). In order to identify significantly changing sites between WT and RH Δ wng1 parasites a one sample t-test was performed applying the following parameters: p-value < 0.05 and $|\log_2|$ fold change > 1 (Figure 6). Furthermore, phosphosite significance was also correlated with the SILAC control sample (WT/WT) and the proteome data to control for differential phosphorylation originating from the technical variation in the system and protein abundance, respectively (Dataset S1). We also identified a number of phosphorylation sites on proteins with consistent loss of phosphorylation in RH Δ wng1 parasite strains, that however, did not pass the t-test significance test (Dataset S1). However, all phosphorylation sites close to the p-value cutoff are predicted or known secreted proteins, indicating that the p-value may be overly stringent in this case.

We identified 10 proteins in which phosphorylation was significantly reduced between the parental and RH Δ wng1 samples (Figure 6, Table 1, and Dataset S1). Among these candidate substrates were 6 proteins well-known to be associated with the PV membrane or IVN tubules (Table 1), including GRA2 and GRA6, which are essential for IVN biogenesis (124). Another hit, GRA37, was identified in a recent proteomics analysis of PV membrane proteins, and was found to colocalize with IVN markers (121). We identified three proteins with WNG1-dependent phosphorylation that have not been previously studied, and are therefore annotated as “hypothetical” in the genomic database (ToxoDB v32 gene models: TGGT1_244530, TGGT1_254000, and TGGT1_267740). We reasoned that if WNG1 is, indeed, a PV-resident kinase, WNG1-dependent phosphorylation should predict PV (and possibly IVN) localization. We therefore engineered strains in which the proteins were endogenously tagged at their C-terminus with a 3xHA epitope. Immunofluorescence revealed that each of these proteins were

secreted into the PV, and co-localized with dense granule markers both within the vacuolar lumen (Figure 7A) and within the parasites (SI Appendix, Fig. S6A). We have thus annotated these three genes as encoding newly described dense granule proteins GRA44, GRA45, GRA46 (Tables 1 and 2).

In addition to the phosphosites that were downregulated in the vacuoles lacking WNG1, we identified 7 sites where phosphorylation was significantly increased in the *RHΔwng1* samples over parental (Table 2). These include 1 site on GRA6, 5 sites on GRA7, and 1 site on GRA44. The phosphorylated states of GRA6 and GRA7 in cells infected with wild-type parasites are readily distinguishable by SDS-PAGE and western blot (Figure 7B, SI Appendix, Fig. S6B; (125,126)). To confirm the changes in phosphorylation of these proteins, we blotted lysates of cells infected with either the parental or *RHΔwng1* strains (Figure 7B). To demonstrate that these changes were due to the presence of WNG1, and to confirm the requirement of WNG1 kinase activity, we also assessed GRA6 and GRA7 phosphorylation in the wild-type and kinase-dead WNG1 complemented strains. The slower migrating, phosphorylated band of GRA6 was apparent in both parental and wild-type complemented lysates, but was undetectable in the knockout and kinase-dead complemented lysates (Figure 7B). Consistent with our phosphoproteomics data, we observed a reduction in, but not complete loss of, phosphorylated GRA7 in the knockout and kinase-dead complemented parasites versus wild-type. These residual phosphorylated species are presumably the novel phospho-states listed in Table 2 that must be due to the activity of an unknown, additional kinase. In support of the idea that WNG1 is acting directly on these potential substrates, recombinant WNG1 robustly phosphorylates bacterially-expressed GRA2, GRA6, and GRA7 *in vitro* (SI Appendix, Fig. S6C). Our data thus demonstrate that WNG1 is an active, PV-resident kinase required for the phosphorylation of luminal proteins associated with the PV and IVN membranes. Notably, each of the WNG1-dependent phosphosites we identified has been previously found exclusively in intracellular

parasites (Figure 7B; (123)), indicating that phosphorylation is occurring only after secretion of the proteins into the PV.

Given that these candidate WNG1 substrates have been demonstrated to either associate with or integrate into PV membranes (33,126–129,30), we asked whether WNG1 itself was membrane associated once secreted into the PV. To test this, we mechanically disrupted a human foreskin fibroblast (HFF) monolayer that had been highly infected with WNG1-3xHA parasites. Intact parasites were separated from host and PV membranes by a low speed (2500 g) spin, and the resulting supernatant was further separated by ultracentrifugation. WNG1, like the known integral membrane protein (and putative WNG1 substrate) GRA5, was found largely in the membrane-associated pellet (Figure 7C). In parallel, we partitioned an aliquot of the same low speed supernatant with Triton-X-114 (130). In this assay, WNG1 partitioned in the aqueous phase (Figure 7D), indicating that it is a soluble protein that is membrane-associated, rather than integrating into the membrane directly. Such a non-integral association of WNG1 with the PV membrane is consistent both with the lack of a predicted transmembrane, amphipathic helix, or other membrane association domain in the WNG1 sequence, and with our ability to purify soluble recombinant protein.

Efficient membrane association of proteins involved in intravacuolar network biogenesis depends on WNG1 kinase activity

The trafficking of IVN-associated proteins is highly unusual. Many GRA proteins integrate amphipathic or transmembrane helices into the IVN membrane, but remain soluble while trafficking through the parasite secretory system (126,127,30), presumably by complexing with an unidentified chaperone. Notably, many of the WNG1-dependent phosphorylation sites are located in, or adjacent to, predicted helical regions of sequence (SI Appendix, Fig. S7A) that have been shown to be required for GRA membrane association (53, 58). We therefore reasoned that phosphorylation of substrates by WNG1 may help regulate the switch from soluble to membranous states of PV GRA proteins. To test this hypothesis, we assessed WNG1

membrane association by comparing fractionated lysates from parental, $RH\Delta wng1$, and the kinase-active and kinase-dead complement strains. We prepared samples from 6 independent infections per condition, which were then separated by SDS-PAGE and analyzed by protein immunoblotting using antibodies recognizing various GRA proteins as indicated in Figure 8. We observed no difference in Triton-X-114 partitioning for any of the strains (SI Appendix, Fig. S7B). We quantified the relative soluble amounts of each protein (Figure 8B), which revealed a requirement for WNG1 kinase activity on IVN GRA membrane association. In particular, GRA4, GRA6, and GRA7 exhibited significant reductions in the fraction of protein that was PV membrane-associated in the $RH\Delta wng1$ and kinase-dead samples. Notably, the phosphorylated forms of GRA6 and GRA7 are found exclusively in the membrane-associated fractions (Figure 8A), and the loss of the slower migrating, phosphorylated states does not appear to result in a concomitant increase in the faster mobility (and presumably unphosphorylated) species at the membrane (SI Appendix, Fig. S7C). Taken together, our results suggest that WNG1-dependent phosphorylation of the GRA proteins promotes their association and is critical for the proper formation of the IVN.

Discussion

We have identified an unusual family of parasite-specific protein kinases that divergently evolved from a canonical protein kinase fold and have lost the typical Gly-rich loop. We have demonstrated that, in spite of missing a structural element thought to be critical to nucleotide binding and catalytic activity, at least one of the WNG kinases can catalyze phosphoryl transfer. Through structural and biochemical analyses, we have delineated subtle changes to the kinase active site that facilitate its catalytic activity. We went on to show that the most conserved member of the family, WNG1/ROP35, is secreted by *Toxoplasma* into the PV, where it associates with the PV membranes. We found that WNG1 kinase activity is required for the phosphorylation of many of the proteins known to be associated with the PV and IVN

membranes. Furthermore, loss of WNG1 kinase activity was correlated with a reduction in membrane association for a subset of the GRA proteins for which there are antibodies available. Finally, we found that parasite vacuoles deficient in catalytically active WNG1 have a substantial reduction in their IVN, suggesting that kinase activity is required for either the efficient formation or stability of the IVN membrane tubules.

The unusual WNG kinase fold raises the question: what may have been the evolutionary pressure that drove the divergence of the WNG family and loss of the Gly-loop? WNG1 is the most conserved member of the family, and appears to preferentially phosphorylate sites on proteins closely associated with the IVN membrane. Moreover, many of the sites we identified are at or near predicted helices (SI Appendix, Fig. S7A) that have been previously implicated in GRA protein interaction with membranes (127,128,131,132), or, in the case of GRA3, within a predicted coiled-coil. The rearrangement of the WNG active site has resulted in an unusually open active site (SI Appendix, Fig. S3B,C) that may better accommodate such folded or otherwise sterically restricted substrates. The atypical “alpha” family of kinases (59) are also able to phosphorylate helical substrates, such as the coiled-coil domains of myosin heavy chains (60). The alpha kinases share no detectable sequence homology to canonical protein kinases in spite of their similar overall folds (61, 62). The active sites of alpha kinases differ in several ways from canonical protein kinases. As with the WNG kinases, the alpha kinases have a more open active site that would accommodate a helical substrate (62). In any event, a comprehensive understanding of the mechanisms of substrate recognition in atypical kinases such as the WNG and alpha kinase families will require structural studies of kinase:substrate complexes.

Notably, the phosphosites we identified as WNG1-dependent are not detectable in extracellular parasites (Figure 7B, (26)), indicating that WNG1 phosphorylates its substrates in the PV lumen rather than while trafficking through the parasite secretory system. Our

phosphoproteomics data revealed both phosphosites are lost in WNG1 knockout parasites, as well as a smaller number of upregulated sites that were only detectable when WNG1 was missing. These data suggest that another kinase is capable of phosphorylating a subset of sites on the IVN GRA proteins, and its activity may be partially compensating for WNG1 loss. Alternatively, this other kinase activity may be acting in competition with that of WNG1. It is possible that these novel sites are phosphorylated by another member of the WNG family. However, we cannot rule out that WNG1 is acting indirectly on IVN GRA phosphorylation, *e.g.* by activating another PV-resident kinase. Regardless, the data we present here are consistent with a role for WNG1-dependent phosphorylation in the regulation of protein-protein and/or protein-membrane interactions of PV-resident proteins. Unfortunately, very little is known about the biochemistry of the GRA proteins secreted into the PV, making it difficult to assess the relevance of individual phosphorylation sites. Nevertheless, elucidating the regulatory functions of WNG-dependent phosphorylation represents a rich avenue of future study.

The multilamellar vesicles we observe in vacuoles deficient in WNG1 kinase activity are reminiscent of structures that have been previously observed during the first steps of IVN biogenesis (15). While bacterially-expressed GRA2 and GRA6, which we assume to be unphosphorylated, are sufficient to tubulate large unilamellar vesicles *in vitro* (20), it is possible that WNG1 kinase activity is required to ensure the efficiency of this process in cells. This may be explained by an apparent paradox that exists in GRA protein trafficking: GRA proteins that are destined to integrate into PV membranes traffic through the parasite secretory system as soluble entities (51–53), presumably in complex with an unknown solubilizing protein (Figure 9). Such a switch ensures that the parasite's intracellular and plasma membranes are protected from the tubulating activity of the GRA proteins. Removal of a solubilizing chaperone normally requires energy provided by ATP hydrolysis. There are no known chaperones secreted into the *Toxoplasma* PV. Consistent with a model in which WNG1 regulates membrane association of a

subset of PV GRAs, we observed that each GRA4, GRA6, and GRA7 were substantially more soluble in the vacuoles of parasites deficient in WNG1 kinase activity. There is thus an intriguing possibility that the ATP used during WNG-mediated phosphorylation is providing the energy to dissociate a chaperoning interaction and drive membrane insertion of a subset of GRA proteins (Figure 9). Such a non-canonical chaperoning mechanism is not without precedent. The mammalian neuropeptide 7B2 solubilizes the prohormone convertase 2 as it traffics to the Golgi (63), where 7B2 is phosphorylated by a resident kinase, resulting in release of the complex (64, 65).

In spite of decades of study, the *Toxoplasma* parasitophorous vacuole remains a mysterious organelle. The major function identified for IVN-associated proteins is in IVN biogenesis, as the deletion of either GRA2 or GRA6 results in a complete loss of the structure (47). Such IVN-deficient parasites have been used to link the IVN to nutrient uptake (17–19) and immune evasion (20, 22), though the precise mechanisms and roles of the IVN have not been established in these processes. Consistent with the pleiotropic effects of disrupting the IVN, knockout of IVN-associated proteins strongly attenuates parasite virulence (25, 66). Infection of mice with WNG1 knockout parasites yields a substantially reduced cyst burden (48), which is consistent with the role we observed for WNG1 in IVN biogenesis and/or stability and the likely resulting pleiotropic effects on the parasite's biology. Our discovery of potential regulatory phosphorylation may facilitate future work to associate specific GRA protein complexes with their biochemical functions and thus better delineate the roles of the IVN in parasite pathogenesis.

Future directions

Kinases are activated by a phosphorylation event that occurs on the activation loop. WNG1 does not have any phosphorylatable residues in the activation loop. This suggests that WNG1 has a unique activation mechanism. Our BPK1 structure lacks data about the activation

loop and thus our model of the WNG1 activation site is incomplete. Since the recombinantly purified protein is unstable and unsuitable for x-ray crystallography, more mutational analysis could yield more information. Using MS, we have now identified WNG1 phosphorylation sites. The analysis yielded 16 possible phosphorylation sites of which 6 were conserved. We then mutated these sites and compared their kinase activity to WT WNG1. We found that T486A has no activity against MBP suggesting that this residue is required for activity (Figure 12). S480A has very low activity while S325A and S349/50A also show a % and % decrease in activity. Some kinases have a conserved Arg that coordinates a phosphorylatable residue in activation loop. These residues are most likely interacting with positively charged Arg or Lys residues. Hence, we have now identified possible residues to mutate and test kinase activities. If when mutated individually they lead to the same drop in activity and when mutated together, the drop in activity is not the sum of the individual mutations, it would strongly suggest that they interact with each other.

We have shown that WNG1 alters GRA protein membrane association but we still need to confirm that this is actually due to the phosphorylation. Questions that need to be addressed include: what phosphosites on IVN GRAs mediate biochemical changes? Does phosphorylation alter membrane association or protein-protein interaction?. We now have the necessary parasite strains to test whether phosphorylation affects GRA2/3/6 membrane association, GRA2/4/6 complex and IVN formation.

How does WNG1 interact with membrane? Treating secreted WNG1 with a cross linker shows that it is a multimer but it is not a clear dimer or trimer. Suggesting that it is interacting at least with one other protein. Since, we have shown that WNG1 is not an integral membrane protein and is instead associating with the membrane, this complex maybe how WNG1 associates with the membrane. Thus we will use Mass spec to identify the interacting protein and test whether this is required for membrane association of WNG1.

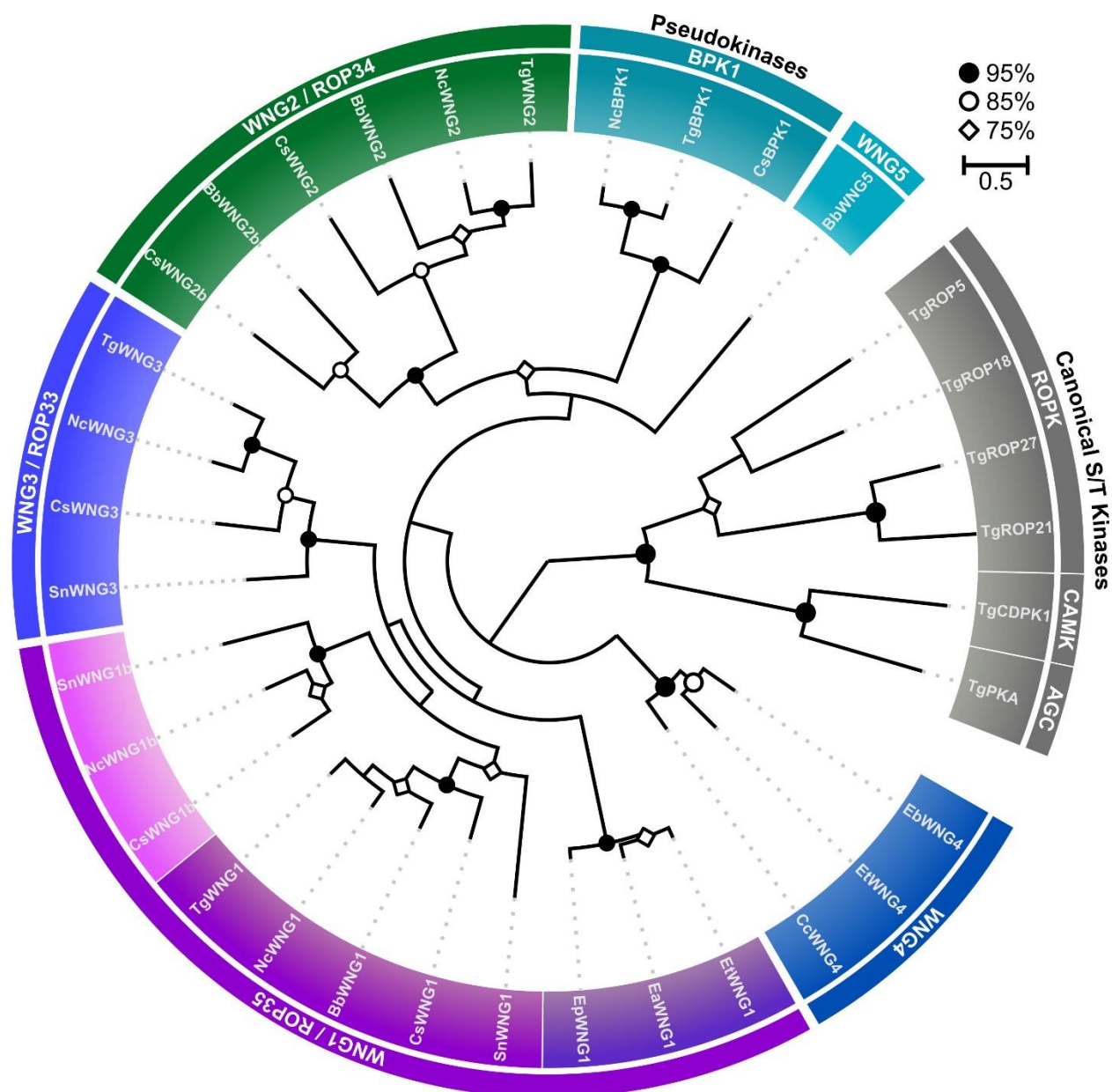


Figure 1 : The WNG kinases comprise a phylogenetic clade that is distinct from canonical protein kinases. A maximum-likelihood phylogenetic tree estimated from the multiple sequence alignment of the indicated kinases. Bootstrap values are indicated as black circles (>95%); white circles (>85%); and white diamonds (>75%). Species: Tg – *Toxoplasma gondii*; Nc – *Neospora caninum*; Bb – *Besnoitia besnoiti*; Sn – *Sarcocystis neurona*; Ea/Ep/Et – *Eimeria* spp.; Cs – *Cystoisospora suis*; Cc – *Cyclospora cayetanensis*

Supplemental Table S1C

Name	Organism	Subfamily	Gene Model/Accession	Alternative gene model
CsBPK1	<i>Cystoisospora suis</i>	BPK1	CSUI_010109	
HhBPK1	<i>Hammondia hammondi</i>	BPK1	HHA_253330	
NcBPK1	<i>Neospora caninum</i>	BPK1	NCLIV_007770	
TgBPK1	<i>Toxoplasma gondii</i>	BPK1	TGGT1_253330	
BbWNG1	<i>Besnoitia besnoiti</i>	WNG1	PFH36021.1	
CsWNG1	<i>Cystoisospora suis</i>	WNG1	CSUI_009154	
CsWNG1b	<i>Cystoisospora suis</i>	WNG1	CSUI_010099	
EaWNG1	<i>Eimeria acervulina</i>	WNG1	EAH_00045380	
EbWNG1	<i>Eimeria brunetti</i>	WNG1	EBH_0002260	
EpWNG1	<i>Eimeria praecox</i>	WNG1	EPH_0003380	
EtWNG1	<i>Eimeria tenella</i>	WNG1	ETH_00005905	
HhWNG1	<i>Hammondia hammondi</i>	WNG1	HHA_304740	
NcWNG1	<i>Neospora caninum</i>	WNG1	NCLIV_044410	
NcWNG1b	<i>Neospora caninum</i>	WNG1	NCLIV_029900	
SnWNG1	<i>Sarcocystic neurona</i>	WNG1	SN3_00501335	SRCN_2183
SnWNG1b	<i>Sarcocystic neurona</i>	WNG1	SRCN_2123	
TgWNG1	<i>Toxoplasma gondii</i>	WNG1	TGGT1_304740	
BbWNG2	<i>Besnoitia besnoiti</i>	WNG2	PFH32376.1	
BbWNG2b	<i>Besnoitia besnoiti</i>	WNG2	PFH32362.1	
CsWNG2	<i>Cystoisospora suis</i>	WNG2	CSUI_004303	

HhWNG2	<i>Hammondia hammondi</i>	WNG2	HHA_240090	
NcWNG2	<i>Neospora caninum</i>	WNG2	NCLIV_000650	
TgWNG2	<i>Toxoplasma gondii</i>	WNG2	TGGT1_240090	
CsWNG2b	<i>Cystoisospora suis</i>	WNG2b	CSUI_008294	
CsWNG3	<i>Cystoisospora suis</i>	WNG3	CSUI_002921	
HhWNG3	<i>Hammondia hammondi</i>	WNG3	HHA_201130	
NcWNG3	<i>Neospora caninum</i>	WNG3	NCLIV_023260	
SnWNG3	<i>Sarcocystic neurona</i>	WNG3	SRCN_4310	SRCN_7082
TgWNG3	<i>Toxoplasma gondii</i>	WNG3	TGGT1_201130	
CcWNG4	<i>Cyclospora cayetanensis</i>	WNG4	cyc_03158	
EaWNG4	<i>Eimeria acervulina</i>	WNG4	EAH_00050320	
EbWNG4	<i>Eimeria brunetti</i>	WNG4	EBH_0025260	
EtWNG4	<i>Eimeria tenella</i>	WNG4	ETH_00026495	
BbWNG5	<i>Besnoitia besnoiti</i>	WNG5	PFH31612.1	

Table S1C: Gene models (for sequences in ToxoDB) or NCBI accession numbers of sequences used in this study.

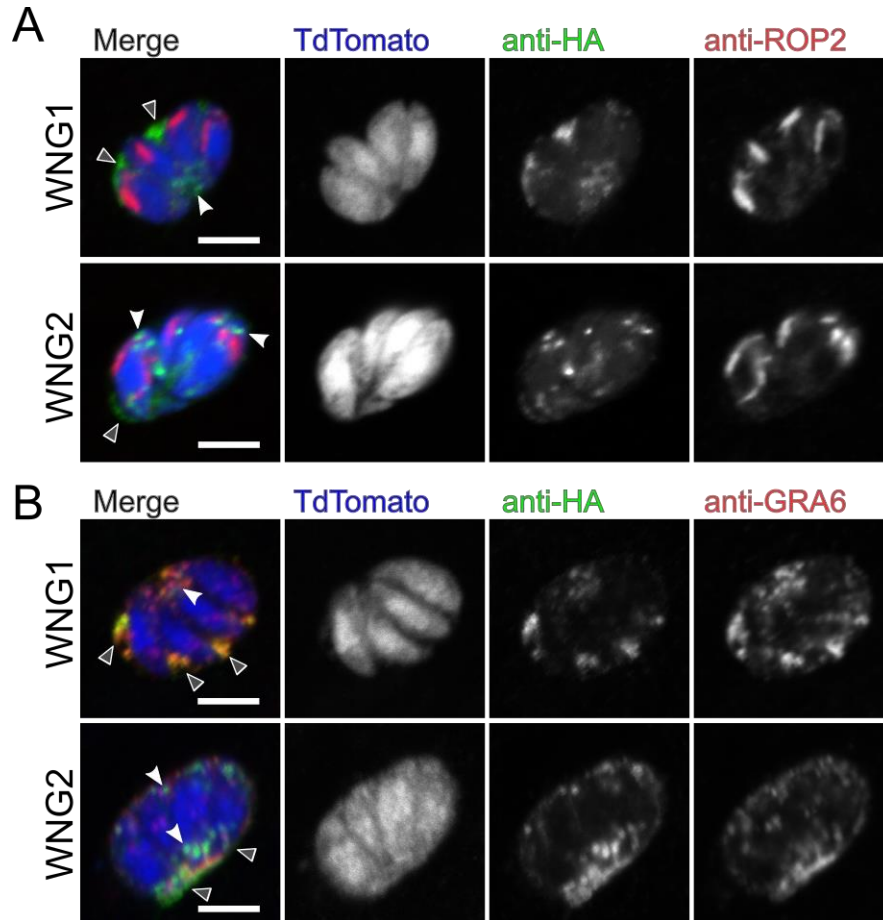


Figure 2 : WNG kinases are secreted into the PV lumen from the dense granules. 0.5 μm confocal slices of WNG1-3xHA or WNG2-3xHA infected cells transiently transfected with TdTomato (blue) and stained with anti-HA (green) and either (A) the rhoptry marker anti-ROP2 (red) or (B) the dense granular/IVN marker anti-GRA6 (red). White arrowheads indicate intracellular signal; Gray arrowheads indicate secreted, PV-localized signal. Scale bars: 5 μm .

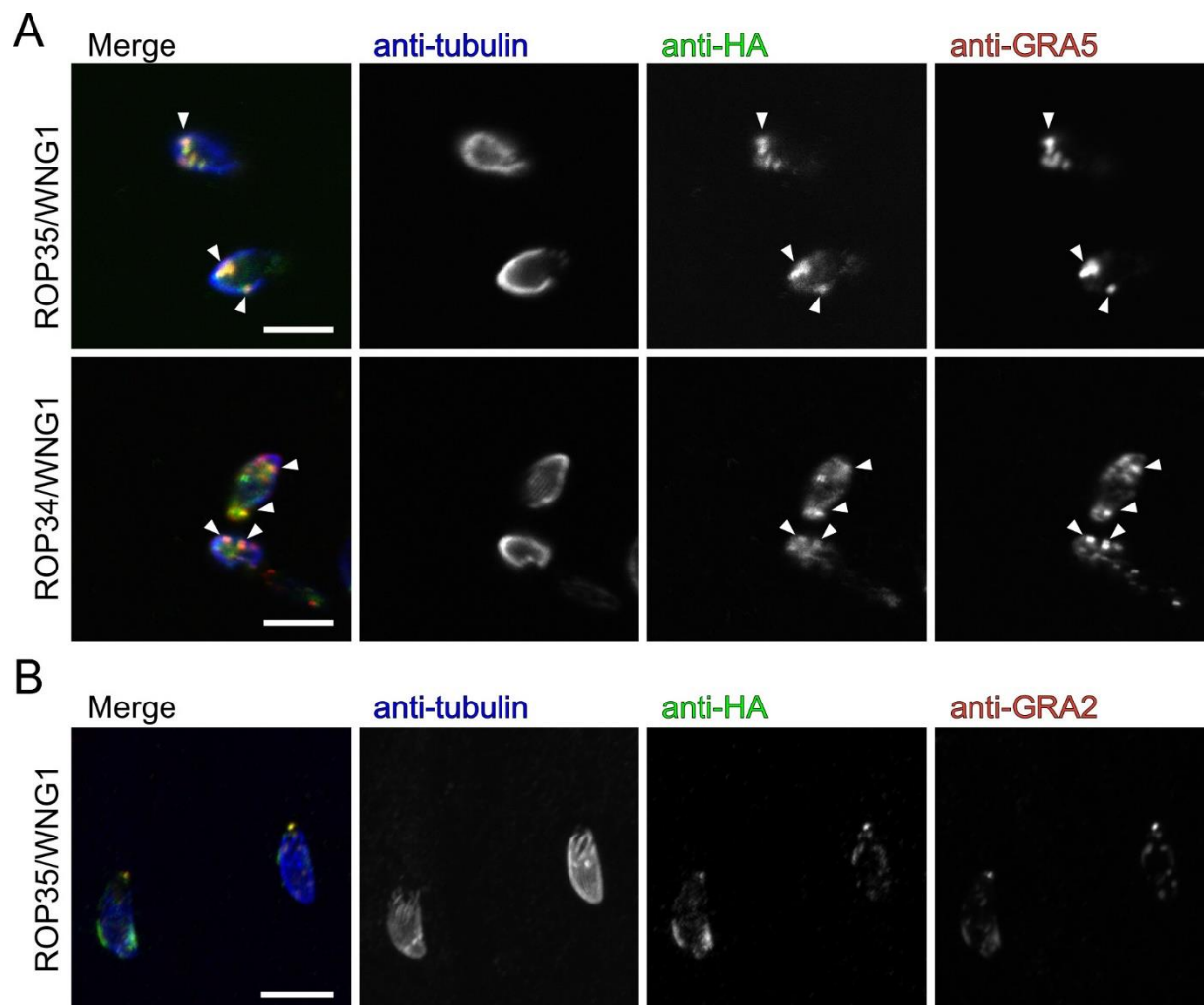


Figure S2: WNG kinases localize to the dense granules. (A) 0.5 μm confocal slices of ROP35/WNG1-3xHA or ROP34/WNG2-3xHA extracellular parasites stained with anti- β -tubulin (blue), anti-HA (green), and the dense granular marker GRA5 (red). Arrowheads indicate punctate co-localization of the HA and GRA5 signal. (B) ROP35/WNG1-3xHA (green) co-localizes with GRA2 (red) in a newly formed parasitophorous vacuoles within 10 minutes after infection. Scale bars: 10 μm .

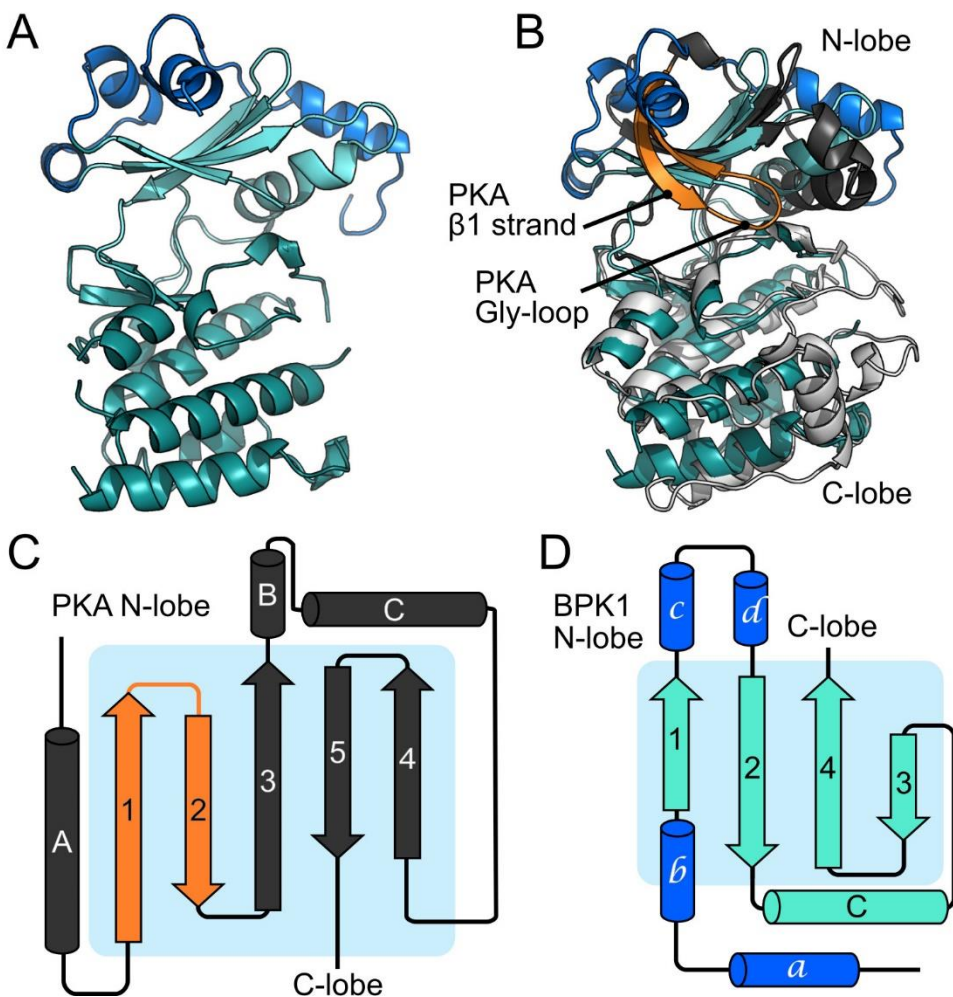


Figure 3: The structure of TgBPK1 reveals an atypical kinase fold lacking the Gly-loop. (A) Stereo view of the TgBPK1 structure. The N-lobe is in cyan, C-lobe colored in teal, and the helical "lid" that is unique to the WNG family is colored blue. (B) Superposition of the TgBPK1 structure with that of PKA (1ATP). TgBPK1 is colored as in (A). The N-lobe of PKA is dark gray, C-lobe is light gray, and β -strands that sandwich the Gly-loop are orange. Cartoon highlighting the differences between the N-lobes of (C) PKA and (D) TgBPK1, colored as in (B). Note the difference in the order of the N-lobe β -strands in PKA versus TgBPK1.

Supplemental Figure S3

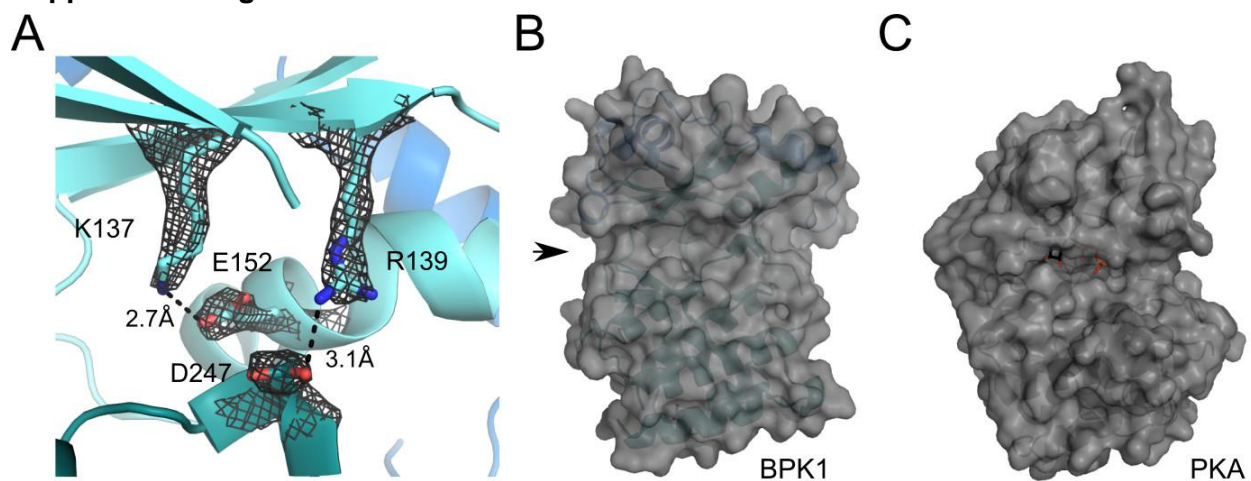


Figure S3: BPK1 has a divergent, open active site. (A) BPK1 active site superposed with the $2F_o - F_c$ electron density map contoured at 2σ . Two salt bridges are highlighted as sticks: the conserved bridge between the αC E152 and the VAIK K137 as well as an unusual, WNG family-specific salt bridge between R139 and D247 (an acidic substitution at the DFG Gly position). The lack of Gly-loop creates an open active site in BPK1, indicated with an arrow in (B). This is compared to the more restricted active site in canonical kinases such as PKA, shown in (C). Note that the two kinases are shown in equivalent orientations.

Supplemental Table S2: Crystallographic Data and Refinement

	TgBPK1 (native)	TgBPK1 (Pt)		
Data collection				
Space group	P2 ₁ 2 ₁ 2	P2 ₁ 2 ₁ 2		
Cell dimensions ^{□□}				
<i>a</i> , <i>b</i> , <i>c</i> (Å)	171.47, 123.07, 86.62	184.77, 120.98, 92.36		
α , β , γ (°)	90, 90, 90	90, 90, 90		
Wavelength (Å)	1.038	Peak 1.07195	Inflection 1.07229	Remote 1.076276
Resolution (Å)	47.7 – 2.50 (2.59 – 2.50)	50.0 – 3.75 (3.81 – 3.75)	50.0 – 3.73 (3.79 – 3.73)	50.0 – 3.92 (3.92 – 3.92)
Total reflections	512518	130864	110497	105514
<i>R</i> _{merge}	9.1 (86.3)	8.3 (1.0)	7.4 (88.2)	8.6 (96.6)
CC _{1/2} (final shell)	0.76	0.63	0.70	0.75
<i>I</i> / <i>I</i> [□]	23.8 (2.0)	25.2 (1.8)	25.3 (2.0)	24.4 (2.2)
†Completeness (%)	90.9 (63.5)	90.3 (61.1)	87.2 (63)	89.8 (60.2)
Redundancy	8.0 (7.3)	6.0 (6.1)	5.0 (5.1)	6.0 (5.9)
Refinement				
No. reflections	58472 (4024)			
<i>R</i> _{free} reflections	2987 (203)			
<i>R</i> _{work} / <i>R</i> _{free}	0.197 / 0.238 (0.238 / 0.289)			
No. atoms				
Protein	12422			
Ligand/ion	64 (EDO), 3 (CL)			
Water	381			
<i>B</i> -factors				
Protein	45.58			
Ligand/ion	47.55			
Water	33.12			
R.m.s. deviations				
Bond lengths (Å)	0.010			
Bond angles (°)	1.37			
Ramachandran (favored/disallowed)	98.48 / 0			
Molprobit score	1.14			
Molprobit clash score	3.48			
No. TLS groups	20 per chain			

†Diffraction was anisotropic, which reduced the completeness, especially in highest resolution shell; for instance, for the native dataset diffraction was measured to 2.2 Å in the strongest dimension and 2.8 Å in the weakest.

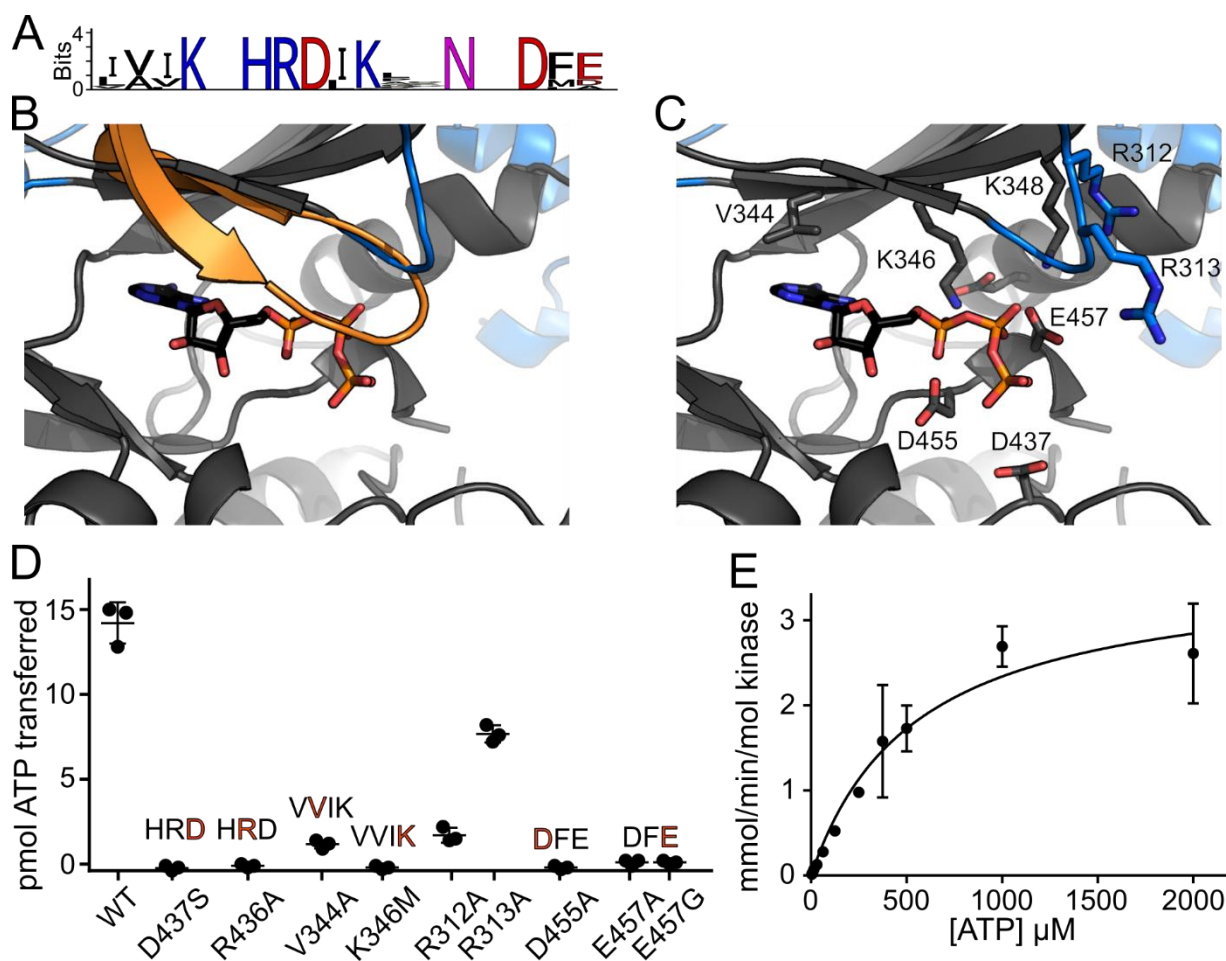


Figure 4: WNG1 has adapted its active site to catalyze phosphoryl transfer without a Gly-loop. (A) Sequence logos of the WNG kinase VAIK, HRD, and DFE motifs indicate conservation of critical catalytic residues. (B) A homology model of the WNG1 structure based on the BPK1 crystal structure, (gray and blue) has been superimposed with the structure of PKA (1.96Å backbone rmsd; 529 atoms compared). For clarity, only the PKA Gly-loop (orange) and bound nucleotide are shown. (C) A model of the WNG1 active site structure, colored as in (B). Bound ATP has been modeled based on superposition of the PKA structure. Residues that comprise either canonical motifs or WNG-specific substitutions are annotated and shown as sticks. (D) Kinase activities of wild-type WNG1 and the indicated mutant proteins using MBP as a protein substrate, quantified by 32 P scintillation. Motifs altered by the mutants are shown above the data points. (E) A representative Michaelis-Menten fit of *in vitro* kinase assays of WNG1 using MBP as a substrate while varying ATP concentration.

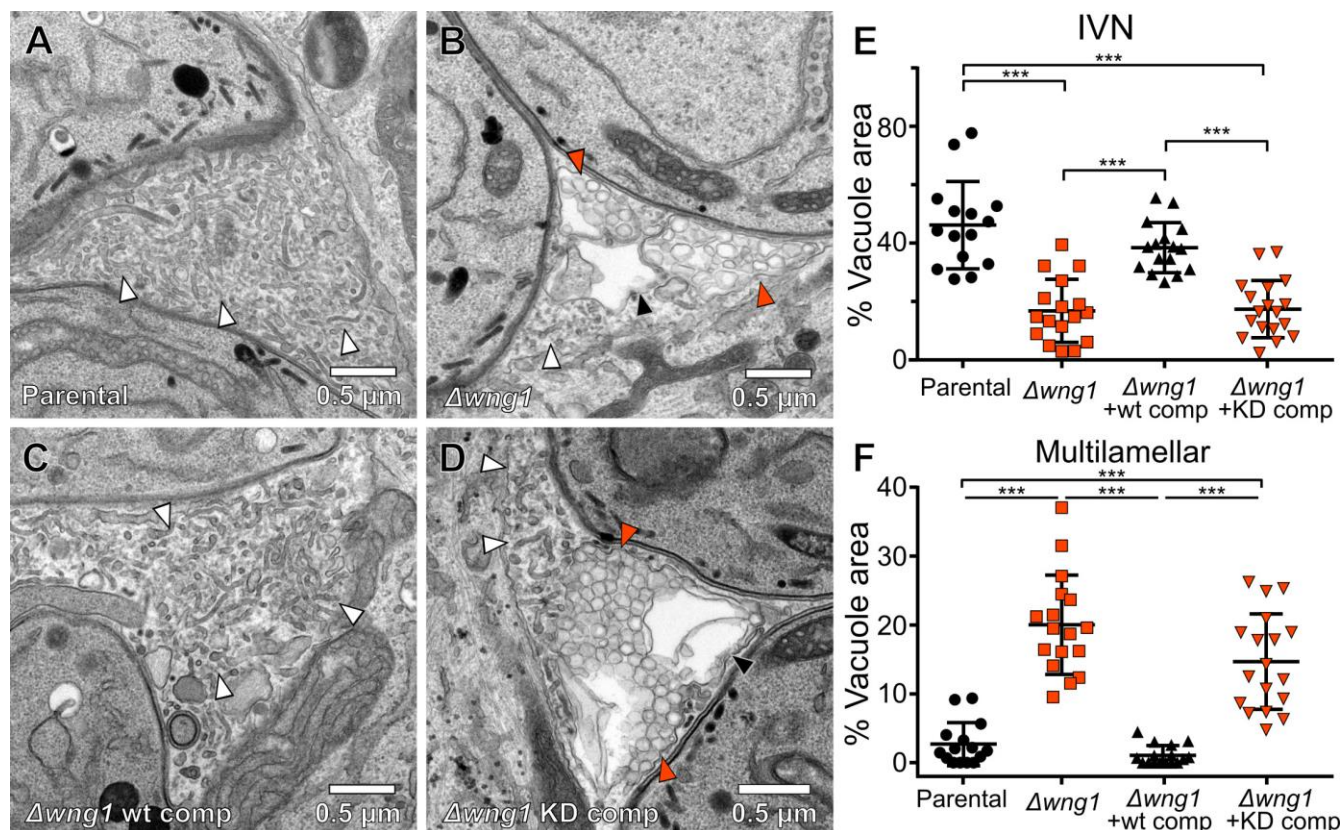


Figure 5: Vacuoles lacking active WNG1 kinase show disrupted IVN membranes. Representative transmission electron microscopic images of the (A) Parental, (B) $RH\Delta wng1$, (C) $RH\Delta wng1$ complemented with wild-type WNG1, and (D) kinase-dead complemented strains. IVN tubules are indicated with white arrowheads. Multilamellar vesicles are indicated with solid orange arrowheads. Multilamellar structures in which internal vesicles appear to have been lost during fixation are indicated with a black arrowhead in (B) and (D). The relative area of each IVN tubules and multilamellar vacuole from EM images as in (A-D) were quantified in ImageJ. Significance was calculated in Prism by ANOVA; $p < 0.0001$ (****); $p < 0.001$ (***); $p < 0.01$ (**); $p < 0.05$ (*).

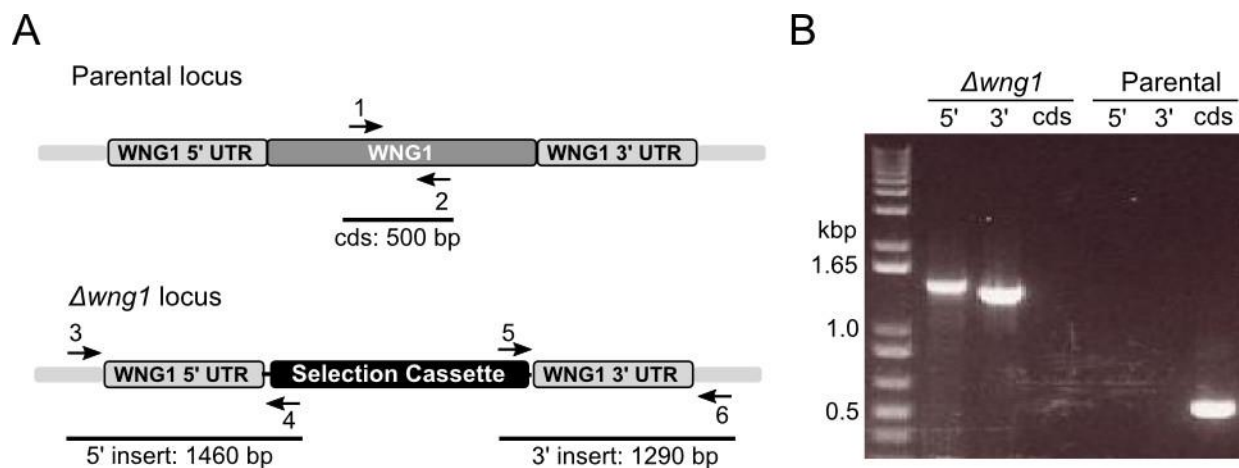


Figure S5a: Generation of WNG1 knockout parasites. RH $\Delta wng1$ parasites were generated by double homologous recombination in which the WNG1 genomic sequence was replaced by a HXGPRT selection cassette. (A) Cartoon of parental and knockout loci indicating binding sites for primers used to verify knockout. (B) PCR demonstrating insertion of selection cassette and loss of coding sequence (cds) in knockout parasites. Primers sequences are listed in Supplemental Table S10.

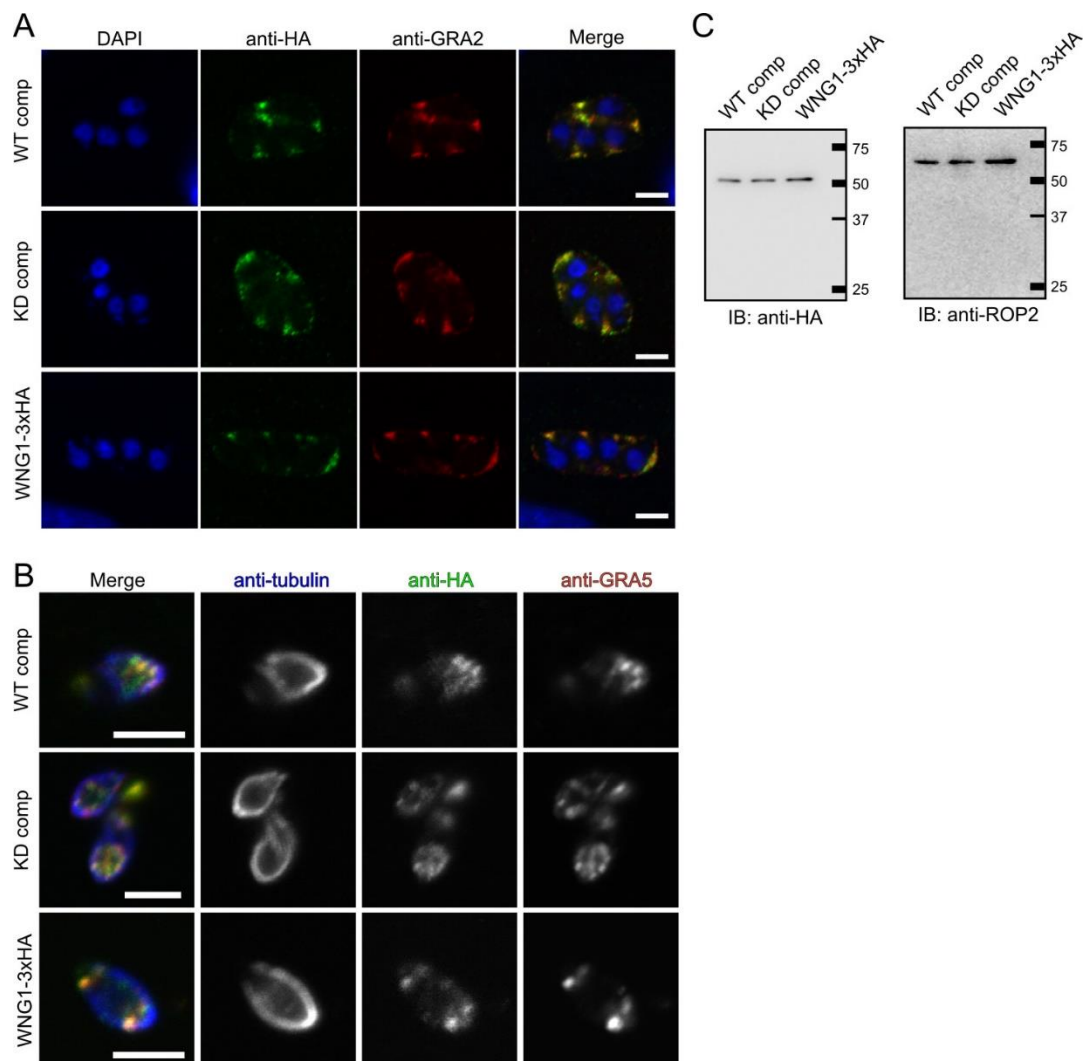


Figure S5b: WNG1 complements faithfully localize to dense granules and PV. (A) 0.5 μm confocal slices of the wild-type (WT) and kinase-dead (KD) WNG1 complemented parasites as well as the endogenously tagged WNG1-3xHA were stained with DAPI (blue), anti-HA (green), and the dense granule and IVN marker GRA2 (red). (B) 0.5 μm confocal slices of the indicated extracellular parasites stained with anti-tubulin (blue), anti-HA (green), and anti-GRA5 (red). (C) Both the WT and KD WNG1-complements are expressed at similar levels to the endogenously 3xHA tagged protein, as demonstrated by western blot, using ROP2 as a loading control.

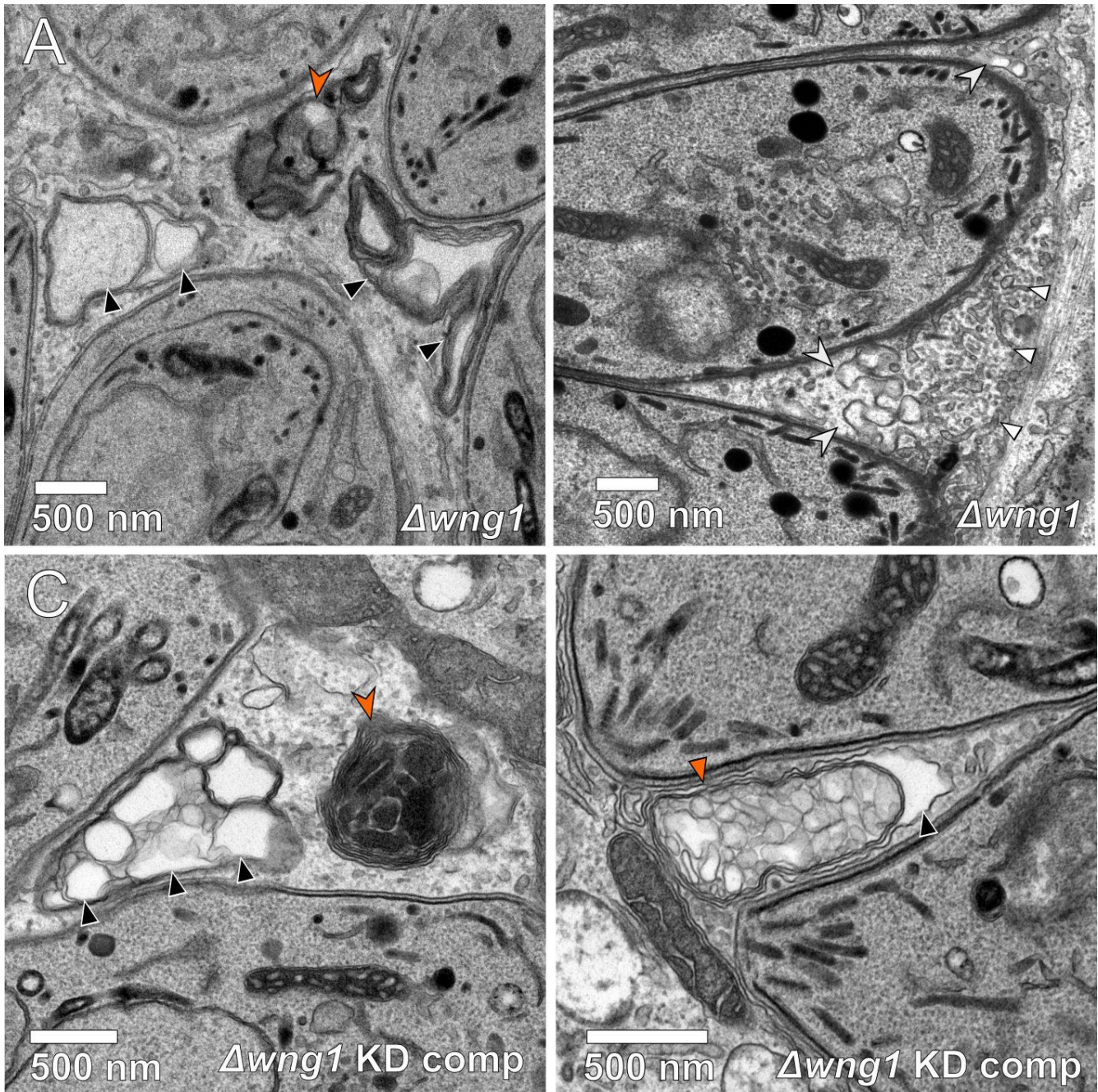


Figure S5c : Unusual membrane structures in vacuoles lacking active WNG1 kinase. Representative transmission electron microscopic images of (A,B) RH $\Delta wng1$ and (C,D) RH $\Delta wng1$ complemented with kinase-dead WNG1. IVN tubules are indicated with small white triangles. Multilamellar vesicles are indicated with small solid orange triangles. Multilamellar structures in which internal vesicles appear to have been lost during fixation or to have collapsed into sheets are indicated with black triangles. Electron dense multilamellar structures are indicated with a large orange arrowheads in (A) and (C). Membrane “whirls” that appear connected with IVN tubules are indicated with large white arrowheads in (B).

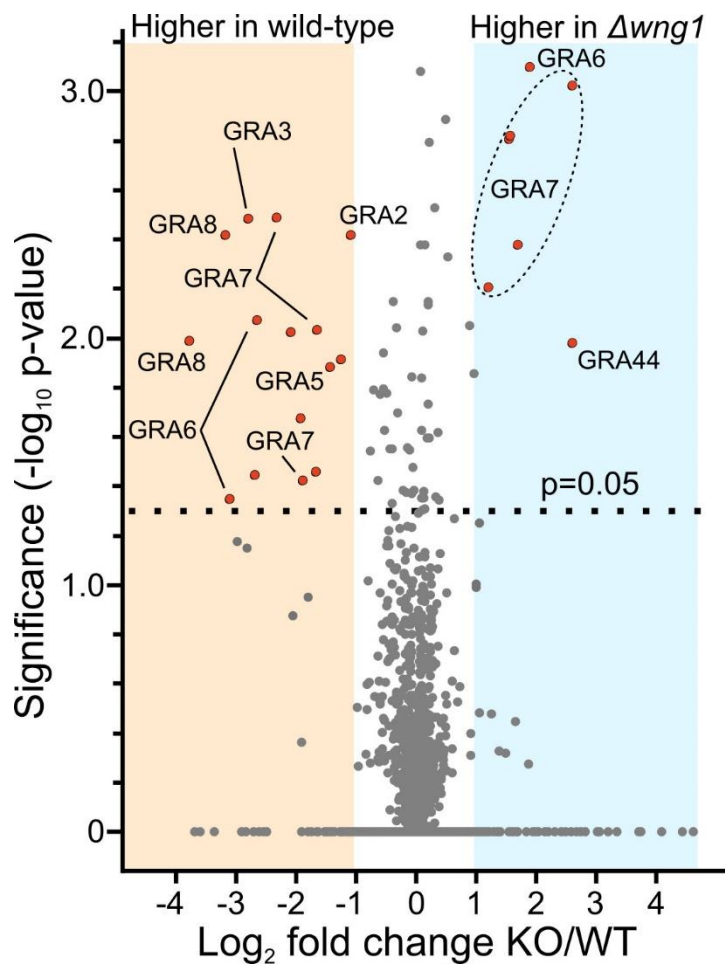


Figure 6: Overview of quantitative phosphoproteomics data. SILAC quantification of change in phosphosite abundance plotted against significance of change for 2296 phosphosites in $RH\Delta wng1$ versus parental parasites. See Supplementary Table 5 for full data set. Significantly changing phosphosites (p -value < 0.05 and $-1 > \log_2$ change > 1) enriched in dense granule proteins are highlighted in red.

Table 1.

Gene Model	Name	Site	Context	Localization
TGGT1_227620	GRA2	T56	G K G E H T P P L P D	IVN membrane (51)
		S72	P E E P V S Q R A S R	
TGGT1_203310	GRA3	S120	V E E E L S LL R R E	PV/IVN membrane (54)
TGGT1_286450	GRA5	S108*	E E S K E S A T A E E	PV membrane (50)
		T110	S K E S A T A E E E E	
TGGT1_286450	GRA6	S112	A N E G K S E A R G P	IVN membrane (56)
		S118	E A R G P S L E E R I	
		T128*	I E E Q G T R R R Y S	
TGGT1_203310	GRA7	S41	S R I R N S D F F D G	PV/IVN membrane (52)
		S77	S M D K A S V E S Q L	
		S227	Q E V P E S G E D G E	
TGGT1_254720	GRA8	S198	P R M G P S D I S T H	PV membrane (53)
		S201	G P S D I S T H V R G	
		T202	P S D I S T H V R G A	
TGGT1_226380	GRA35	S85*	R Y G E A S V D D T Q	PV/IVN (48)
TGGT1_236890	GRA37	S72	T V R K Q S N D A D G	PV/IVN (48)
TGGT1_254000	GRA45	S420*	D A K E R S H A S E D	PV (this study)
		S423	E R S H A S E D E D D	
TGGT1_267740	GRA46	S186**	E A E L I S L S P G G	PV (this study)

* Not significant in t-test due to variability between replicates ($p > 0.05$) or quantified in only one

type of labeling (Rv samples only)

** Identified in preliminary dataset, not statistically significant in final data

Table 1: Phosphosites downregulated in RHΔwng1 vacuoles. The sequence context of each of the phosphosites is indicated. Acidic residues are red, basic residues are blue. Note that some regions appear to be hyperphosphorylated in a WNG1-dependent manner. Such potential priming sites are indicated bolded with a gray background in the phosphosite context.

Table 2

Gene Model	Name	Site	Context
TGGT1_286450	GRA6	S133	T RRRY S SVQ E P
TGGT1_203310	GRA7	T70*	T DD H L T T S M D K
		S80*	K AS V E S QL P RR
		T90	R E P L E T E P D E Q
		T112	S D A E V T D D N I Y
		T121	I Y E E H T D R K V V
TGGT1_244530	GRA44	S548	Q A K S L S V D N T P

* Not significant in t-test due to variability between replicates ($p > 0.05$) or quantified in only one

type of labeling (Rv samples only)

Table 2: Phosphosites upregulated in WNG1-deficient vacuoles. Table is formatted as in Table 1.

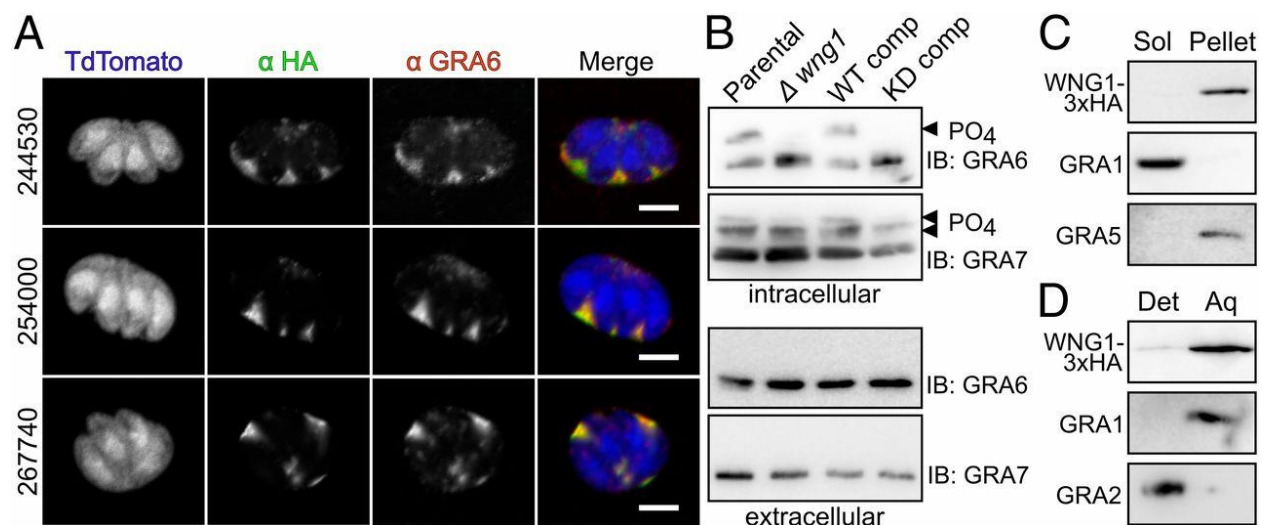


Figure 7: WNG1 and its substrates are membrane associated. (A) 0.5 μm confocal slices of cells infected with parasites in which the indicated unannotated candidate substrates are endogenously 3xHA tagged (anti-HA; green), transiently transfected with TdTomato (blue), and co-stained with the dense granular and IVN marker GRA6 (red). Scale bars 5 μm . (B) Western blot of lysates of cells infected with the indicated wild-type, knockout, or complement strains probed with anti-GRA6 and anti-GRA7 antisera. Phosphorylated bands are indicated with arrowheads. (C) Western blot of host and PV membranes that have been ultracentrifuged. WNG1-3xHA is detected with anti-HA, GRA1 and GRA2 are used as soluble and membrane-associated controls, respectively. (D) Western blot of host and PV membranes that have been subjected to Triton-X-114 partitioning between detergent (Det) and aqueous (Aq) phases.

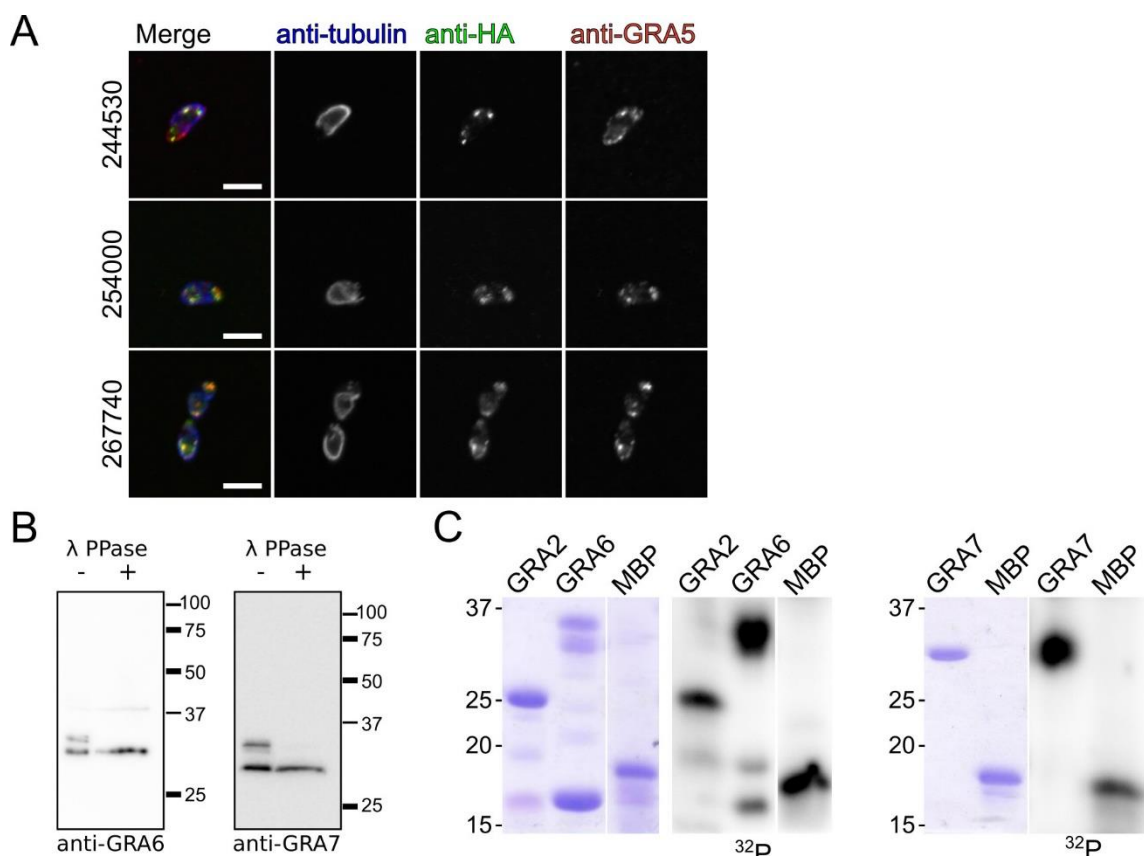


Figure S6: WNG1 substrates are dense granular proteins. (A) 0.5 μm confocal slices of extracellular parasites with the indicated candidate WNG1 substrate endogenously tagged with 2xHA and stained with anti-HA (green), anti β -tubulin (blue), and anti-GRA5 (red). (B) The slower migrating GRA6 and GRA7 bands correspond to phosphorylated species. Lysate from cells infected with parasites with a wild-type WNG1 locus were either treated with λ -phosphatase (+) for 30 minutes at 30°C or left untreated (-) and western blotted with the indicated antibody. (C) Bacterially expressed His₆-tagged GRA2, GRA6, and GRA7 were purified on NiNTA resin and used as substrates for a WNG1 kinase assay with γ [³²P]-ATP and visualized by autoradiogram. 4 μg MBP was used as a positive control. Coomassie stained

gels indicate relative protein amounts used in the assay.

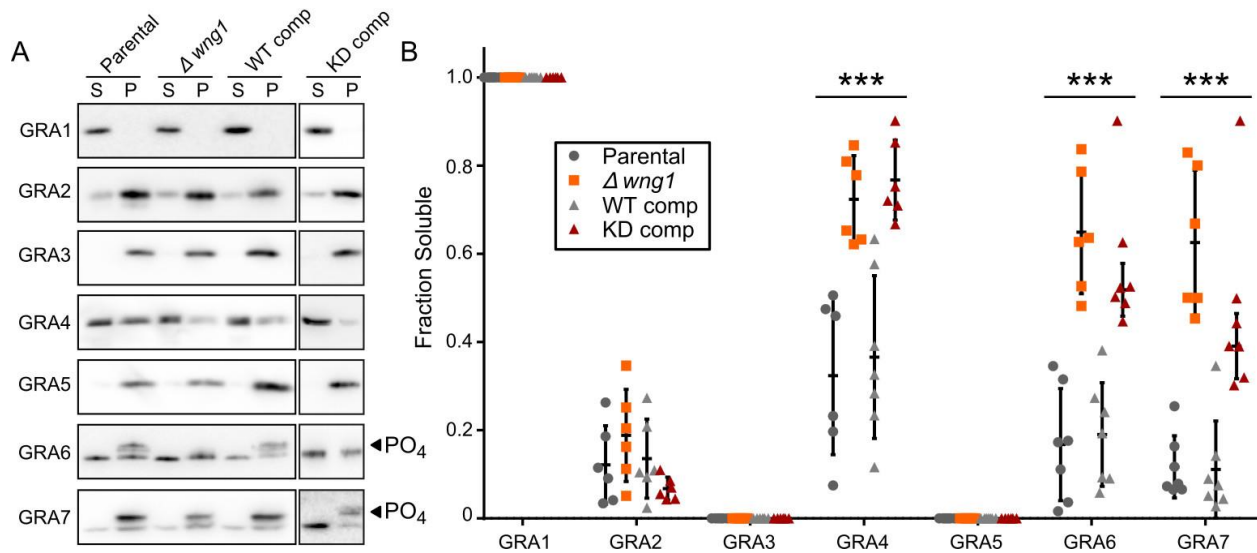


Figure 8: Membrane association of GRA proteins correlates with WNG1 kinase activity. (A) Representative western blot of samples in which host and PV membranes were ultracentrifuged and the soluble (S) and pellet (P) fractions were separated by SDS-PAGE and probed with the indicated antisera. Phosphorylated bands are indicated with arrowheads. (B) Quantification of $n=6$ biological replicates as in (A). Significance was calculated by ANOVA in Prism; $p < 0.001$ (***).

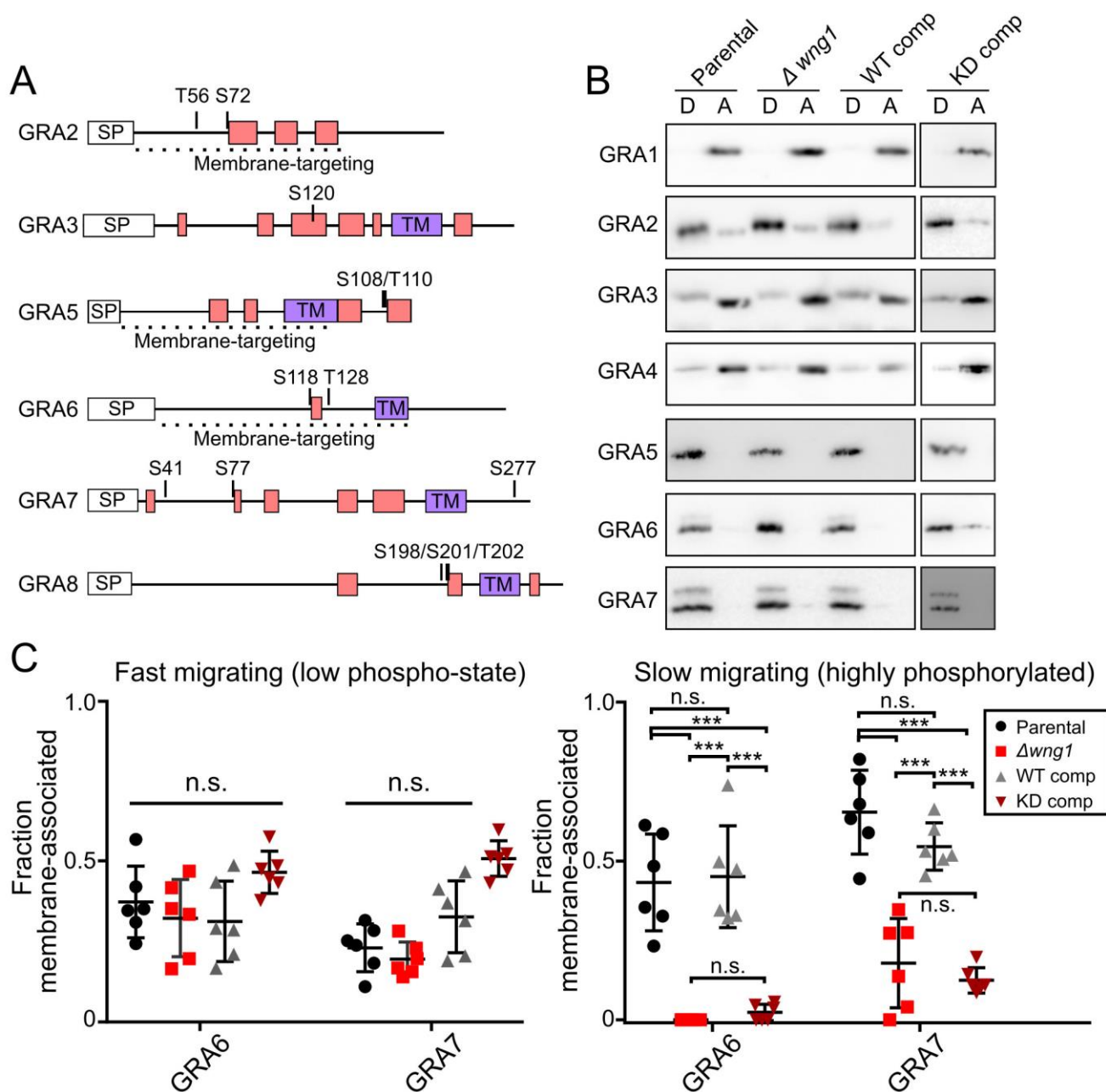


Figure S7: WNG1 activity does not affect TX-114 partitioning of IVN GRA proteins. (A) WNG1-dependent phosphosites are mapped onto the predicted secondary structures of the indicated GRA proteins. Predicted α -helices are shown as rectangles. Predicted transmembrane helices

(TM) are shaded purple. (B) Host and PV membranes from cells infected with the indicated strains were partitioned in TX-114 and the detergent [D] and aqueous [A] phases were separated by SDS-PAGE and analyzed by western blot probed with antibodies to the indicated GRA proteins. We note that GRA2 and GRA3 appear to exhibit a slightly slower electrophoretic mobility in the detergent-phase samples. While detergent concentrations were normalized between samples, this may be due to an artifact of the proteins' behavior in the SDS-PAGE. (C) Data from Figure 8 were requantified to compare the fractional membrane-association of the faster migrating, unphosphorylated species (left panel) with the the slower migrating, highly phosphorylated species (right panel) of GRA6 and GRA7 in vacuoles of the parental, knockout, and complement strains. Significance was analyzed by 2-way ANOVA with Tukey's test (***, $p < 0.001$; n.s., not significant). Note that while the difference between the fast migrating GRA7 band from kinase-dead WNG1 complemented vacuoles appears to be borderline significant ($p \sim 0.05$) when compared to the other samples; it is unlikely to be biologically relevant.

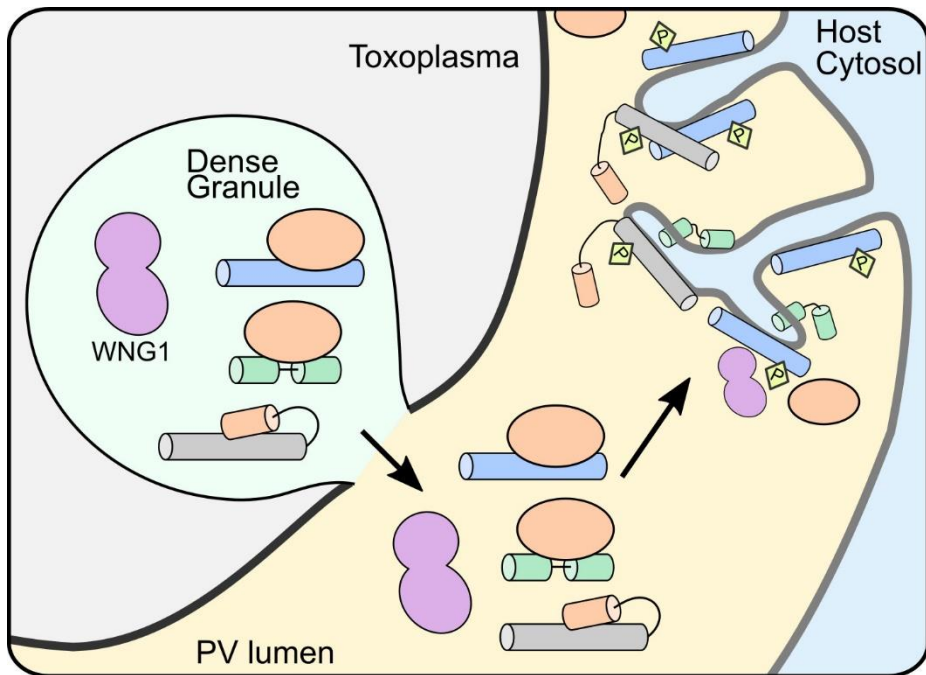


Figure 9: Model for WNG1 regulation of IVN GRA protein membrane association. Within the parasite secretory pathway, membrane-seeking GRA proteins (blue, green, and gray cylinders) are complexed with solubilizing proteins or domains (orange). Once secreted into the PV lumen, WNG1 is activated through an unknown mechanism and phosphorylates the GRAs, leading to their eventual insertion into the PV membrane and efficient stabilization of the IVN tubules.

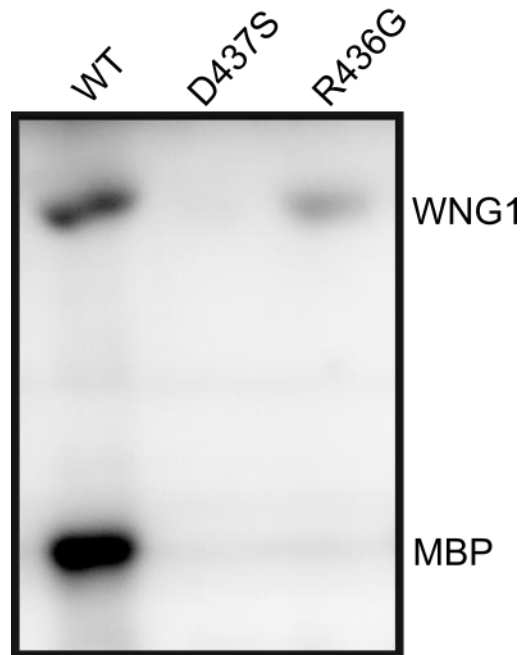


Figure 10: The HRD R is required for WNG1 substrate phosphorylation. Autoradiogram of kinase activities of wild-type WNG1 and the indicated mutant proteins using MBP as a protein substrate, and ^{32}P scintillation.

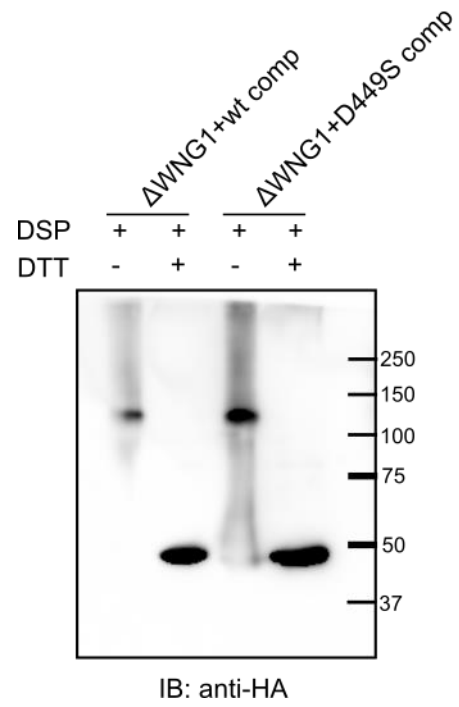


Figure 11: WNG1 forms a multimer. Western blot of lysates of cells infected with the 3xHA tagged wild-type or D449S complement strains probed with anti-HA.

Site	Context	Conservation
S325	RVPHV S EALAD	Yes; except Et/Ea=D
S349,S350	VIKVK SS TDAEA	Yes; except Sn=AF
S480	FAPEL S RATDH	Yes; except Sn=R
T486	RATDH T EKSDV	Tg/Nc/Sn=Yes; Ea/Et=R= Gln
T534	PEERP T LKQVM	Tg/Nc/Sn=Yes; Ea/Et=R

Table 3: Phosphosites downregulated in recombinant WNG1 D449S. The sequence context of each of the phosphosites is indicated. Acidic residues are red, basic residues are blue.

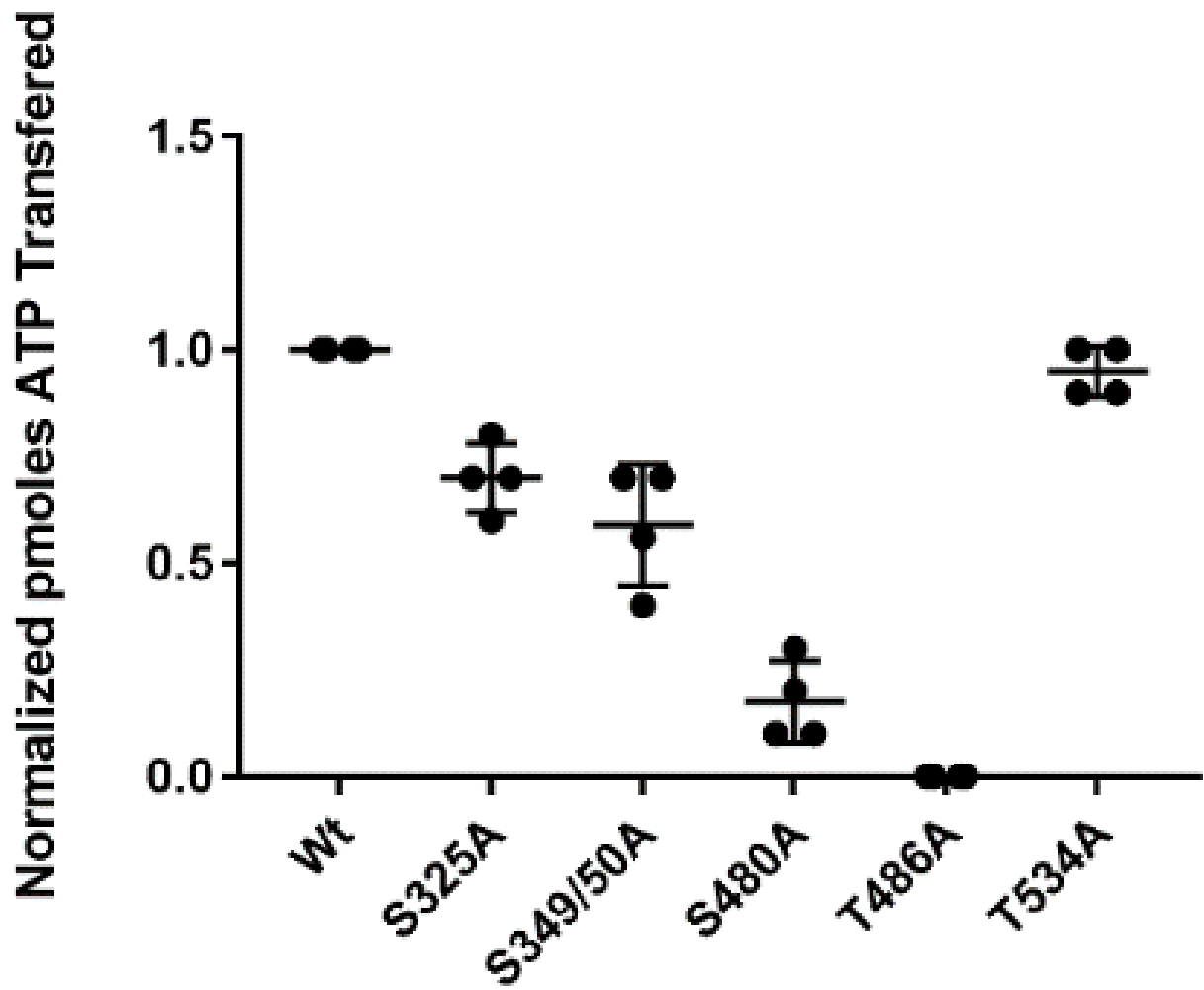


Figure 12: WNG1 autophosphorylation is required for activity. Kinase activities of wild-type WNG1 and the indicated mutant proteins using MBP as a protein substrate, quantified by ^{32}P scintillation.

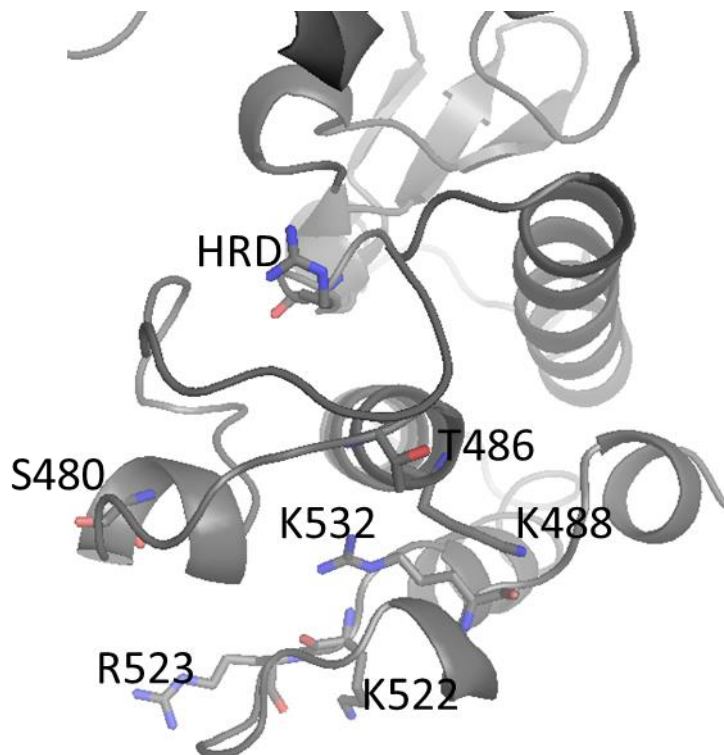


Figure 13: WNG1 autophosphorylation is required for activity. A homology model of the WNG1 structure based on the BPK1 crystal structure with the autophosphorylation sites indicated. The K and R residues that are in close proximity with these sites are also shown.

Chapter 3: WNG2 and WNG3

Materials and Methods

PCR and plasmid generation – Same as per methods in chapter 2

Parasite culture and transfection – Same as per methods in chapter 2

Immunofluorescence – Same as per methods in chapter 2

In vitro kinase assays – Same as per methods in chapter 2. Except recombinant WNG2 and GRAs were used.

Protein purification – Same as per methods in chapter 2

Transmission electron microscopy – Same as per methods in chapter 2

Work on WNG2 and WNG3

In order to identify potential functions for WNG2 and WNG3 we created KO parasites. We used double homologous recombination to knock out the WNG2 and WNG3 locus in the *RH Δ ku80 Δ hxgprt* background (Figure 3.1 and 3.2). The resulting *RH Δ wng2* and *RH Δ wng3* parasites showed no obvious growth phenotype in normal culture conditions. Next, we sought to examine the ultrastructure within the vacuoles of parasites with and without active WNG2 and WNG3, using transmission electron microscopy (TEM). We compared the vacuoles of HFFs that had been infected for 24 hours with either parental or WNG KO.

There was no obvious phenotype in the *Δ wng2* parasites. We have only done EM on these parasites, once and have yet to do EM on the wild-type and kinase dead complements. There was also an issue with the sample preparation where there was potential loss of parasite structure resulting in areas that had holes (not surrounded by membrane unlike in the WNG1 IVN phenotype). Hence, more EM data will be needed to conclusively show a phenotype for WNG2. Preliminary quantitative phosphoproteomics data have yielded potential WNG2 substrates. Five sites in three different proteins were downregulated in the *Δ wng2* vacuole (Table.4). These potential substrates have not been characterized which will make it harder to determine the function of WNG2. Interestingly, recombinantly expressed WNG2 is actually active and can phosphorylate MBP as well as IVN GRAs (Figure 3.3). This suggests that there might be some redundancy in the WNG kinase family.

A group looking to identify effector proteins that are processed by ASP5 showed that WNG2 is processed by ASP5. Potential ASP5 clients were identified using quantitative proteomics approaches such as SILAC, heavy dimethyl labeling, and label-free quantitation coupled with Terminal Amine Isotopic Labeling of Substrates (TAILS) and Hydrophobic Tagging-Assisted N-Terminal Enrichment (HYTANE) to enrich N-terminally derived peptides. ASP5 cleavage of WNG2 was then confirmed by inserting an HA tag into the endogenous locus

just before the stop codon in WT, $\Delta asp5$, RRL mutant parasites and blotting for anti-HA. This showed that the WNG2, with an expected MW of 62 KDa, runs at 55kDa in the WT while it runs at 60 KDa, in the $\Delta asp5$, RRL mutant parasites. These data have also been confirmed by our lab.

We have not been able to endogenously tag WNG3 at the C-terminus but our overexpression localization data suggest that it is localized within the parasite and in particular to the parasite plasma membrane (Figure 3.4). Yet, while WNG3 does have a signal peptide which should allow it to be secreted it does not have any predicted transmembrane domain. It is possible that the overexpression may have caused a change in localization though, hence we will have to either successfully endogenously tag it or raise an antibody to the protein. Multiple constructs have also failed to yield recombinant protein.

While most animals, plants and bacteria replicate by binary fission, *Toxoplasma* replicates by assembling two daughter cells within the mother cell per mitotic cell cycle (2). This method of replication is called endodyogeny. Endopolygeny, one parasite giving rise to more than two daughter cells, is observed at a frequency of 0.6% (33). In the $\Delta wng3$ parasites, we observed one vacuole (out of 16 we took EM images of) that exhibited aberrant cytokinesis where one mother cell gave rise to 3 daughter cells (Figure 3.5). Three out of the 16 vacuoles also had odd number of parasites. We also observed "mislocalization" of organelles within the PV where organelles such as mitochondria and dense granules that should be localized to within the parasite, instead were localized to the residual body (Figure 3.6). The residual body is what is left of the mother cell after it divides (3). It is thought to serve as a center for sharing material in large vacuoles where not all the parasites have access to the PVM. I am currently in the process of testing the aberrant cytokinesis phenotype by infecting HFF cells with WT or $\Delta wng3$ parasites, letting them replicate once and taking phase images of at least 500 vacuoles.

This will allow me to determine if the percentage of parasites giving rise to multiple daughter cells is significantly higher in the Δwng parasites.

Preliminary quantitative phosphoproteomics data have yielded GRA5 and several hypothetical proteins as potential substrates (Table 3.2). Similarly to WNG2, we have only done EM on these parasites, once and have yet to do EM on the wild-type and kinase dead complements. Hence, more EM data will be needed to conclusively show a phenotype for WNG3.

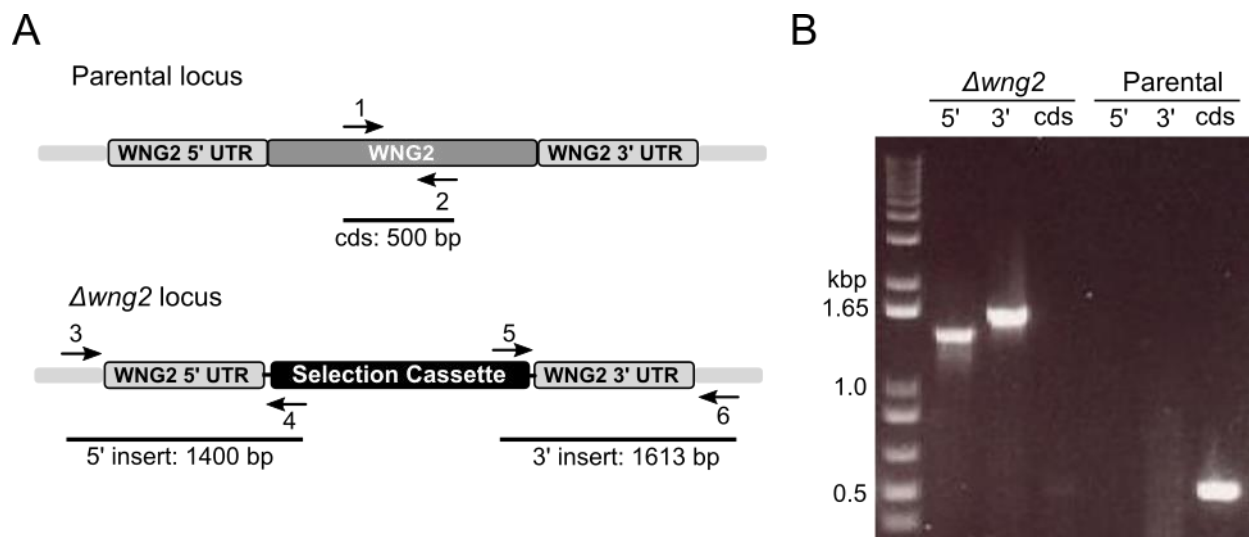


Figure 3.1: Generation of WNG2 knockout parasites. RH $\Delta wng1$ parasites were generated by double homologous recombination in which the WNG2 genomic sequence was replaced by a HXGPRT selection cassette. (A) Cartoon of parental and knockout loci indicating binding sites for primers used to verify knockout. (B) PCR demonstrating insertion of selection cassette and loss of coding sequence (cds) in knockout parasites. Primers sequences are listed in Table 3.3.

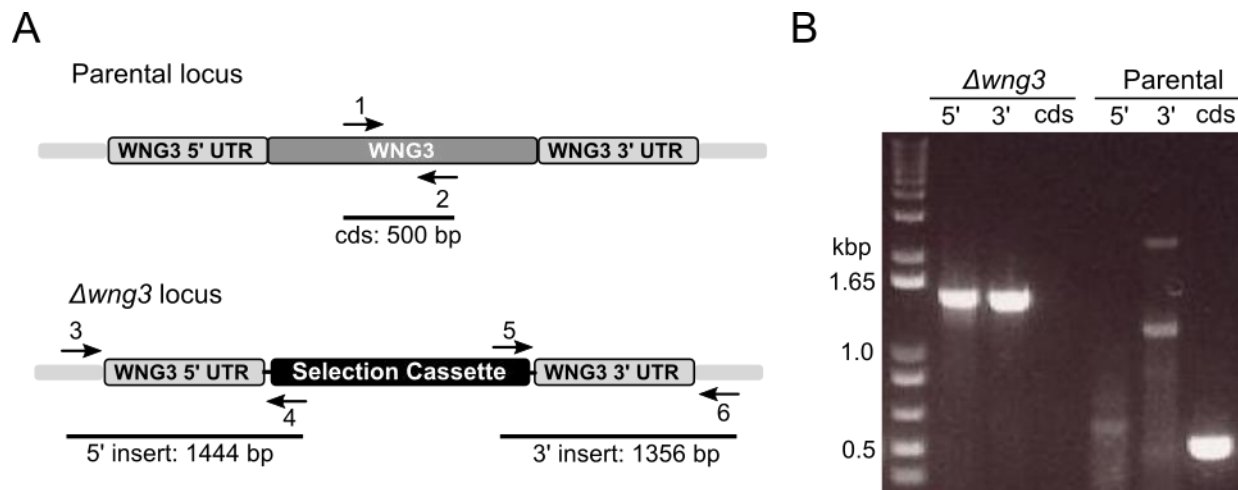


Figure 3.2: Generation of WNG3 knockout parasites. RH $\Delta wng1$ parasites were generated by double homologous recombination in which the WNG3 genomic sequence was replaced by a HXGPRT selection cassette. (A) Cartoon of parental and knockout loci indicating binding sites for primers used to verify knockout. (B) PCR demonstrating insertion of selection cassette and loss of coding sequence (cds) in knockout parasites. Primers sequences are listed in Table 3.3.

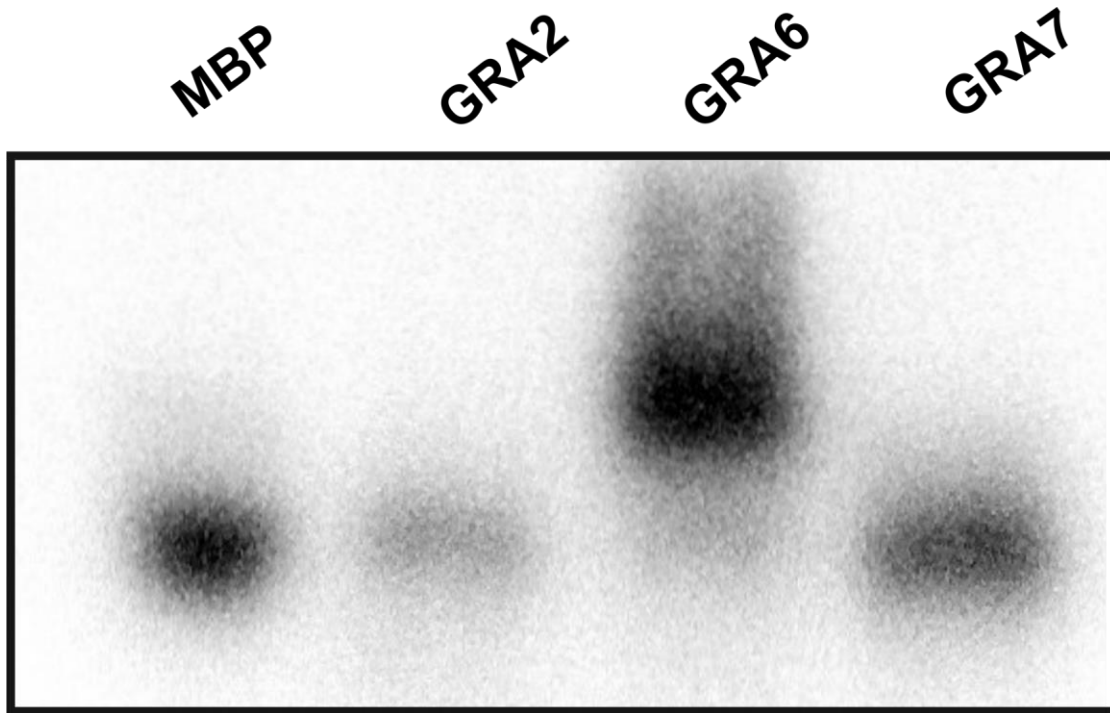


Figure 3.3: WNG2 is an active kinase. Autoradiogram of kinase activity of recombinant WNG2 against the indicated GRA proteins and MBP as substrates, using ^{32}P scintillation.

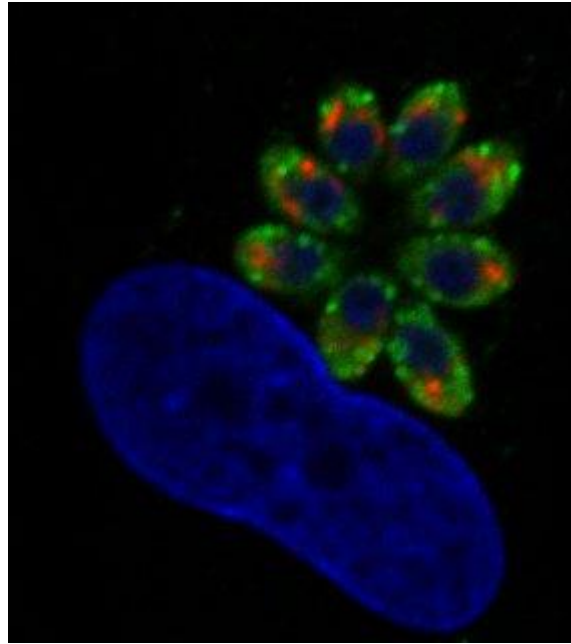


Figure 3.4. WNG3 localizes within the parasite. WNG3 (green) was visualized by immunohistochemistry. Nucleus (Blue), Rhoptry (red).

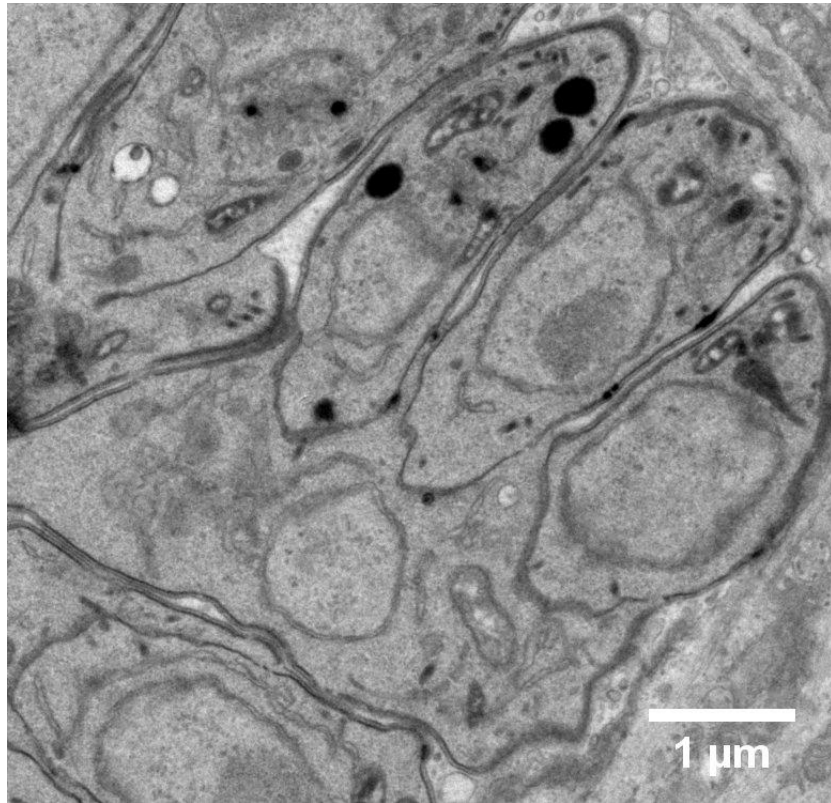


Figure 3.5. Vacuole of WNG3 KO parasites showing aberrant cytokinesis. One mother cell is giving rise to three daughter cells. Representative transmission electron microscopic images of the $RH\Delta wng3$.

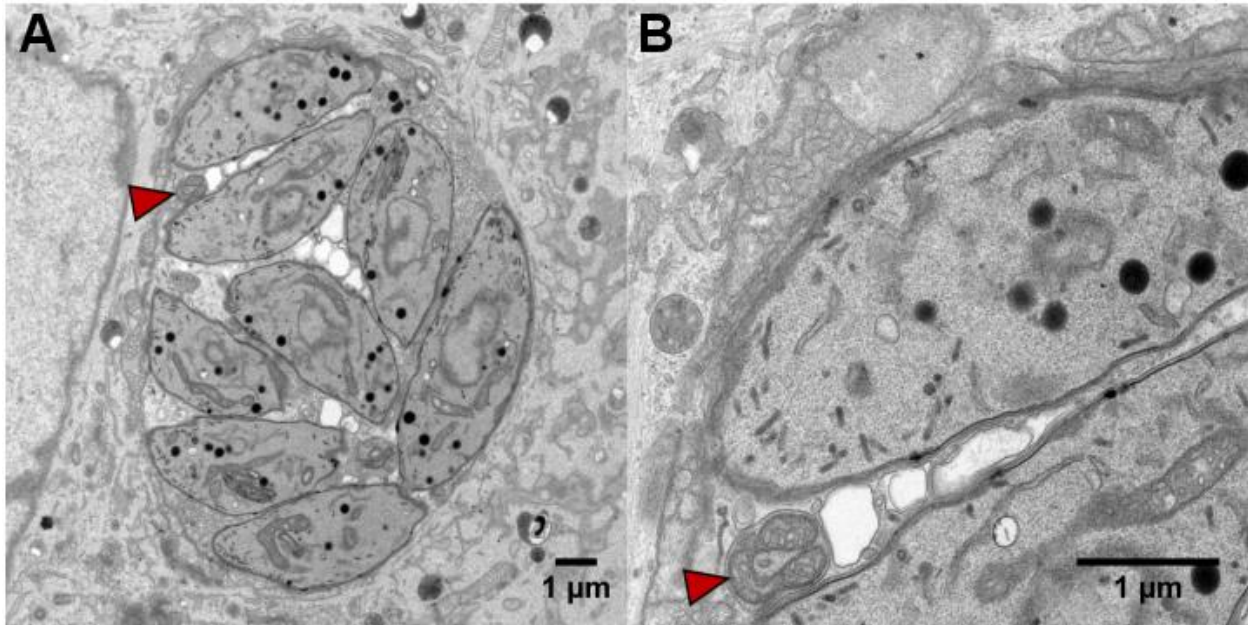


Figure 3.6. Vacuoles of WNG3 KO parasites show mislocalized organelles (mitochondria). Representative transmission electron microscopic images of the (A) $RH\Delta wng3$ (B) zoom in of the vacuole in A. Mitochondria that are localized to vesicles are indicated with solid red arrowheads.

Gene model	Name	Context
TGGT1_220370	hypothetical protein	SLGL SS GDRLA
TGGT1_220370	hypothetical protein	D RLAE T RRRES
TGGT1_315140	WD domain, G-beta repeat-containing protein	AASGD S DDERKR
TGVEG_234560	hypothetical protein	VRRSR S PEAEA

Table 3.1: Phosphosites downregulated in RHΔwng2 vacuoles. The sequence context of each of the phosphosites is indicated. Acidic residues are red, basic residues are blue.

Gene model	Name	Context
TGGT1_220370	hypothetical protein	SLGLS S GDRLA
TGGT1_220370	hypothetical protein	D RLAE T RRRES
TGGT1_239083	hypothetical protein	I DSMQ T sIPRN
TGGT1_217680	hypothetical protein	P ERRR S FFGNL
TGGT1_286450	GRA5	Q N EDR S LF E RG
TGVEG_273560	kinesin heavy chain, putative;putative kinesin heavy chain	K KRSE S PEG D E

Table 3.2: Phosphosites downregulated in RH Δ wng3 vacuoles. The sequence context of each of the phosphosites is indicated. Acidic residues are red, basic residues are blue.

APPENDICES

Construct	Primer name	Primer sequence
WNG1 KO	f TgWNG1ko(5targ-ga) [56]	ggatcccaccgcggtggcgg GGAACAGAGTCGATGTTCTAGAC
	r TgWNG1ko(5targ-ga) [57]	cgaacggtagcattcgatat ATGTCACACTCGACTCCGTACC
	f TgWNG1ko(3targ-ga) [61]	atacgaacggtacagcttgc AGCAAAGTGCGCGGCAGG
	r TgWNG1ko(3targ-ga) [58]	ggaacaaaagctgggtacgg CACATGTCCTGCATGATGTGATACC
	r pTKO_ga_prep1	ggatcccaccgcggtggcggCCGTACCCAGCTTTTGTTC
	f pTKO_ga_prep2	CCGCCACCGCGGTGGG
	f HXGPRT(ptko-ga)	CTAGCAAGCTGTACCGTTCGTATAATG
	r HXGPRT/gra2-3'utr(ptko-ga)	ATATCGAATGCTACCGTTCGTATAGC
	f cds (1)	ACTGACTGCGGATAGACGCGT
	r cds (2)	TACCACAGAGACACACGCAGACAG
	f testWNG1ko 5p (3)	GCTCTCTGCGTCTGTGGAGC
	r testWNG1ko 5p (4)	CATCACTTTTCGTCTGTAGTCATAACTTC
	f testWNG1ko 3p (5)	GAATGCAAGGTTTCGTGCTGAT
	r testWNG1ko 3p (6)	CGCTTTCTGGCGTCTGGGC
WNG1and WNG2 3xHA	f 1xHA/f HA seq	TACCCGTACGACGTCCCGGAC
	f DHFRp	GATCAGCACGAAACCTTGCATTCAAAC
	f WNG1(-1500*) DHFRp-ga	tgcaaggtttcgtgctgacTACAGCTCGTACAAGCATGGTGG
	r WNG1(E628) HA-ga [57]	tccgggacgtcgtacgggtaTTCGTTTTCTGTTTCATGGTCTTG
	f WNG2(ex3) DHFRp-ga [57]	tgcaaggtttcgtgctgacATAGGACGAGAAGCTTCTCTCTG
	r WNG2(S553) HA-ga [56]	tccgggacgtcgtacgggtaGCTCTCCTGTGCGTCTTCC
WNG1 WT and D437S complement	f_OriginAmp-ga[61]	GCGAGCGGTATCAGCTCACTC
	r Ku80 5p vec-ga [60]	agtgagctgataccgctcgcCGCTACTTGTGTGTCTTCACTGC
	f Ku80 3p vec-ga [59]	cgattaagtgggtaaaccgcGTGTAGGCATTTGCCGTGCG
	r_OriginAmp-ga[60]	GCGTTTACCCAACCTAATCGCCTTG
	r SAG1 3p [57]	TCGGGGGGGCAAGAATTGTG
	r Ku80 3p SAG13p-ga [60]	cacaattctgccccccgaGCAGATGCGAGAGGGCTGG
	f SAG1p [58]	AAGCTTTTACATCCGTTGCCTTTTC
	F_TgWNG1 (ATG -1384) [58]	GCTCTCTGCGTCTGTGGAGC
	F_TgWNG1 (ATG-197)[59]	AAGCAGTTGTGTCTCGAGCGATC
	f TgWNG1(M1) blunt [58]	ATGAGGGACAGAGGCTGGCG
	r WNG1 start-ga [61]	CGCCAGCCTCTGTCCCTCAT
	r WNG1 HA-ga [58]	tccgggacgtcgtacgggatgTTCGTTTTCTGTTTCATGGTC
	f WNG1p sag1p-ga [58]	ggcaacggatgtaaaagcttGCTCTCTGCGTCTGTGGAG
	f 3xHA_1 SAG1p-ga [59]	ggcaacggatgtaaaagcttTACCCGTACGACGTCCCGGAC
	f HA seq [58]	TACCCGTACGACGTCCCGGAC
	r x1HA blunt [61]	AGCGTAGTCCGGGACGTCGTAC
	f_pHPT_GRA2_3utr_ga[60]	GACTACGACGAAAGTGATGCGC
	f Ku80 5p gra2-ga [60]	acaccgtagtccagtcgacCTCCGAGCAGCACATGCATT
	r GRA2 3p utr [60]	GTCGACTGGAACACTACGGTGTGTTGTT

Pet28-sumo WNG1 WT and mutants	WNG1 (aa310) R312A [59]	TGG CTG GCA AGA GGG GCG C
	R_WNG1 (aa309) [59]	CGG CAA AAT GTC TTC AAA CTC CGG GAA
	F_WNG1 (aa310) R313A [59]	TGG CTG AGG GCA GGG GCG
	F_TgWNG1 K346M	GTGATAATGGTAAAGTCTTCAACGGACG
	R_TgWNG1 K346M [57]	AATCCCTGTCCTCCGCGTCTC
	F_WNG1 (aa342) V344A [58]	GGG ATT GCA ATA AAG GTA AAG TCT TCA ACG
	R_WNG1 (aa341) [58]	TGT CCT CCG CGT CTC CTC GT
	F_WNG1 D455A PhQC	GCCTTCGAAGGCGTTGGCG
	F_WNG1 E457G PhQC	GACTTCGGCGGCGTTGGCGTGC
	F_WNG1 (aa455) E469A[59]	GAC TTC GCA GGC GTT GGC G
	R_WNG1 (aa454 [58]	AGC GAG AAC GAC ATG GCC GTC
	F_WNG1 (aa446) R448G [59]	CAT GGC GAC ATC AAG GCT CAC AAC
	R_WNG1 (aa433) [59]	CAG GAA GCC GTG TGT ATG GAG AAT GTA
	F_TgWNG1 D437S [59]	CATCGGAGCATCAAGGCTCACAAAC
	R_TgWNG1 D437S	CAGGAAGCCGTGTGTATGGAGAAT
	F_WNG1(aa265)[59]	GGTGGCCCGCGGGTCCG
	R_BAMHI pet28SUMO 5p [58]	GGATCCACCAATCTGTTCTCTGTGAG
	WNG2KO	f TgWNG2ko(5targ-ga) [57]
r TgWNG2ko(5targ-ga) [59]		cgaacggtagcattcgatat CCTTCTTTCGGACAGTCGCG
f TgWNG2ko(3targ-ga) [58]		atacgaacggtagcagcttgc GCAGAGGAGGAAGGACGTCAAC
r TgWNG2ko(3targ-ga) [59]		ggaacaaaagctgggtacgg GCGAGTGCCAGTCGTTTCCC
r pTKO_ga_prep1		ggatcccaccgcggtggcggCCGTACCCAGCTTTTGTTC
f pTKO_ga_prep2		CCGCCACCGCGGTGGG
f HXGPRT(ptko-ga)		CTAGCAAGCTGTACCGTTCGTATAATG
r HXGPRT/gra2-3'utr(ptko-ga)		ATATCGAATGCTACCGTTCGTATAAGC
f cds (1)		GCCTTCGACTTCTACGAGTCCG
r cds (2)		CACCTGAACGCCAGTCCTTCG
f testWNG2ko 5p (3)		CTC GTC TTC ACA ACT CAC CGG G
r testWNG2ko 5p (4)		CATCACTTTCGTGCTAGTCATAACTTC
f testWNG2ko 3p (5)		GAATGCAAGGTTTCGTGCTGAT
r testWNG2ko 3p (6)		CTC AGC TAA ATA CAG AGG AGA GTG G
		f WNG3ko(5targ-ga) [59]
	r WNG3ko(5targ-ga) [59]	cgaacggtagcattcgatat GGAAGAACGGAGGGCGAGAAAC
	f WNG3ko(3targ-ga) [59]	atacgaacggtagcagcttgc CCAAGTCGAATGGAGGGACTGG
	r WNG3ko(3targ-ga) [59]	ggaacaaaagctgggtacgg AAGGTTCTCTGGAGTCGGCAC
	r pTKO_ga_prep1	ggatcccaccgcggtggcggCCGTACCCAGCTTTTGTTC
	f pTKO_ga_prep2	CCGCCACCGCGGTGGG
	f HXGPRT(ptko-ga)	CTAGCAAGCTGTACCGTTCGTATAATG

WNG3KO	r HXGPRT/gra2-3'utr(ptko-ga)	ATATCGAATGCTACCGTTCGTATAGC
	f cds (1)	CCGAAGAACGCCTTTATCCTGCC
	r cds (2)	CAGCTTGTCTACGTCGGCTGTC
	f testWNG3ko 5p (3)	CGA GCC TCT TAC AAC TGA AAT CGG
	r testWNG3ko 5p (4)	CATCACTTTTCGTTCGTAGTCATAACTTC
	f testWNG3ko 3p (5)	GAATGCAAGGTTTCGTGCTGAT
	r testWNG3ko 3p (6)	GTT TTT TCA TTA GCA AAG CGT CAA AGA G

Table 3.3. Primers used in this study.

BIBLIOGRAPHY

References (Chapter 1&3)

1. Tenter AM, Heckerroth AR, Weiss LM. *Toxoplasma gondii*: from animals to humans. *Int J Parasitol.* 2000 Nov;30(12-13):1217–58.
2. Weiss LM, Kim K. *Toxoplasma Gondii: The Model Apicomplexan. Perspectives and Methods.* Academic Press; 2011. 801 p.
3. Periz J, Whitelaw J, Harding C, Gras S, Del Rosario Minina MI, Latorre-Barragan F, et al. *Toxoplasma gondii* F-actin forms an extensive filamentous network required for material exchange and parasite maturation. Akhmanova A, editor. *eLife.* 2017 Mar 21;6:e24119.
4. Brown MS, Goldstein JL. Receptor-mediated control of cholesterol metabolism. *Science.* 1976 Jan 16;191(4223):150–4.
5. Coppens I, Sinai AP, Joiner KA. *Toxoplasma gondii* exploits host low-density lipoprotein receptor-mediated endocytosis for cholesterol acquisition. *J Cell Biol.* 2000 Apr 3;149(1):167–80.
6. Bottova I, Hehl AB, Štefanić S, Fabriàs G, Casas J, Schraner E, et al. Host Cell P-glycoprotein Is Essential for Cholesterol Uptake and Replication of *Toxoplasma gondii*. *J Biol Chem.* 2009 Jun 26;284(26):17438–48.
7. Sehgal A, Bettiol S, Pypaert M, Wenk MR, Kaasch A, Blader IJ, et al. Peculiarities of Host Cholesterol Transport to the Unique Intracellular Vacuole Containing *Toxoplasma*. *Traffic.* 2005;6(12):1125–41.
8. Ehrenman K, Sehgal A, Lige B, Stedman TT, Joiner KA, Coppens I. Novel roles for ATP-binding cassette G transporters in lipid redistribution in *Toxoplasma*. *Mol Microbiol.* 2010;76(5):1232–49.
9. Krug EC, Marr JJ, Berens RL. Purine metabolism in *Toxoplasma gondii*. *J Biol Chem.* 1989 Jun 25;264(18):10601–7.
10. Chaudhary K, Darling JA, Fohl LM, Sullivan WJ, Donald RGK, Pfefferkorn ER, et al. Purine salvage pathways in the apicomplexan parasite *Toxoplasma gondii*. *J Biol Chem.* 2004 Jul 23;279(30):31221–7.
11. Ngô HM, Ngo EO, Bzik DJ, Joiner KA. *Toxoplasma gondii*: Are Host Cell Adenosine Nucleotides a Direct Source for Purine Salvage? *Exp Parasitol.* 2000 Jun 1;95(2):148–53.
12. De Koning HP, Al-Salabi MI, Cohen AM, Coombs GH, Wastling JM. Identification and characterisation of high affinity nucleoside and nucleobase transporters in *Toxoplasma gondii*. *Int J Parasitol.* 2003 Jul 30;33(8):821–31.

13. Conrad Schwab J, Afifi Afifi M, Pizzorno G, Handschumacher RE, Joiner KA. *Toxoplasma gondii* tachyzoites possess an unusual plasma membrane adenosine transporter. *Mol Biochem Parasitol*. 1995 Mar 1;70(1):59–69.
14. Schwartzman JD, Pfefferkorn ER. *Toxoplasma gondii*: Purine synthesis and salvage in mutant host cells and parasites. *Exp Parasitol*. 1982 Feb 1;53(1):77–86.
15. White EL, Ross LJ, Davis RL, Ginkel SZ, Vasanthakumar G, Borhani DW. The Two *Toxoplasma gondii* Hypoxanthine-Guanine Phosphoribosyltransferase Isozymes Form Heterotetramers. *J Biol Chem*. 2000 Jun 23;275(25):19218–23.
16. Sibley LD, Niesman IR, Asai T, Takeuchi T. *Toxoplasma gondii*: secretion of a potent nucleoside triphosphate hydrolase into the parasitophorous vacuole. *Exp Parasitol*. 1994 Nov;79(3):301–11.
17. Carruthers VB, Sibley LD. Sequential protein secretion from three distinct organelles of *Toxoplasma gondii* accompanies invasion of human fibroblasts. *Eur J Cell Biol*. 1997 Jun;73(2):114–23.
18. Asai T, O'Sullivan WJ, Kobayashi M, Gero AM, Yokogawa M, Tatibana M. Enzymes of the de novo pyrimidine biosynthetic pathway in *Toxoplasma gondii*. *Mol Biochem Parasitol*. 1983 Feb 1;7(2):89–100.
19. Asai T, Miura S, Sibley LD, Okabayashi H, Takeuchi T. Biochemical and molecular characterization of nucleoside triphosphate hydrolase isozymes from the parasitic protozoan *Toxoplasma gondii*. *J Biol Chem*. 1995 May 12;270(19):11391–7.
20. Bermudes D, Peck KR, Afifi MA, Beckers CJ, Joiner KA. Tandemly repeated genes encode nucleoside triphosphate hydrolase isoforms secreted into the parasitophorous vacuole of *Toxoplasma gondii*. *J Biol Chem*. 1994 Nov 18;269(46):29252–60.
21. Davis RH. Compartmental and regulatory mechanisms in the arginine pathways of *Neurospora crassa* and *Saccharomyces cerevisiae*. *Microbiol Rev*. 1986 Sep;50(3):280–313.
22. Makoff AJ, Radford A. Genetics and biochemistry of carbamoyl phosphate biosynthesis and its utilization in the pyrimidine biosynthetic pathway. *Microbiol Rev*. 1978 Jun;42(2):307–28.
23. Botero-Kleiven S, Fernández V, Lindh J, Richter-Dahlfors A, von Euler A, Wahlgren M. Receptor-mediated endocytosis in an apicomplexan parasite (*Toxoplasma gondii*). *Exp Parasitol*. 2001 Jul;98(3):134–44.
24. Dou Z, McGovern OL, Cristina MD, Carruthers VB. *Toxoplasma gondii* Ingests and Digests Host Cytosolic Proteins. *mBio*. 2014 Aug 29;5(4):e01188–14.
25. Marino ND, Panas MW, Franco M, Theisen TC, Naor A, Rastogi S, et al. Identification of a novel protein complex essential for effector translocation across the parasitophorous vacuole membrane of *Toxoplasma gondii*. *PLOS Pathog*. 2018 Jan 22;14(1):e1006828.

26. Lopez J, Bittame A, Massera C, Vasseur V, Effantin G, Valat A, et al. Intravacuolar Membranes Regulate CD8 T Cell Recognition of Membrane-Bound *Toxoplasma gondii* Protective Antigen. *Cell Rep*. 2015 Dec 15;13(10):2273–86.
27. Reese ML, Boothroyd JC. A helical membrane-binding domain targets the *Toxoplasma* ROP2 family to the parasitophorous vacuole. *Traffic*. 2009 Oct;10(10):1458–70.
28. Reese ML, Zeiner GM, Saeij JPJ, Boothroyd JC, Boyle JP. Polymorphic family of injected pseudokinases is paramount in *Toxoplasma* virulence. *Proc Natl Acad Sci U S A*. 2011 Jun 7;108(23):9625–30.
29. Labruyere E, Lingnau M, Mercier C, Sibley LD. Differential membrane targeting of the secretory proteins GRA4 and GRA6 within the parasitophorous vacuole formed by *Toxoplasma gondii*. *Mol Biochem Parasitol*. 1999 Aug 20;102(2):311–24.
30. Ossorio PN, Dubremetz JF, Joiner KA. A soluble secretory protein of the intracellular parasite *Toxoplasma gondii* associates with the parasitophorous vacuole membrane through hydrophobic interactions. *J Biol Chem*. 1994 May 27;269(21):15350–7.
31. Neudeck A, Stachelhaus S, Nischik N, Striepen B, Reichmann G, Fischer H-G. Expression variance, biochemical and immunological properties of *Toxoplasma gondii* dense granule protein GRA7. *Microbes Infect*. 2002 May 1;4(6):581–90.
32. Alaganan A, Fentress SJ, Tang K, Wang Q, Sibley LD. *Toxoplasma* GRA7 effector increases turnover of immunity-related GTPases and contributes to acute virulence in the mouse. *Proc Natl Acad Sci*. 2014 Jan 21;111(3):1126–31.
33. Carey KL, Donahue CG, Ward GE. Identification and molecular characterization of GRA8, a novel, proline-rich, dense granule protein of *Toxoplasma gondii*. *Mol Biochem Parasitol*. 2000 Jan 5;105(1):25–37.
34. Manning G, Plowman GD, Hunter T, Sudarsanam S. Evolution of protein kinase signaling from yeast to man. *Trends Biochem Sci*. 2002 Oct;27(10):514–20.
35. Tagliabracci VS, Wiley SE, Guo X, Kinch LN, Durrant E, Wen J, et al. A Single Kinase Generates the Majority of the Secreted Phosphoproteome. *Cell*. 2015 Jun 18;161(7):1619–32.
36. Cori GT, Green AA. Crystalline Muscle Phosphorylase li. Prosthetic Group. *J Biol Chem*. 1943 Nov 1;151(1):31–8.
37. Burnett G, Kennedy EP. The enzymatic phosphorylation of proteins. *J Biol Chem*. 1954 Dec;211(2):969–80.
38. Fischer EH, Krebs EG. Conversion of phosphorylase b to phosphorylase a in muscle extracts. *J Biol Chem*. 1955 Sep;216(1):121–32.
39. Sutherland EW, Wosilait WD. The relationship of epinephrine and glucagon to liver phosphorylase. I. Liver phosphorylase; preparation and properties. *J Biol Chem*. 1956 Jan;218(1):459–68.

40. Krebs EG, Fischer EH. Phosphorylase and Related Enzymes of Glycogen Metabolism. In: Harris RS, Wool IG, Loraine JA, Marrian GF, Thimann KV, editors. *Vitamins & Hormones* [Internet]. Academic Press; 1964. p. 399–410. Available from: <http://www.sciencedirect.com/science/article/pii/S0083672908603453>
41. Sutherland EW, Rall TW. Fractionation and characterization of a cyclic adenine ribonucleotide formed by tissue particles. *J Biol Chem*. 1958 Jun;232(2):1077–91.
42. Walsh DA, Perkins JP, Krebs EG. An Adenosine 3',5'-Monophosphate-dependant Protein Kinase from Rabbit Skeletal Muscle. *J Biol Chem*. 1968 Jul 10;243(13):3763–5.
43. Takai Y, Kishimoto A, Inoue M, Nishizuka Y. Studies on a cyclic nucleotide-independent protein kinase and its proenzyme in mammalian tissues. I. Purification and characterization of an active enzyme from bovine cerebellum. *J Biol Chem*. 1977;252(21):7603–9.
44. Cyclic Nucleotide-dependent Protein Kinases [Internet]. [cited 2019 Mar 14]. Available from: <http://www.jbc.org/content/245/10/2493.short>
45. Taylor SS, Radzio-Andzelm E. Three protein kinase structures define a common motif. *Structure*. 1994 May;2(5):345–55.
46. Jeffrey PD, Russo AA, Polyak K, Gibbs E, Hurwitz J, Massagué J, et al. Mechanism of CDK activation revealed by the structure of a cyclinA-CDK2 complex. *Nature*. 1995 Jul;376(6538):313.
47. Sicheri F, Moarefi I, Kuriyan J. Crystal structure of the Src family tyrosine kinase Hck. *Nature*. 1997 Feb 13;385(6617):602–9.
48. Cowan-Jacob SW, Fendrich G, Manley PW, Jahnke W, Fabbro D, Liebetanz J, et al. The crystal structure of a c-Src complex in an active conformation suggests possible steps in c-Src activation. *Struct Lond Engl* 1993. 2005 Jun;13(6):861–71.
49. Pearce LR, Komander D, Alessi DR. The nuts and bolts of AGC protein kinases. *Nat Rev Mol Cell Biol*. 2010 Jan;11(1):9–22.
50. Yang J, Cron P, Good VM, Thompson V, Hemmings BA, Barford D. Crystal structure of an activated Akt/protein kinase B ternary complex with GSK3-peptide and AMP-PNP. *Nat Struct Biol*. 2002 Dec;9(12):940–4.
51. Biondi RM, Komander D, Thomas CC, Lizcano JM, Deak M, Alessi DR, et al. High resolution crystal structure of the human PDK1 catalytic domain defines the regulatory phosphopeptide docking site. *EMBO J*. 2002 Aug 15;21(16):4219–28.
52. Steinberg GR, Kemp BE. AMPK in Health and Disease. *Physiol Rev*. 2009 Jul;89(3):1025–78.
53. Oliver AW, Knapp S, Pearl LH. Activation segment exchange: a common mechanism of kinase autophosphorylation? *Trends Biochem Sci*. 2007 Aug;32(8):351–6.

54. Zhang X, Gureasko J, Shen K, Cole PA, Kuriyan J. An allosteric mechanism for activation of the kinase domain of epidermal growth factor receptor. *Cell*. 2006 Jun 16;125(6):1137–49.
55. Clapéron A, Therrien M. KSR and CNK: two scaffolds regulating RAS-mediated RAF activation. *Oncogene*. 2007 May 14;26(22):3143–58.
56. Udell CM, Rajakulendran T, Sicheri F, Therrien M. Mechanistic principles of RAF kinase signaling. *Cell Mol Life Sci CMLS*. 2011 Feb;68(4):553–65.
57. Xu B, English JM, Wilsbacher JL, Stippec S, Goldsmith EJ, Cobb MH. WNK1, a novel mammalian serine/threonine protein kinase lacking the catalytic lysine in subdomain II. *J Biol Chem*. 2000 Jun 2;275(22):16795–801.
58. Manning G, Plowman GD, Hunter T, Sudarsanam S. Evolution of protein kinase signaling from yeast to man. *Trends Biochem Sci*. 2002 Oct;27(10):514–20.
59. Scheeff ED, Eswaran J, Bunkoczi G, Knapp S, Manning G. Structure of the pseudokinase VRK3 reveals a degraded catalytic site, a highly conserved kinase fold, and a putative regulatory binding site. *Struct Lond Engl* 1993. 2009 Jan 14;17(1):128–38.
60. Middelbeek J, Clark K, Venselaar H, Huynen MA, van Leeuwen FN. The alpha-kinase family: an exceptional branch on the protein kinase tree. *Cell Mol Life Sci*. 2010 Mar;67(6):875–90.
61. Tagliabracci VS, Engel JL, Wen J, Wiley SE, Worby CA, Kinch LN, et al. Secreted kinase phosphorylates extracellular proteins that regulate biomineralization. *Science*. 2012 Jun 1;336(6085):1150–3.
62. Koike T, Izumikawa T, Tamura J-I, Kitagawa H. FAM20B is a kinase that phosphorylates xylose in the glycosaminoglycan-protein linkage region. *Biochem J*. 2009 Jun 26;421(2):157–62.
63. Bordoli MR, Yum J, Breitkopf SB, Thon JN, Italiano JE, Xiao J, et al. A secreted tyrosine kinase acts in the extracellular environment. *Cell*. 2014 Aug 28;158(5):1033–44.
64. Dudkiewicz M, Lenart A, Pawłowski K. A Novel Predicted Calcium-Regulated Kinase Family Implicated in Neurological Disorders. *PLOS ONE*. 2013 Jun 28;8(6):e66427.
65. Yaffe MB, Elia AEH. Phosphoserine/threonine-binding domains. *Curr Opin Cell Biol*. 2001 Apr 1;13(2):131–8.
66. Salah Z, Alian A, Aqeilan RI. WW domain-containing proteins: retrospectives and the future. *Front Biosci Landmark Ed*. 2012 Jan 1;17:331–48.
67. Durocher D, Jackson SP. The FHA domain. *FEBS Lett*. 2002;513(1):58–66.
68. Kipreos ET, Pagano M. The F-box protein family. *Genome Biol*. 2000;1(5):reviews3002.1–reviews3002.7.

69. Adams JA. Kinetic and catalytic mechanisms of protein kinases. *Chem Rev.* 2001 Aug;101(8):2271–90.
70. Chan KF, Hurst MO, Graves DJ. Phosphorylase kinase specificity. A comparative study with cAMP-dependent protein kinase on synthetic peptides and peptide analogs of glycogen synthase and phosphorylase. *J Biol Chem.* 1982 Apr 10;257(7):3655–9.
71. Luo K, Zhou P, Lodish HF. The specificity of the transforming growth factor beta receptor kinases determined by a spatially addressable peptide library. *Proc Natl Acad Sci U S A.* 1995 Dec 5;92(25):11761–5.
72. Manning G, Whyte DB, Martinez R, Hunter T, Sudarsanam S. The Protein Kinase Complement of the Human Genome. *Science.* 2002 Dec 6;298(5600):1912–34.
73. Pappas G, Roussos N, Falagas ME. Toxoplasmosis snapshots: Global status of *Toxoplasma gondii* seroprevalence and implications for pregnancy and congenital toxoplasmosis. *Int J Parasitol.* 2009 Oct 1;39(12):1385–94.
74. Boothroyd JC, Dubremetz J-F. Kiss and spit: the dual roles of *Toxoplasma* rhoptries. *Nat Rev Microbiol.* 2008 Jan;6(1):79–88.
75. Hakimi M-A, Olias P, Sibley LD. *Toxoplasma* Effectors Targeting Host Signaling and Transcription. *Clin Microbiol Rev.* 2017 Jul 1;30(3):615–45.
76. Peixoto L, Chen F, Harb OS, Davis PH, Beiting DP, Brownback CS, et al. Integrative genomic approaches highlight a family of parasite-specific kinases that regulate host responses. *Cell Host Microbe.* 2010 Aug 19;8(2):208–18.
77. Boothroyd JC. Have it your way: how polymorphic, injected kinases and pseudokinases enable *Toxoplasma* to subvert host defenses. *PLoS Pathog.* 2013;9(4):e1003296.
78. Bradley PJ, Sibley LD. Rhoptries: an arsenal of secreted virulence factors. *Curr Opin Microbiol.* 2007 Dec;10(6):582–7.
79. Jones NG, Wang Q, Sibley LD. Secreted Protein Kinases Regulate Cyst Burden During Chronic Toxoplasmosis. *Cell Microbiol.* 2016 Jul 23;
80. Walker JE, Saraste M, Runswick MJ, Gay NJ. Distantly related sequences in the alpha- and beta-subunits of ATP synthase, myosin, kinases and other ATP-requiring enzymes and a common nucleotide binding fold. *EMBO J.* 1982;1(8):945–51.
81. Etheridge RD, Alaganaan A, Tang K, Lou HJ, Turk BE, Sibley LD. The *Toxoplasma* pseudokinase ROP5 forms complexes with ROP18 and ROP17 kinases that synergize to control acute virulence in mice. *Cell Host Microbe.* 2014 May 14;15(5):537–50.
82. Hanks SK, Hunter T. Protein kinases 6. The eukaryotic protein kinase superfamily: kinase (catalytic) domain structure and classification. *FASEB J Off Publ Fed Am Soc Exp Biol.* 1995 May;9(8):576–96.

83. Buchholz KR, Bowyer PW, Boothroyd JC. Bradyzoite pseudokinase 1 is crucial for efficient oral infectivity of the *Toxoplasma gondii* tissue cyst. *Eukaryot Cell*. 2013 Mar;12(3):399–410.
84. Huynh M-H, Carruthers VB. Tagging of endogenous genes in a *Toxoplasma gondii* strain lacking Ku80. *Eukaryot Cell*. 2009 Apr;8(4):530–9.
85. Donald RG, Carter D, Ullman B, Roos DS. Insertional tagging, cloning, and expression of the *Toxoplasma gondii* hypoxanthine-xanthine-guanine phosphoribosyltransferase gene. Use as a selectable marker for stable transformation. *J Biol Chem*. 1996 Jun 14;271(24):14010–9.
86. Soldati D, Kim K, Kampmeier J, Dubremetz JF, Boothroyd JC. Complementation of a *Toxoplasma gondii* ROP1 knock-out mutant using phleomycin selection. *Mol Biochem Parasitol*. 1995 Oct;74(1):87–97.
87. PyMOL Molecular Graphics System - Browse /pymol/1.7 at SourceForge.net [Internet]. [cited 2019 Mar 24]. Available from: <https://sourceforge.net/projects/pymol/files/pymol/1.7/>
88. Stivala A, Wybrow M, Wirth A, Whisstock JC, Stuckey PJ. Automatic generation of protein structure cartoons with Pro-origami. *Bioinforma Oxf Engl*. 2011 Dec 1;27(23):3315–6.
89. Otwinowski Z, Minor W. [20] Processing of X-ray diffraction data collected in oscillation mode. In: *Methods in Enzymology* [Internet]. Academic Press; 1997. p. 307–26. (Macromolecular Crystallography Part A; vol. 276). Available from: <http://www.sciencedirect.com/science/article/pii/S007668799776066X>
90. Sheldrick GM. A short history of SHELX. *Acta Crystallogr A*. 2008 Jan;64(Pt 1):112–22.
91. Terwilliger TC, Berendzen J. Automated MAD and MIR structure solution. *Acta Crystallogr D Biol Crystallogr*. 1999 Apr;55(Pt 4):849–61.
92. Terwilliger T. SOLVE and RESOLVE: automated structure solution, density modification and model building. *J Synchrotron Radiat*. 2004 Jan 1;11(Pt 1):49–52.
93. Adams PD, Afonine PV, Bunkóczi G, Chen VB, Davis IW, Echols N, et al. PHENIX: a comprehensive Python-based system for macromolecular structure solution. *Acta Crystallogr D Biol Crystallogr*. 2010 Feb 1;66(2):213–21.
94. Emsley P, Lohkamp B, Scott WG, Cowtan K. Features and development of Coot. *Acta Crystallogr D Biol Crystallogr*. 2010 Apr;66(Pt 4):486–501.
95. Winn MD, Murshudov GN, Papiz MZ. Macromolecular TLS Refinement in REFMAC at Moderate Resolutions. In: *Methods in Enzymology* [Internet]. Academic Press; 2003. p. 300–21. (Macromolecular Crystallography, Part D; vol. 374). Available from: <http://www.sciencedirect.com/science/article/pii/S0076687903740142>
96. MolProbity: all-atom structure validation for macromolecular crystallography [Internet]. [cited 2013 Jul 15]. Available from: <http://scripts.iucr.org/cgi-bin/paper?S0907444909042073>

97. Sali A, Blundell TL. Comparative protein modelling by satisfaction of spatial restraints. *J Mol Biol.* 1993 Dec 5;234(3):779–815.
98. Sievers F, Wilm A, Dineen D, Gibson TJ, Karplus K, Li W, et al. Fast, scalable generation of high-quality protein multiple sequence alignments using Clustal Omega. *Mol Syst Biol.* 2011 Oct 11;7:539.
99. Schindelin J, Arganda-Carreras I, Frise E, Kaynig V, Longair M, Pietzsch T, et al. Fiji: an open-source platform for biological-image analysis. *Nat Methods.* 2012 Jun 28;9(7):676–82.
100. Cox J, Mann M. MaxQuant enables high peptide identification rates, individualized p.p.b.-range mass accuracies and proteome-wide protein quantification. *Nat Biotechnol.* 2008 Dec;26(12):1367–72.
101. Cox J, Neuhauser N, Michalski A, Scheltema RA, Olsen JV, Mann M. Andromeda: a peptide search engine integrated into the MaxQuant environment. *J Proteome Res.* 2011 Apr 1;10(4):1794–805.
102. Tyanova S, Temu T, Sinitcyn P, Carlson A, Hein MY, Geiger T, et al. The Perseus computational platform for comprehensive analysis of (prote)omics data. *Nat Methods.* 2016;13(9):731–40.
103. Talevich E, Kannan N. Structural and evolutionary adaptation of rhoptyr kinases and pseudokinases, a family of coccidian virulence factors. *BMC Evol Biol.* 2013;13:117.
104. Fox BA, Sanders KL, Rommereim LM, Guevara RB, Bzik DJ. Secretion of Rhoptyr and Dense Granule Effector Proteins by Nonreplicating *Toxoplasma gondii* Uracil Auxotrophs Controls the Development of Antitumor Immunity. *PLoS Genet.* 2016;12(7):e1006189.
105. Coffey MJ, Dagley LF, Seizova S, Kapp EA, Infusini G, Roos DS, et al. Aspartyl Protease 5 Matures Dense Granule Proteins That Reside at the Host-Parasite Interface in *Toxoplasma gondii*. *mBio.* 2018 Nov 7;9(5):e01796–18.
106. Ossorio PN, Schwartzman JD, Boothroyd JC. A *Toxoplasma gondii* rhoptyr protein associated with host cell penetration has unusual charge asymmetry. *Mol Biochem Parasitol.* 1992 Jan;50(1):1–15.
107. Brennan DF, Dar AC, Hertz NT, Chao WCH, Burlingame AL, Shokat KM, et al. A Raf-induced allosteric transition of KSR stimulates phosphorylation of MEK. *Nature.* 2011 Apr 21;472(7343):366–9.
108. Murphy JM, Czabotar PE, Hildebrand JM, Lucet IS, Zhang J-G, Alvarez-Diaz S, et al. The pseudokinase MLKL mediates necroptosis via a molecular switch mechanism. *Immunity.* 2013 Sep 19;39(3):443–53.
109. Reese ML, Shah N, Boothroyd JC. The *Toxoplasma* Pseudokinase ROP5 Is an Allosteric Inhibitor of the Immunity-related GTPases. *J Biol Chem.* 2014 Oct 3;289(40):27849–58.
110. Zhang H, Zhu Q, Cui J, Wang Y, Chen MJ, Guo X, et al. Structure and evolution of the Fam20 kinases. *Nat Commun.* 2018 Mar 23;9(1):1218.

111. Zhu Q, Venzke D, Walimbe AS, Anderson ME, Fu Q, Kinch LN, et al. Structure of protein O-mannose kinase reveals a unique active site architecture. Gilmore R, editor. *eLife*. 2016 Nov 23;5:e22238.
112. Murphy JM, Zhang Q, Young SN, Reese ML, Bailey FP, Evers PA, et al. A robust methodology to subclassify pseudokinases based on their nucleotide-binding properties. *Biochem J*. 2014 Jan 15;457(2):323–34.
113. Levinson NM, Kuchment O, Shen K, Young MA, Koldobskiy M, Karplus M, et al. A Src-Like Inactive Conformation in the Abl Tyrosine Kinase Domain. *PLOS Biol*. 2006 May 2;4(5):e144.
114. A dynamic mechanism for allosteric activation of Aurora kinase A by activation loop phosphorylation | *eLife* [Internet]. [cited 2019 Mar 24]. Available from: <https://elifesciences.org/articles/32766>
115. Huang H, Zeqiraj E, Dong B, Jha BK, Duffy NM, Orlicky S, et al. Dimeric structure of pseudokinase RNase L bound to 2-5A reveals a basis for interferon-induced antiviral activity. *Mol Cell*. 2014 Jan 23;53(2):221–34.
116. A Comparison of Protein Kinases Inhibitor Screening Methods Using Both Enzymatic Activity and Binding Affinity Determination [Internet]. [cited 2019 Mar 24]. Available from: <https://journals.plos.org/plosone/article?id=10.1371/journal.pone.0098800>
117. Schwab JC, Beckers CJ, Joiner KA. The parasitophorous vacuole membrane surrounding intracellular *Toxoplasma gondii* functions as a molecular sieve. *Proc Natl Acad Sci U S A*. 1994 Jan 18;91(2):509–13.
118. Gold DA, Kaplan AD, Lis A, Bett GCL, Rosowski EE, Cirelli KM, et al. The *Toxoplasma* Dense Granule Proteins GRA17 and GRA23 Mediate the Movement of Small Molecules between the Host and the Parasitophorous Vacuole. *Cell Host Microbe*. 2015 May;17(5):642–52.
119. Yoshida T, Kakizuka A, Imamura H. BTeam, a Novel BRET-based Biosensor for the Accurate Quantification of ATP Concentration within Living Cells. *Sci Rep*. 2016 Dec 21;6:39618.
120. Fox BA, Rommereim LM, Guevara RB, Falla A, Hortua Triana MA, Sun Y, et al. The *Toxoplasma gondii* Rhoptry Kinome Is Essential for Chronic Infection. *mBio*. 2016 10;7(3).
121. Nadipuram SM, Kim EW, Vashisht AA, Lin AH, Bell HN, Coppens I, et al. In Vivo Biotinylation of the *Toxoplasma* Parasitophorous Vacuole Reveals Novel Dense Granule Proteins Important for Parasite Growth and Pathogenesis. *mBio*. 2016;7(4).
122. Treeck M, Sanders JL, Gaji RY, LaFavers KA, Child MA, Arrizabalaga G, et al. The calcium-dependent protein kinase 3 of *Toxoplasma* influences basal calcium levels and functions beyond egress as revealed by quantitative phosphoproteome analysis. *PLoS Pathog*. 2014 Jun;10(6):e1004197.

123. Treeck M, Sanders JL, Elias JE, Boothroyd JC. The phosphoproteomes of *Plasmodium falciparum* and *Toxoplasma gondii* reveal unusual adaptations within and beyond the parasites' boundaries. *Cell Host Microbe*. 2011 Oct 20;10(4):410–9.
124. Mercier C, Dubremetz J-F, Rauscher B, Lecordier L, Sibley LD, Cesbron-Delauw M-F. Biogenesis of Nanotubular Network in *Toxoplasma* Parasitophorous Vacuole Induced by Parasite Proteins. *Mol Biol Cell*. 2002 Jul 1;13(7):2397–409.
125. Coppens I, Dunn JD, Romano JD, Pypaert M, Zhang H, Boothroyd JC, et al. *Toxoplasma gondii* sequesters lysosomes from mammalian hosts in the vacuolar space. *Cell*. 2006 Apr 21;125(2):261–74.
126. Labruyere E, Lingnau M, Mercier C, Sibley LD. Differential membrane targeting of the secretory proteins GRA4 and GRA6 within the parasitophorous vacuole formed by *Toxoplasma gondii*. *Mol Biochem Parasitol*. 1999 Aug 20;102(2):311–24.
127. Lecordier L, Mercier C, Sibley LD, Cesbron-Delauw M-F. Transmembrane Insertion of the *Toxoplasma gondii* GRA5 Protein Occurs after Soluble Secretion into the Host Cell. *Mol Biol Cell*. 1999 Apr;10(4):1277–87.
128. Mercier C, Cesbron-Delauw MF, Sibley LD. The amphipathic alpha helices of the toxoplasma protein GRA2 mediate post-secretory membrane association. *J Cell Sci*. 1998 Aug;111 (Pt 15):2171–80.
129. Jacobs D, Dubremetz J-F, Loyens A, Bosman F, Saman E. Identification and heterologous expression of a new dense granule protein (GRA7) from *Toxoplasma gondii*1Note: Nucleotide sequence data reported in this paper have been submitted to the GenBank™ Data Bank with the accession number U79158.1. *Mol Biochem Parasitol*. 1998 Mar 15;91(2):237–49.
130. Bordier C. Phase separation of integral membrane proteins in Triton X-114 solution. *J Biol Chem*. 1981 Feb 25;256(4):1604–7.
131. Travier L, Mondragon R, Dubremetz J-F, Musset K, Mondragon M, Gonzalez S, et al. Functional domains of the *Toxoplasma* GRA2 protein in the formation of the membranous nanotubular network of the parasitophorous vacuole. *Int J Parasitol*. 2008 Jun;38(7):757–73.
132. Gendrin C, Bittame A, Mercier C, Cesbron-Delauw M-F. Post-translational membrane sorting of the *Toxoplasma gondii* GRA6 protein into the parasite-containing vacuole is driven by its N-terminal domain. *Int J Parasitol*. 2010 Sep;40(11):1325–34.
133. Hu K, Mann T, Striepen B, Beckers CJM, Roos DS, Murray JM. Daughter Cell Assembly in the Protozoan Parasite *Toxoplasma gondii*. *Mol Biol Cell*. 2002 Feb;13(2):593–606.